$H \rightarrow WW^* \rightarrow \ell\nu\ell\nu$ d'ATLAS

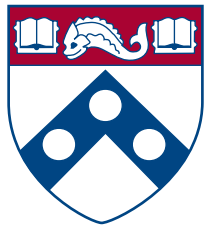

Univ. de Pennsylvanie

Dr. Tae Min Hong

Expérience d'ATLAS

Higgs Hunting, 26 juillet 2013

http://www.hep.upenn.edu/~tmhong/hh
http://higgshunting.fr

Outline

Analysis

Signatures of production & decay

Event selection & backgrounds

Results

Yields & systematics

Coupling strengths

Extra material

I will not cover some related topics (p30-32): spin (see T. Doyle, S. Luyckx); high M_H (see J. Wang); WH, ZH.

More slides (p19-39), tables (p40-50), plots (p51-104)

Physics context

Hong

HWW results part of [1] in July 2013. μ_{hat} at 20 - 30%. (p56-62)

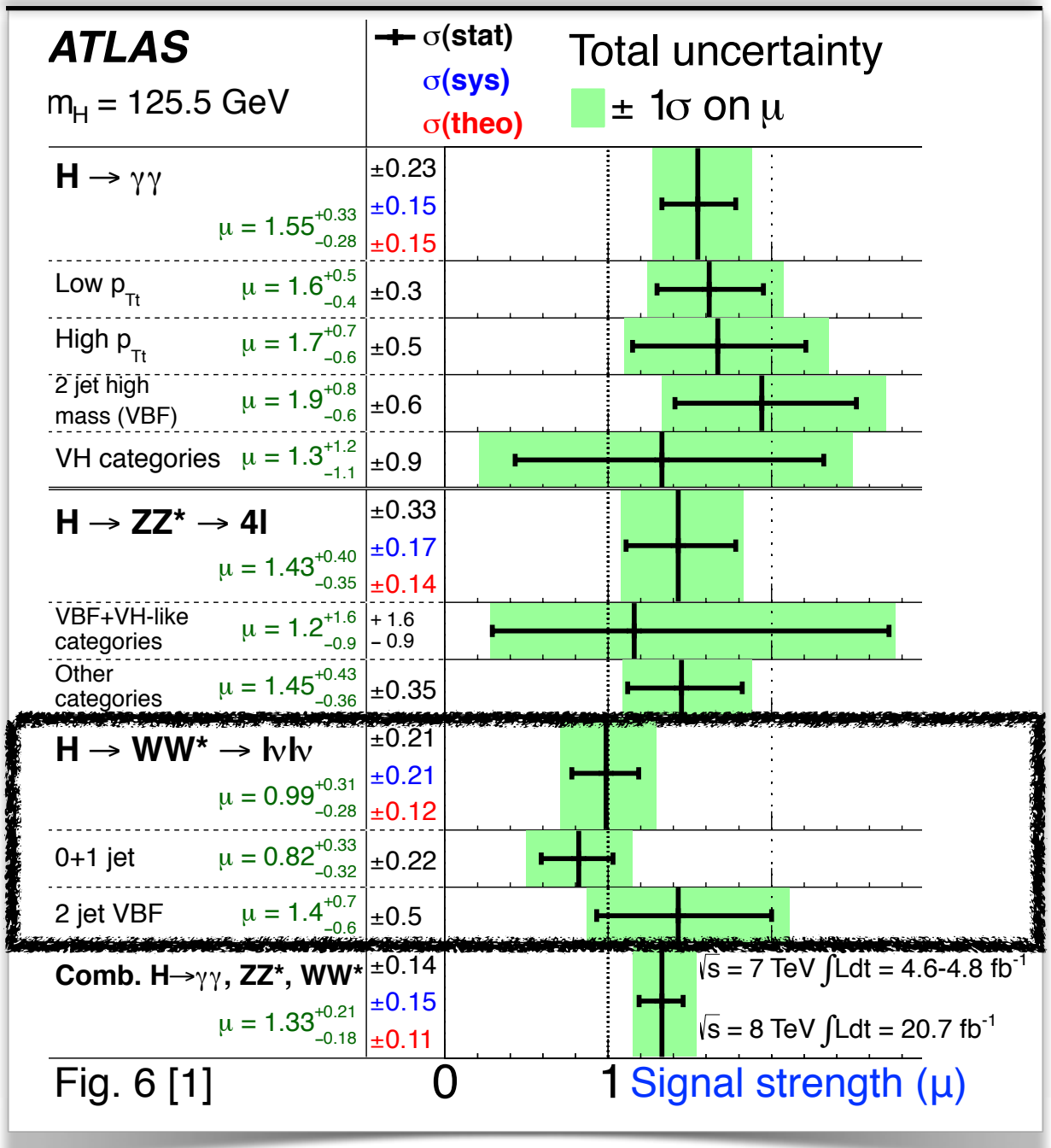

Fig. 6 [1]

HWW improved

- 2x data & 7 TeV
- Bkg. treatment
- ee, μμ channels
- VBF measurement
- VBF v. ggF contour

← Comparison with prev.

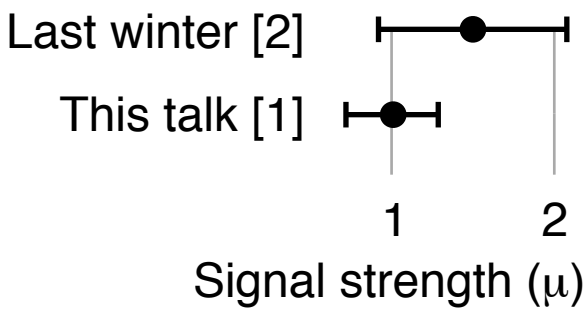

Higgs decay & production

Hong

H→WW*→ℓνℓν is clean with large rate, but no mass sensitivity. (p35)

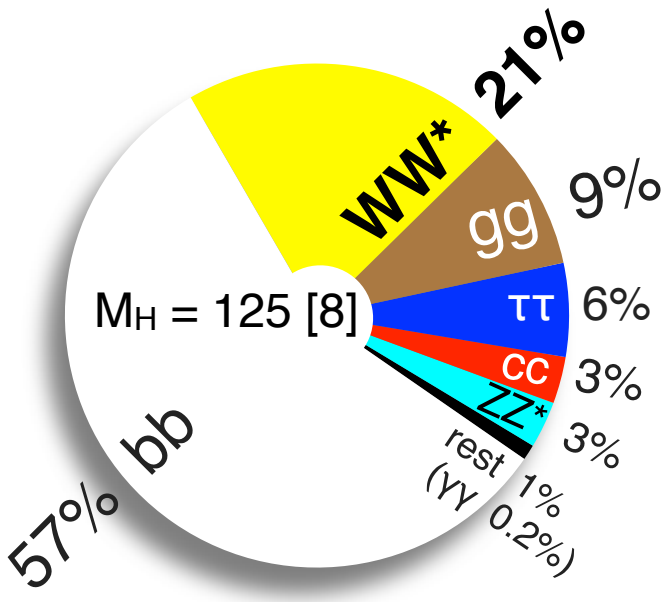

H→WW* →eμ $\nu_e\nu_\mu$ is most sensitive; focus of this talk.

→ee $\nu_e\nu_e$ } Large DY, so 10-15% gain in μ_{hat} wrt eμ.

→μμ $\nu_\mu\nu_\mu$ }

	σ (fb) [8] M_H=125	# of H 20.7fb^{-1}	# →WW* BR = 0.21	# →ℓνℓν BR = 0.04	After cuts This analysis
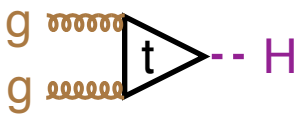	19,500	400,000	92,000	3,700	137
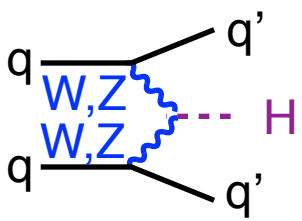	1,580	33,000	6,900	280	11

Physics with N_{Jet}

Hong

N_{Jet} distribution can separate the production mechanism. (p67-68)

ggF production

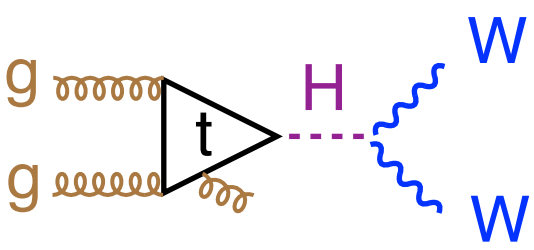

VBF production

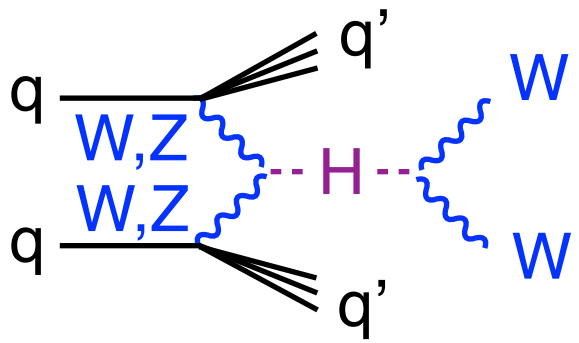

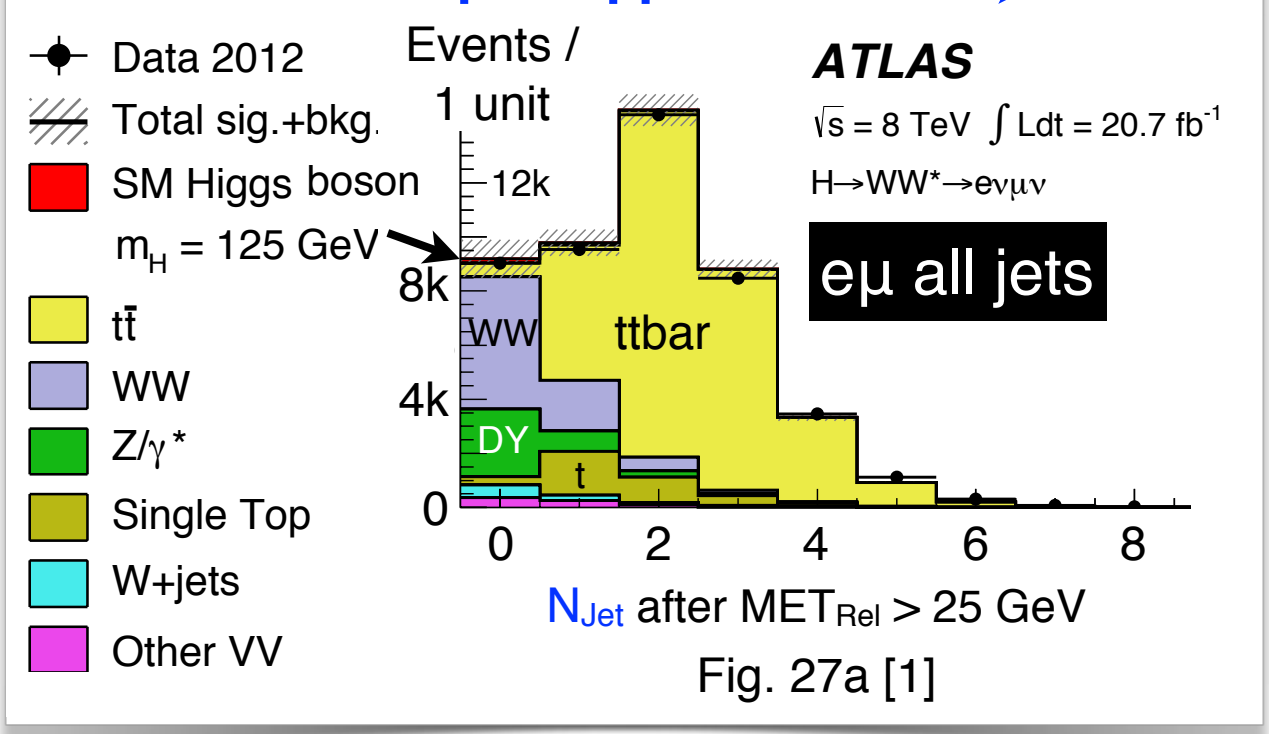

Fig. 27a [1]

Define jet from clusters:

- $P_T > 25$ in tracking vol.
  - Jet-vertex association to suppress pile-up (p103-104)
  - $f_{JVF} > 0.5$ for $P_T < 50$ GeV
- $P_T > 30$ if forward
  - $2.4 < |\eta| < 4.5$

Breakdown after all cuts:

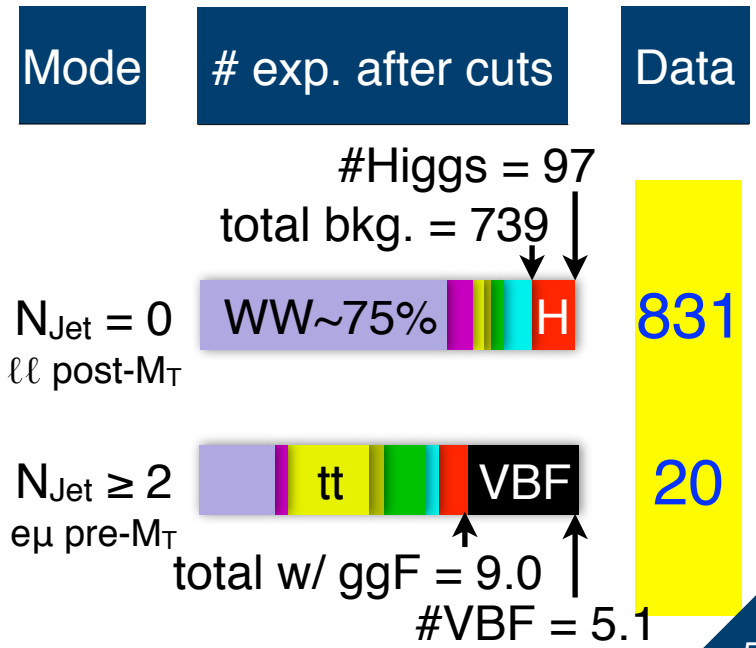

H→WW*→ℓνℓν signature

Hong

Conserving helicity (spin 0 + weak decay) gives collinear ℓℓ. (p70-75)

Diagram in rest frame of decay vertex

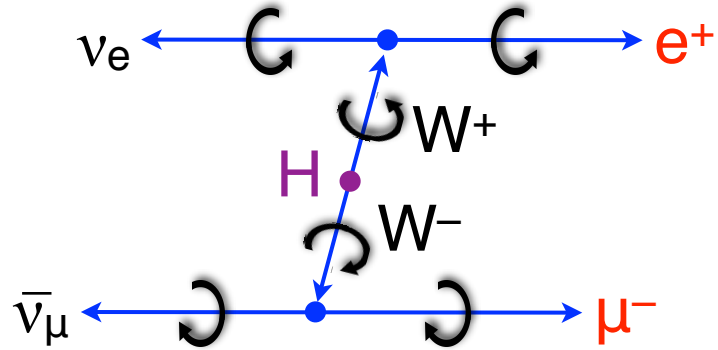

- Low $M_{\ell\ell}$ (bottom left plot)
- Small $\Delta\phi_{\ell\ell}$ (bottom right plot)
- Large MET (p10)

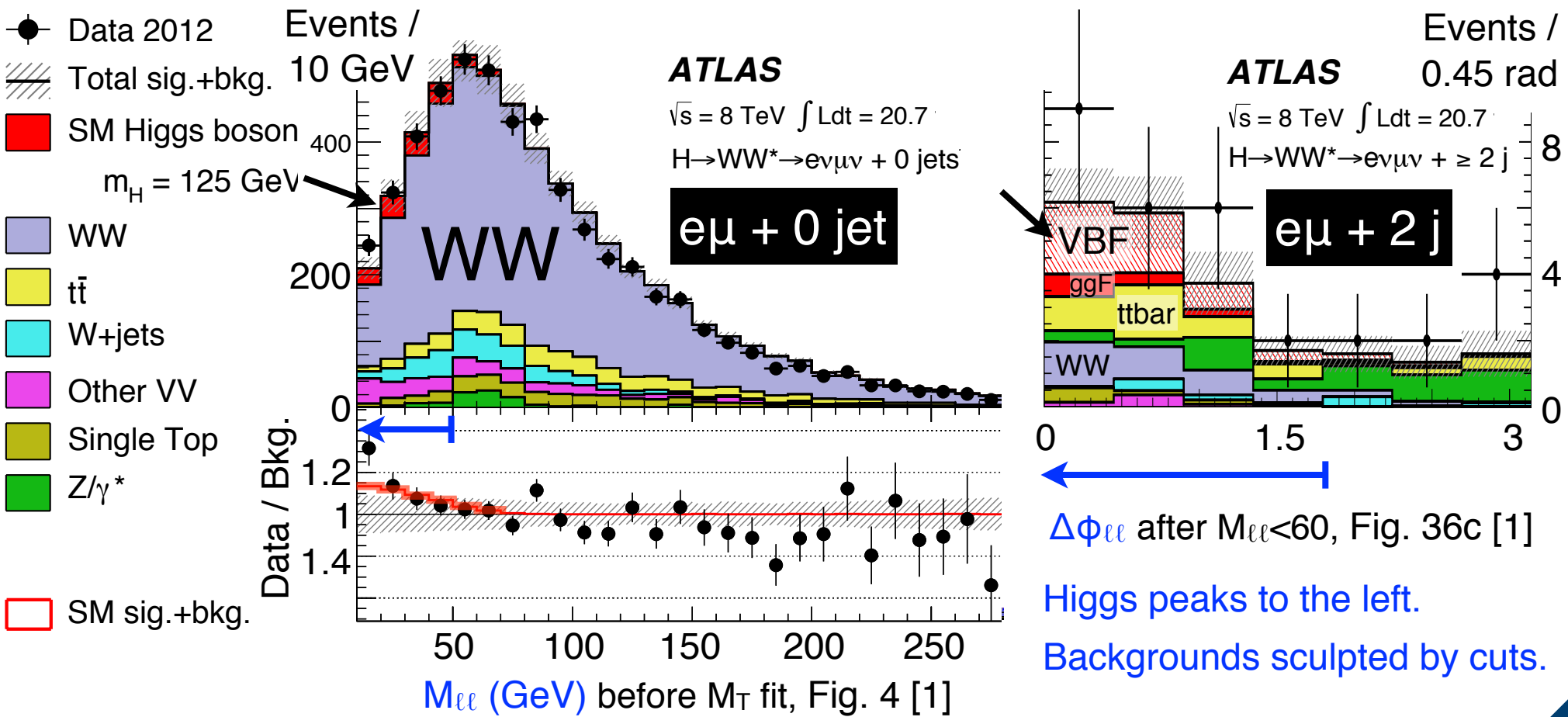

Higgs peaks to the left.

Backgrounds sculpted by cuts.

VBF signature

Hong

WW or ZZ collision has two recoiling well-separated jets. (p89-94)

Diagram in lab frame

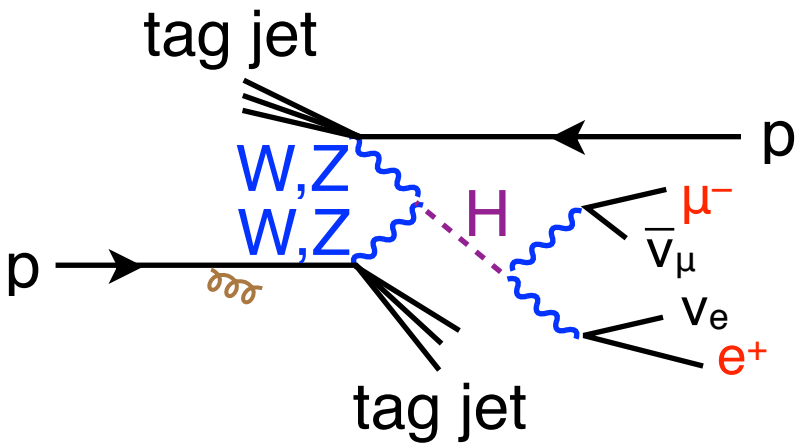

- W or Z exchange, so low QCD activity between tag jets
- Large ΔY_{JJ} & M_{JJ} (bottom plots)
- No b-jets at 85% eff. operating pt.

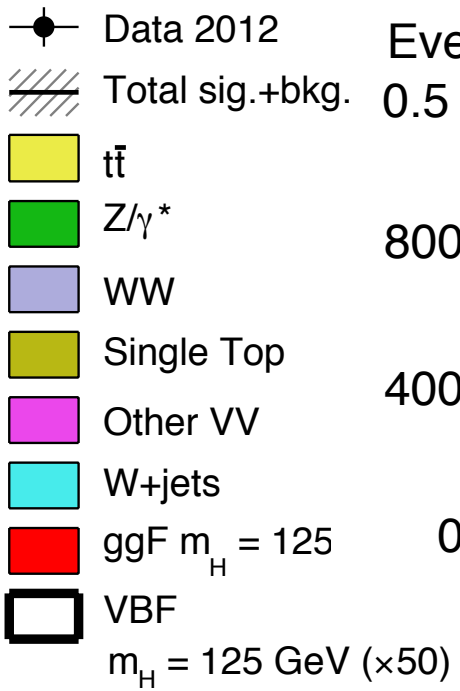

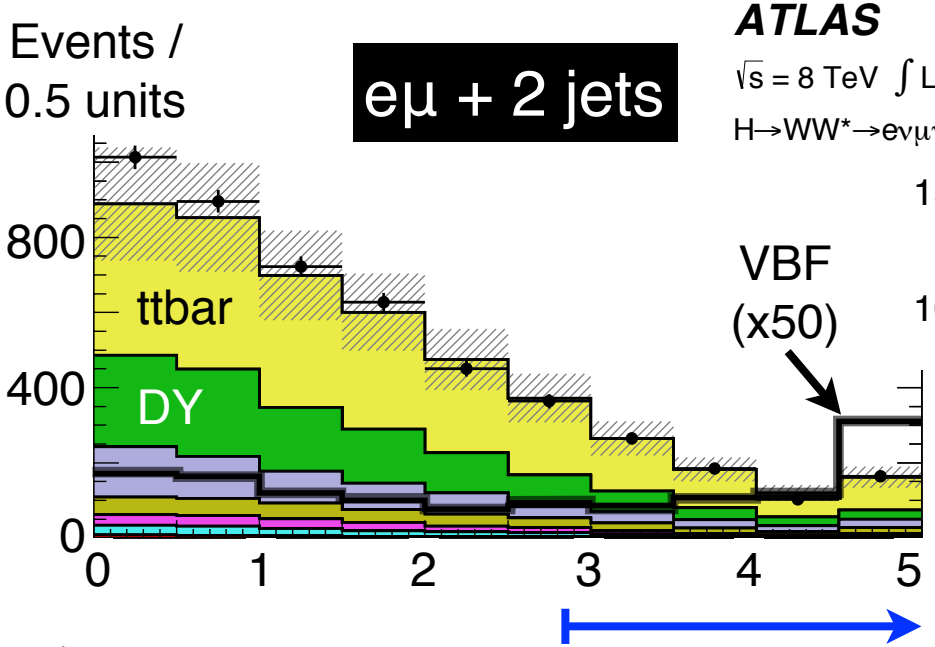

ΔY_{JJ} after $P_{T,tot} < 45$ GeV

Fig. 35a [1]

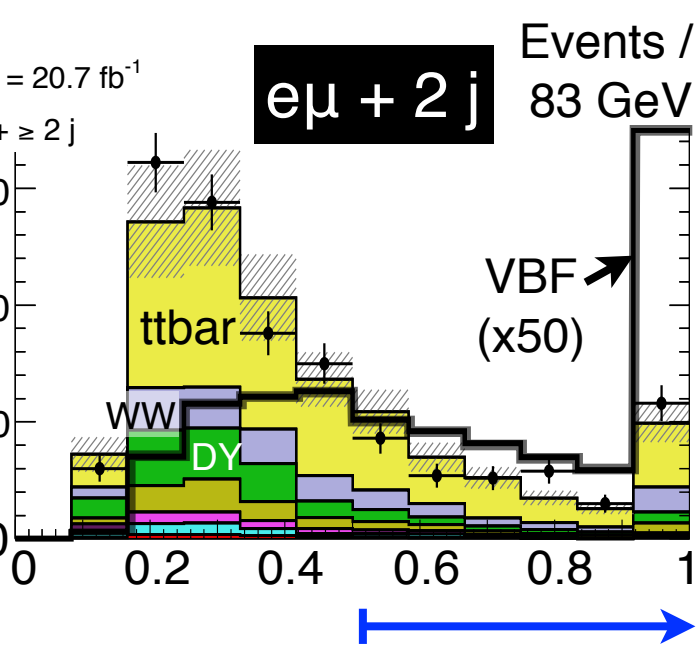

M_{JJ} (TeV) after $\Delta Y_{JJ} > 2.8$

Fig. 33c [1]

eμ + two forward jets

Run 214680, Event 271333760
Nov. 17, 2012, 07:42:05 CET [1]

Hong

VBF-like in JJ & Higgs-like in decay (more displays in p21-23)

ΔY_{JJ} = 6.6

M_{JJ} = 1.5 TeV

$M_{e\mu}$ = 21 GeV

M_T = 95 GeV

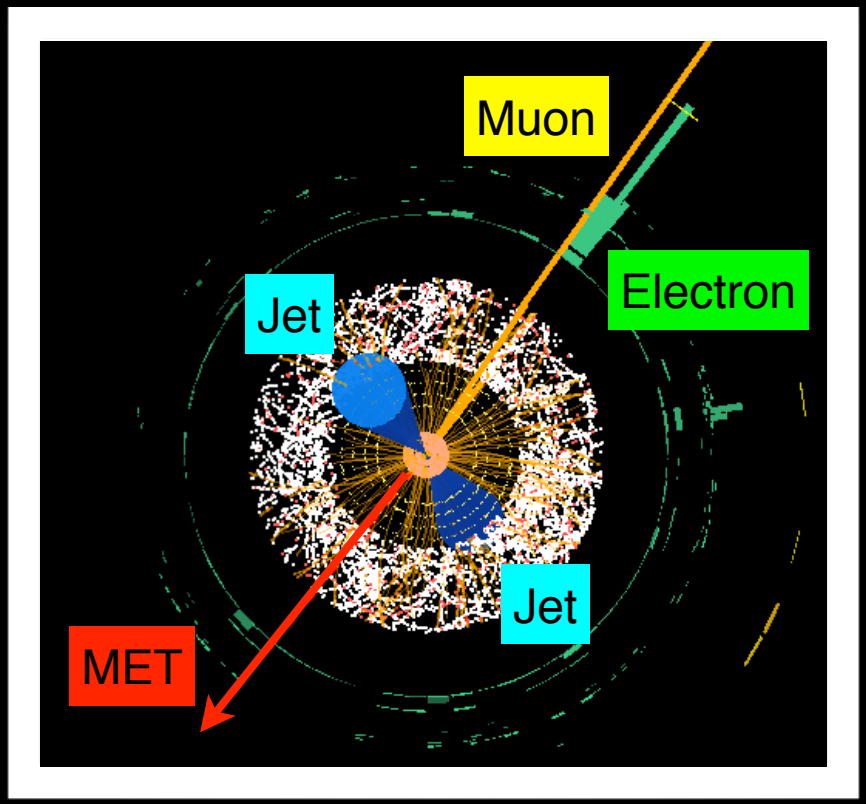

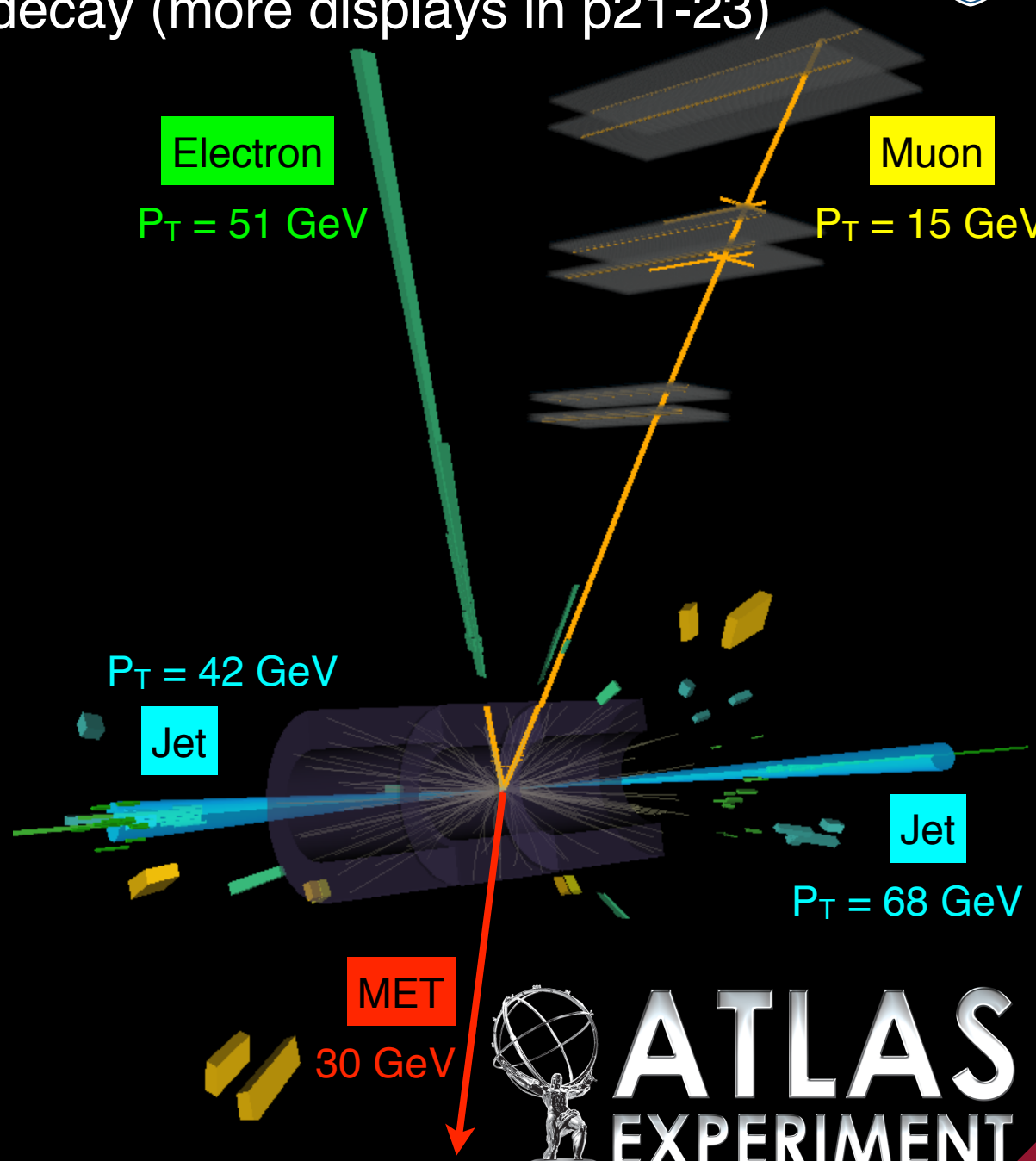

ATLAS EXPERIMENT

Backgrounds overview

Hong

Use data control regions to normalize backgrounds. (p44-47)

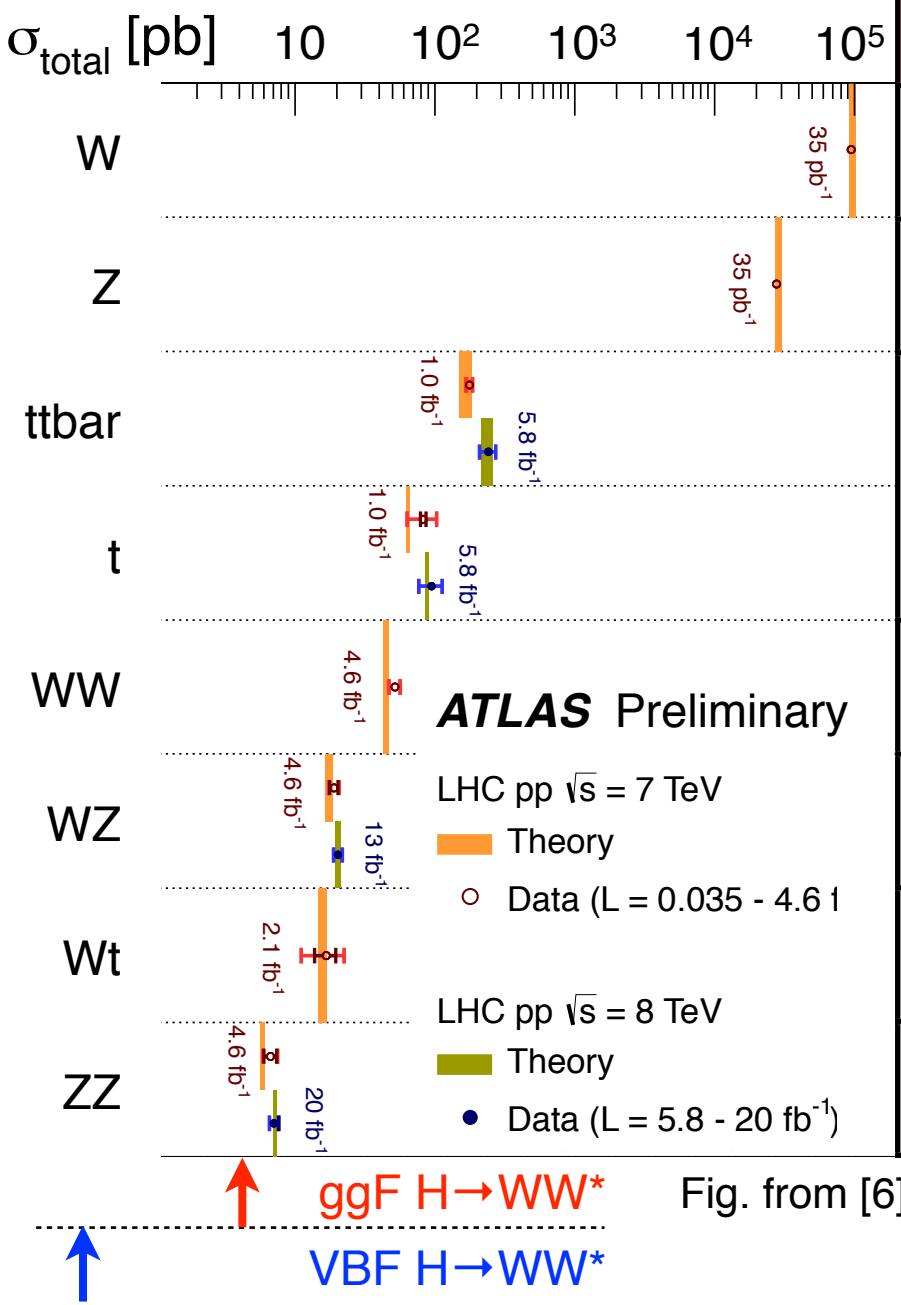

Fig. from [6]

How it fakes signal		Estimate	
W → ℓν	Jet fakes ℓ	Data	← p12 (24-25)
Z → ℓℓ Z → ττ	Fake MET Real MET	Data	← p10 (26-28, 63-66)
t → bℓν	Lose b	Data	← p13 (29, 76 -80, 89, 90)
Irreducible	Large	Data	← p11 (46, 47, 81-82)
WZ → ℓνℓℓ	Lose ℓ	MC	
W → ℓν	Lose b	Data	← p13 (29, 76 -80, 89, 90)
Irreducible	Small	MC	

Caveat emptor: The plot is for total cross sections, not for the dilepton final state in the HWW phase space.

MET selection

Hong

Reduce DY. For ee & μμ, use soft hadronic recoil (p26-28, 63-66).

Adjust MET relative to ℓ or jet

$MET_{Rel} = MET \cdot \sin\Delta\phi$ if $\Delta\phi < 180°$

$= MET$ else

for nearest ℓ, jet in transv. plane

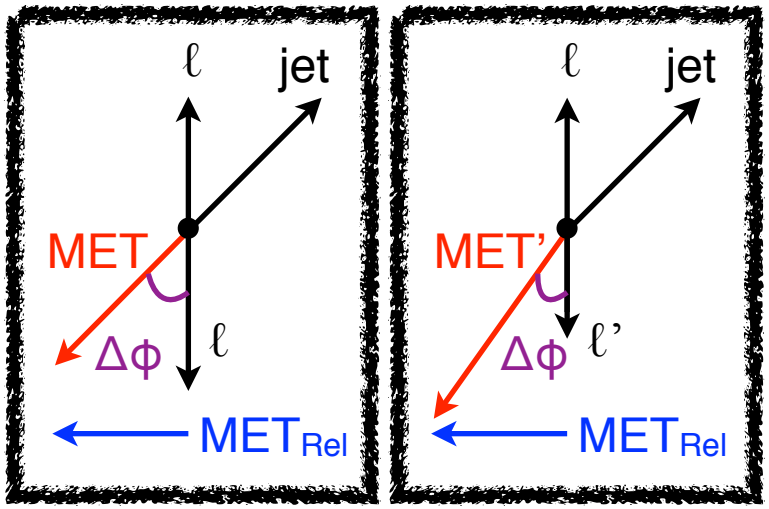

In this cartoon, MET_{Rel} immune to energy loss / mismeas't of nearest ℓ or jet.

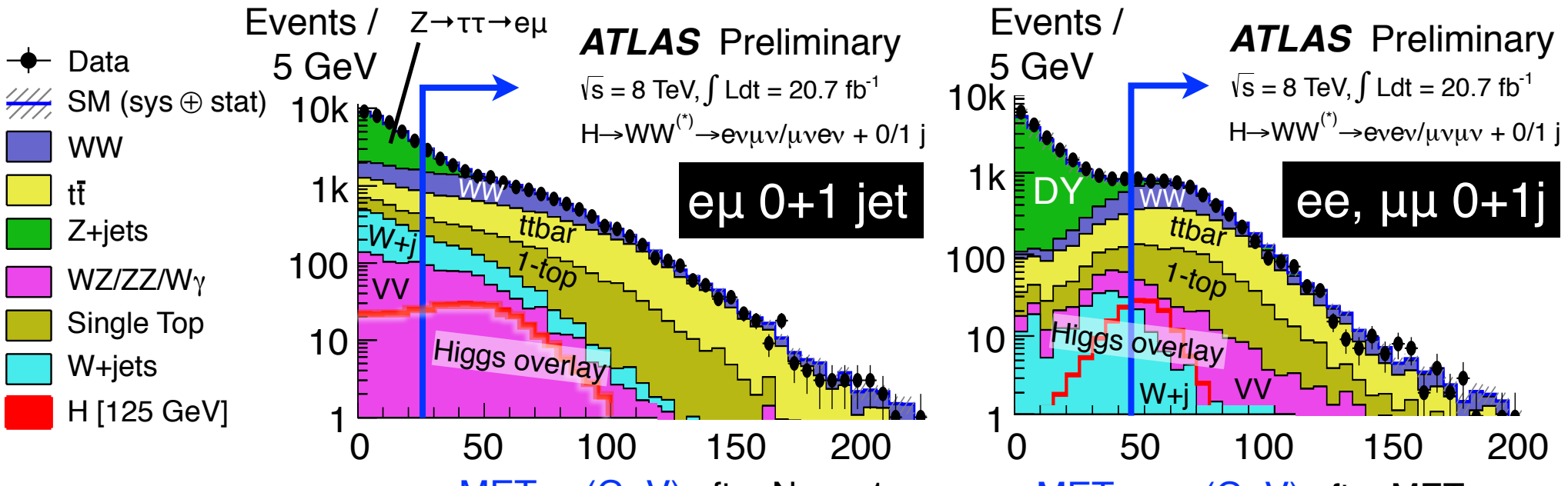

Fig. 1a [2]

Fig. 1b [2]

WW in $N_{Jet} \leq 1$

Hong

Use a data C.R. to normalize & MC to extrapolate to S.R. (p45-47)

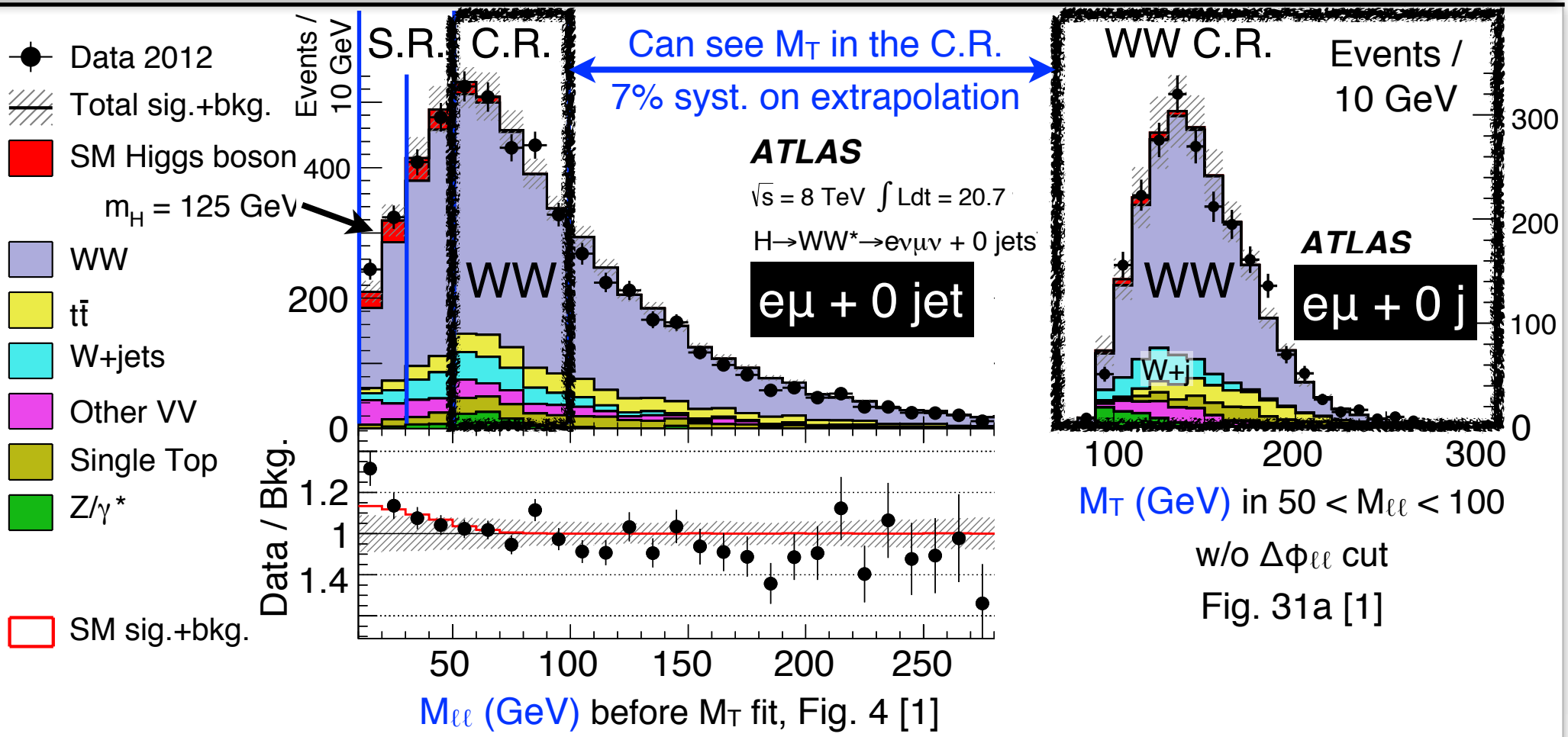

- Define C.R. as $50 < M_{\ell\ell} < 100$
- Define S.R. as $M_{\ell\ell} < 50$ GeV

Norm = 1.16 ± 0.04 (stat.) 0j
1.03 ± 0.06 (stat.) 1j

- Normalize S.R. from C.R. & fit $M_T = \sqrt{\left(E_{T,\ell\ell} + \text{MET}\right)^2 - \left|\vec{P}_{T,\ell\ell} + \vec{\text{MET}}\right|^2}$

W+jet in N_{Jet} = 0, 1, 2, ...

Hong

Use a data C.R. to normalize & di-jet data to extrapolate to S.R.

$$N_{\text{obs}} = \left(N_{\text{pass+pass ID}}\right)_{\text{S.R.}}$$

Pass + Pass / Fail

Extrapolate w/ di-jet data

$$N_{W+j} = \left(N_{\text{pass+fail ID}}\right)_{\text{S.R.}} \cdot \left(\frac{N_{\text{pass ID}}}{N_{\text{fail ID}}}\right)_{\text{di-jet}}$$

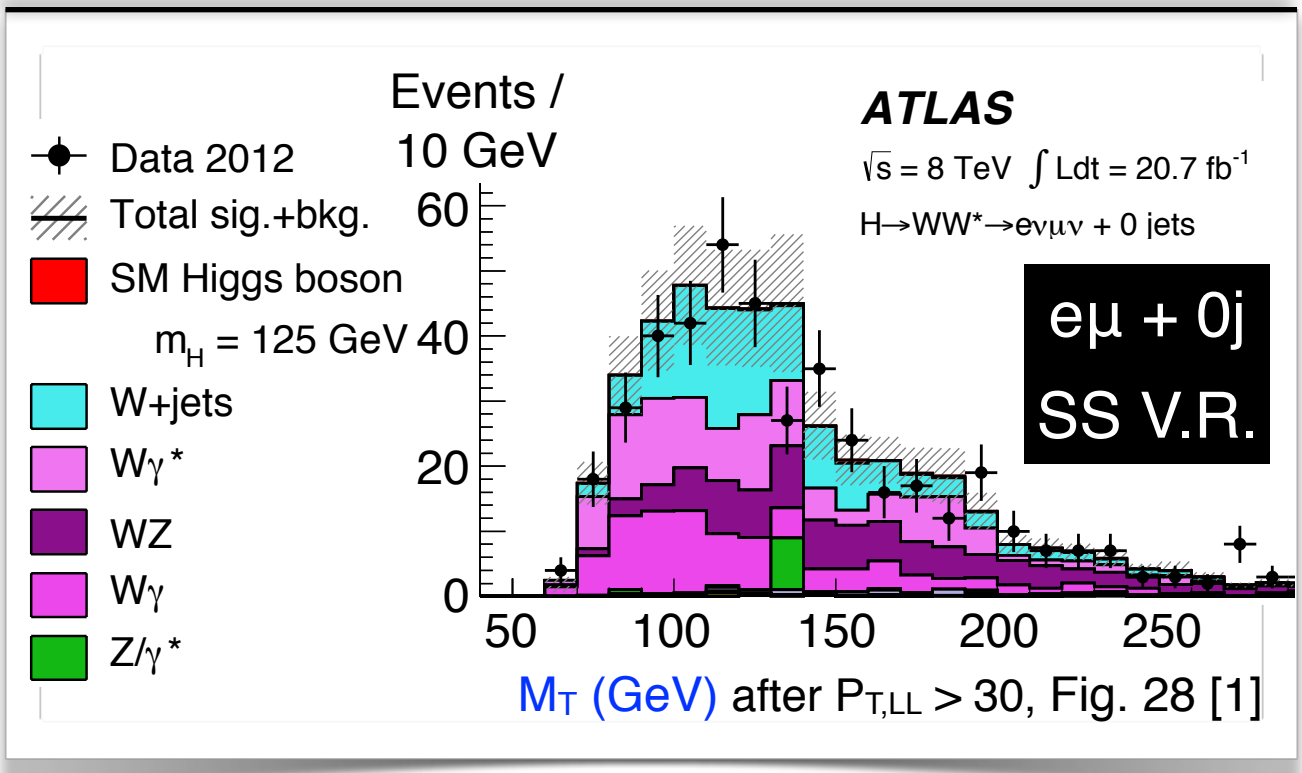

- Extrapolation assumes OK to use di-jet for W+j.
- Syst. at 40% on the est. by comparing MC (see back-up p24-25).
- Check shape & norm. of the estimate with MC in the same-sign validation region (left).

Top in N_{Jet} = 0, 1, 2, ...

Hong

Use a data C.R. to normalize & MC to extrapolate to S.R.

- 0-jet estimate uses

  Norm 0j = 1.07 ± 0.03 (stat) ± 0.12 (syst)

- 1-jet & VBF use $N_{b\text{-tag}} = 1$

  Norm 1j = 1.04 ± 0.02

  Norm VBF= 0.59 ± 0.07 (stat) ± 0.09 (syst)

  (see back-up p29)

$$N_{t\bar{t}} = \left(N_{\text{All jets}}\right)_{\text{data}} \cdot \left[\left(\frac{N_{0\text{jet}}}{N_{\text{All jets}}}\right)_{\text{MC}} \cdot f_{b\text{-tag}}\right]$$

- eμ $N_{Data} - N_{non\text{-}top}$ after MET_{Rel}>25 = 32k events
- MC extrapol. = 2 - 4% (±5%)
- b-tag correction data v. MC = 1.02 ± 0.02

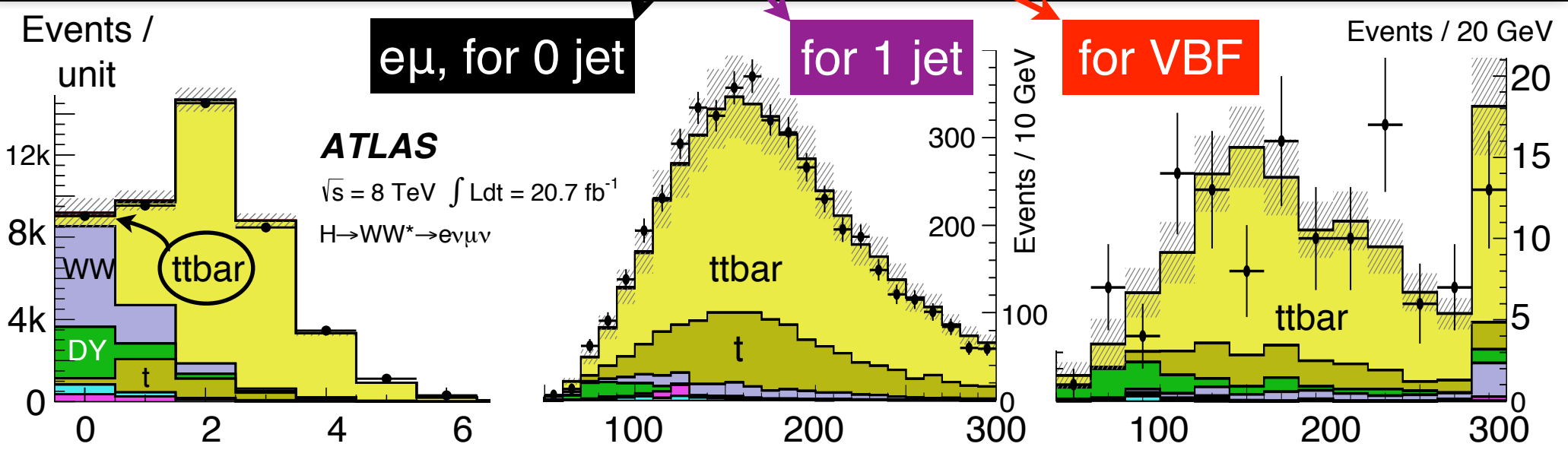

Fig. 27a [1]

Fig. 30a [1]

Fig. 30b [1]

Fit M_T after all cuts (p36, 42 cuts; 48-50 cutflow)

Hong

Data – Bkg. shows normalization & shape consistent with M_H=125.

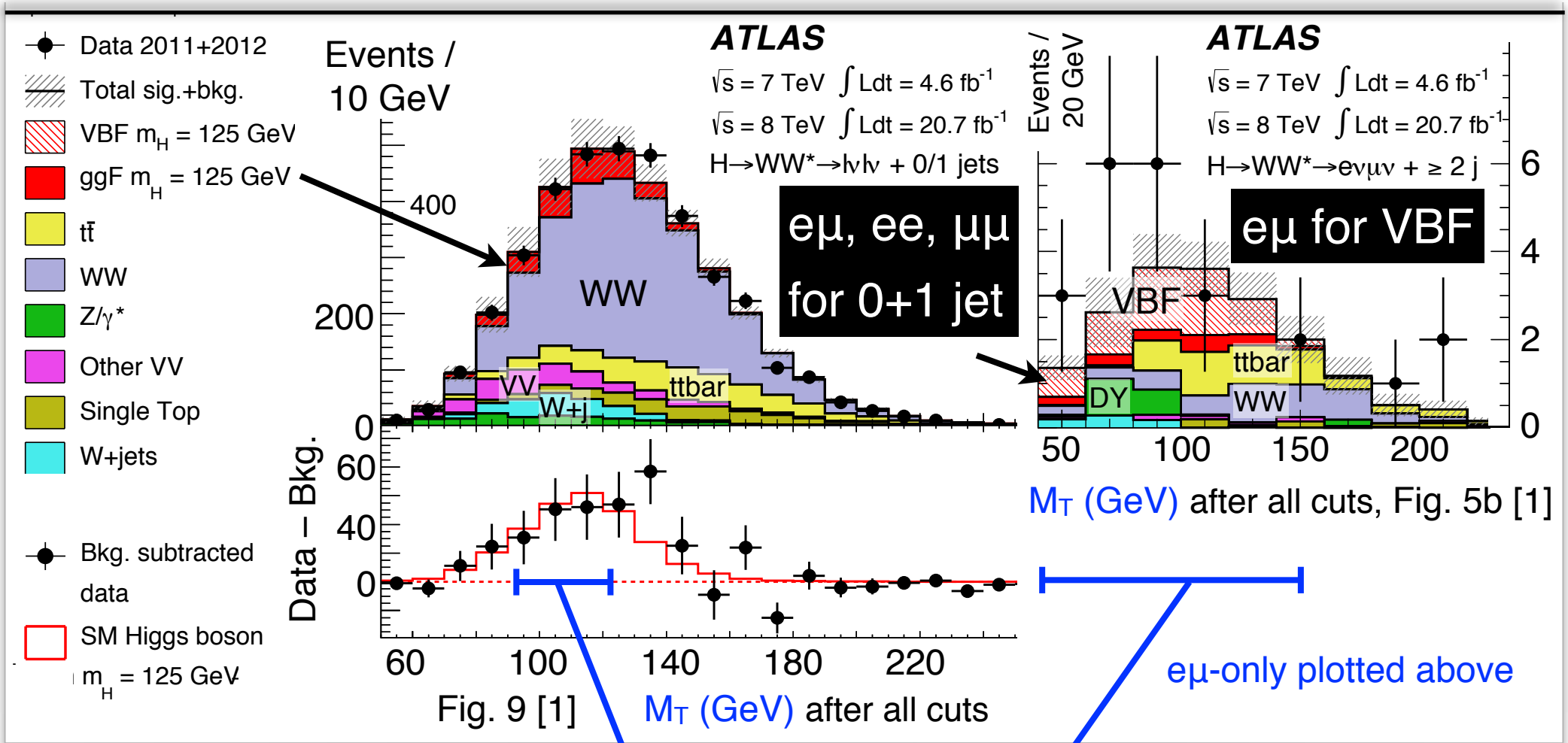

	$N_{\text{jet}} = 0$	$N_{\text{jet}} = 1$	$N_{\text{jet}} \geq 2$
Observed	831	309	55
Signal	100 ± 21	41 ± 14	10.9 ± 1.4
Total background	739 ± 39	261 ± 28	36 ± 4

After M_T cut in range shown in plot. Sum of eμ+ee+μμ. Table 9 [1]

Signal strength

Hong

Fit M_T on the prev. pg. to extract μ_{hat}. (p56-62)

	μ_{hat}	stat	expt syst	theo syst
Total	0.99	± 0.21	± 0.17	± 0.12
$N_{Jet} \leq 1$	0.82	± 0.22	± 0.25	
$N_{Jet} \geq 2$	1.4	± 0.5	± 0.4	

Caveat emptor: The table is using 7 & 8 TeV data at M_H = 125.5 GeV combining all the production modes.

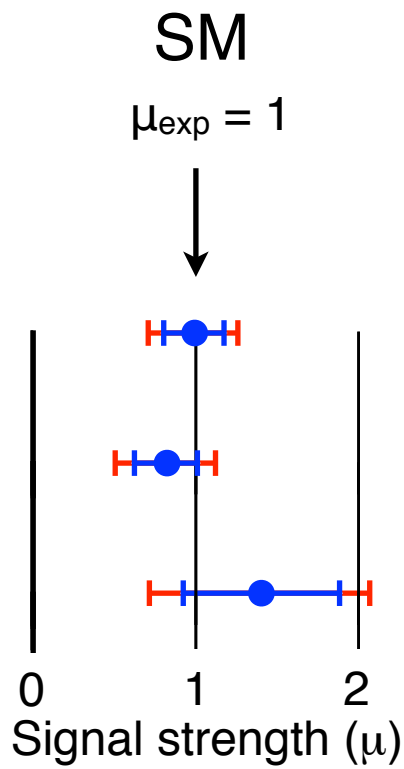

Signal significance for HWW is 3.8σ (3.8σ)
observed expected

Sources of uncertainties

Hong

Largest sources for μ_{hat} (ggF & VBF combined). (p43)

% of μ_{hat}	Source	Category	Key words
30	Total		
21	Statistics		$\sqrt{N_{exp}}$
21	Systematic sources	All	
$^{+12}_{-9}$	Signal yield (σ • BR)	Theory	QCD scale, PDF
12	WW normalization	Theory	Modeling ← Discussed
9	Objects & DY estimation	Experimental	JES, JER, b-tag
8	Signal acceptance	Theory	Jet binning
7	MC statistics	Experimental	-
5	W+jet fake factor	Experimental	Di-jet v. W+jet ← Discussed
5	Backgrounds, excluding WW	Theory	-
4	Integrated luminosity	Luminosity	-

Same size

Signal strength VBF v. ggF

Hong

Scan 2-d contour & VBF/ggF ratio = $2.0 \pm {}^{2.2}_{1.0}$ (p99-102)

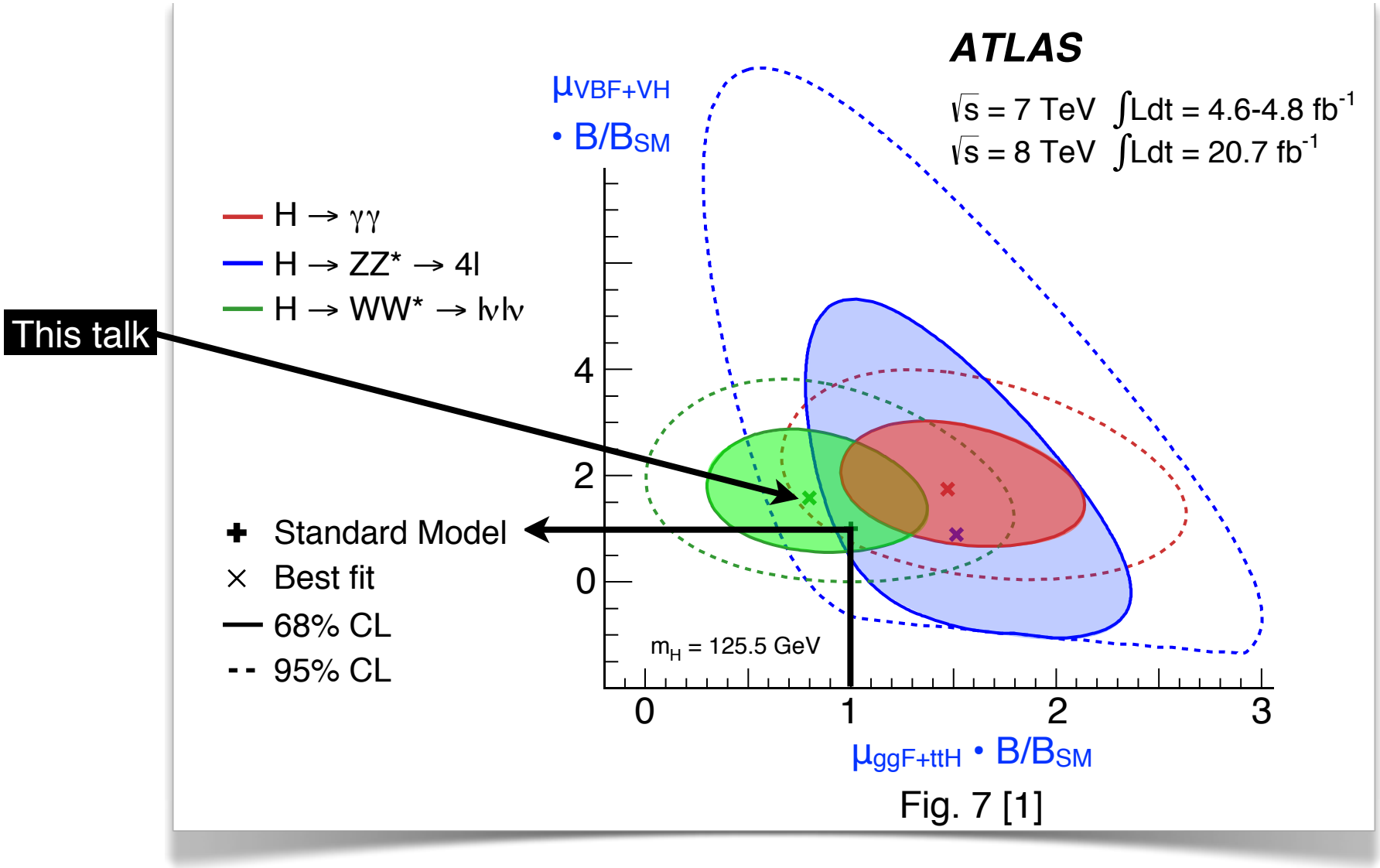

Fig. 7 [1]

Signal significance for VBF HWW is 2.5σ (1.6σ)
observed expected

Conclusions

• Results

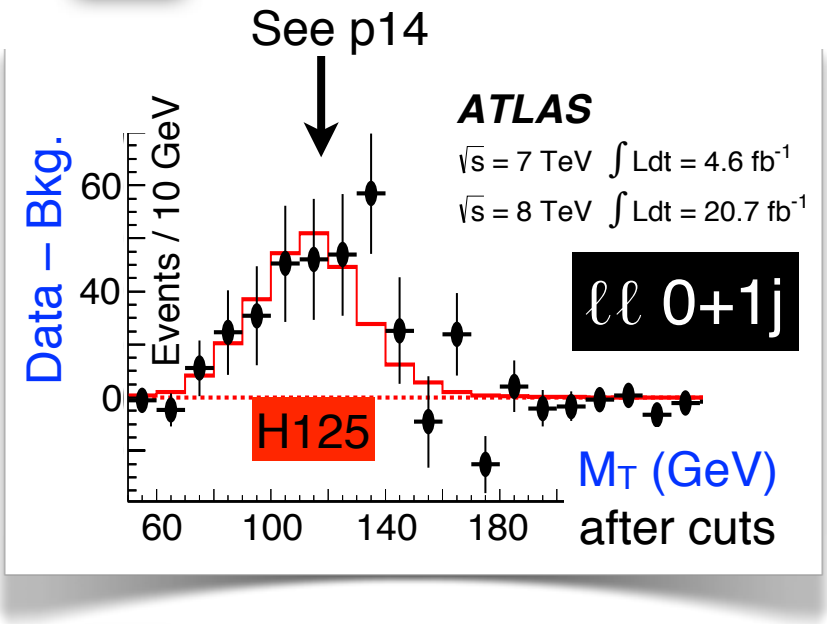

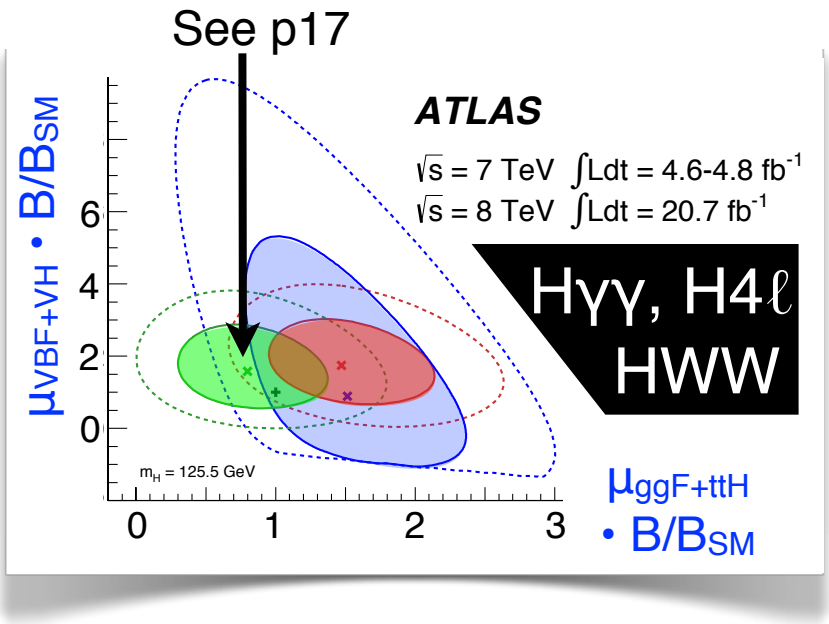

• Outlook (p38)

Expect improved μ_{hat} (ggF driven) with more data & reduced syst. with better understanding (e.g., W+jet)

Expect better μ_{VBF} since stat. limited & small theory err.

Expect more production modes: WH, ZH at 1-2σ

Extra slides

References

Hong

This talk → Details →

Ref.	What	Link
[1]	ATLAS Higgs coupling → PLB, July 2013	https://cern.ch/Atlas/GROUPS/PHYSICS/PAPERS/HIGG-2013–02/
[2]	ATLAS HWW note, March 2013	https://cern.ch/Atlas/GROUPS/PHYSICS/CONFNOTES/ATLAS-CONF-2013–030/
[3]	ATLAS Higgs combination note, Dec. 2012	https://cern.ch/Atlas/GROUPS/PHYSICS/CONFNOTES/ATLAS-CONF-2012–170/
[4]	ATLAS HWW note, Aug. 2011	https://cern.ch/Atlas/GROUPS/PHYSICS/CONFNOTES/ATLAS-CONF-2011–134/
[5]	ATLAS SM WW note, March 2011	https://cern.ch/Atlas/GROUPS/PHYSICS/CONFNOTES/ATLAS-CONF-2011–015/
[6]	ATLAS SM summary webpage, 2013	https://cern.ch/twiki/bin/view/AtlasPublic/CombinedSummaryPlots
[7]	ATLAS luminosity webpage	https://cern.ch/twiki/bin/view/AtlasPublic/LuminosityPublicResults
[8]	LHC cross section webpage	https://cern.ch/twiki/bin/view/LHCPhysics/CrossSections
[9]	ATLAS event display webpage	https://cern.ch/twiki/bin/view/AtlasPublic/EventDisplayStandAlone
[10]	ATLAS HWW 7 TeV paper, June 2012	https://cern.ch/Atlas/GROUPS/PHYSICS/PAPERS/HIGG-2012–04
[11]	ATLAS HWW 5.8 fb^{-1} 8 TeV note, July 2012	https://cern.ch/Atlas/GROUPS/PHYSICS/CONFNOTES/ATLAS-CONF-2012–098/
[12]	ATLAS Higgs spin paper → PLB, July 2013	https://cern.ch/Atlas/GROUPS/PHYSICS/PAPERS/HIGG-2013–01/
[13]	ATLAS HWW spin note, March 2013	https://cern.ch/Atlas/GROUPS/PHYSICS/CONFNOTES/ATLAS-CONF-2013–031/
[14]	ATLAS HWW high mass note, July 2013	https://cern.ch/Atlas/GROUPS/PHYSICS/CONFNOTES/ATLAS-CONF-2013–067/
[15]	ATLAS HWW WH, ZH note, July 2013	https://cern.ch/Atlas/GROUPS/PHYSICS/CONFNOTES/ATLAS-CONF-2013–075/
[16]	ATLAS High lumi. study , Oct. 2012	https://cern.ch/Atlas/GROUPS/PHYSICS/PUBNOTES/ATL-PHYS-PUB-2012–004/
-	ATLAS HWW animation, floating scale	https://cern.ch/twiki/pub/AtlasPublic/HiggsPublicResults//WW-FloatingScale.gif
-	ATLAS HWW animation, fixed scale	https://cern.ch/twiki/pub/AtlasPublic/HiggsPublicResults//WW-FixedScale.gif

eμ + 0 jet in 2010

Run 167576, Event 120642801
Oct. 24, 2010, 13:06:00 EDT [5]

Hong

Higgs like in decay

$\Delta\phi_{\ell\ell}$ = 0.93

MET = 69 GeV

μ P_T = 68 GeV

e P_T = 21 GeV

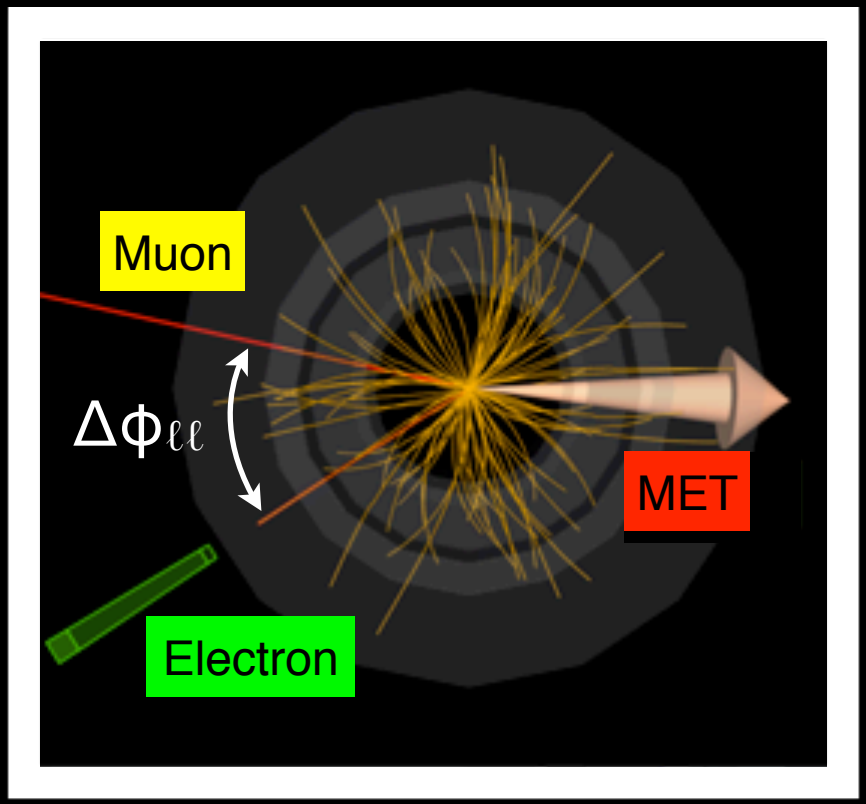

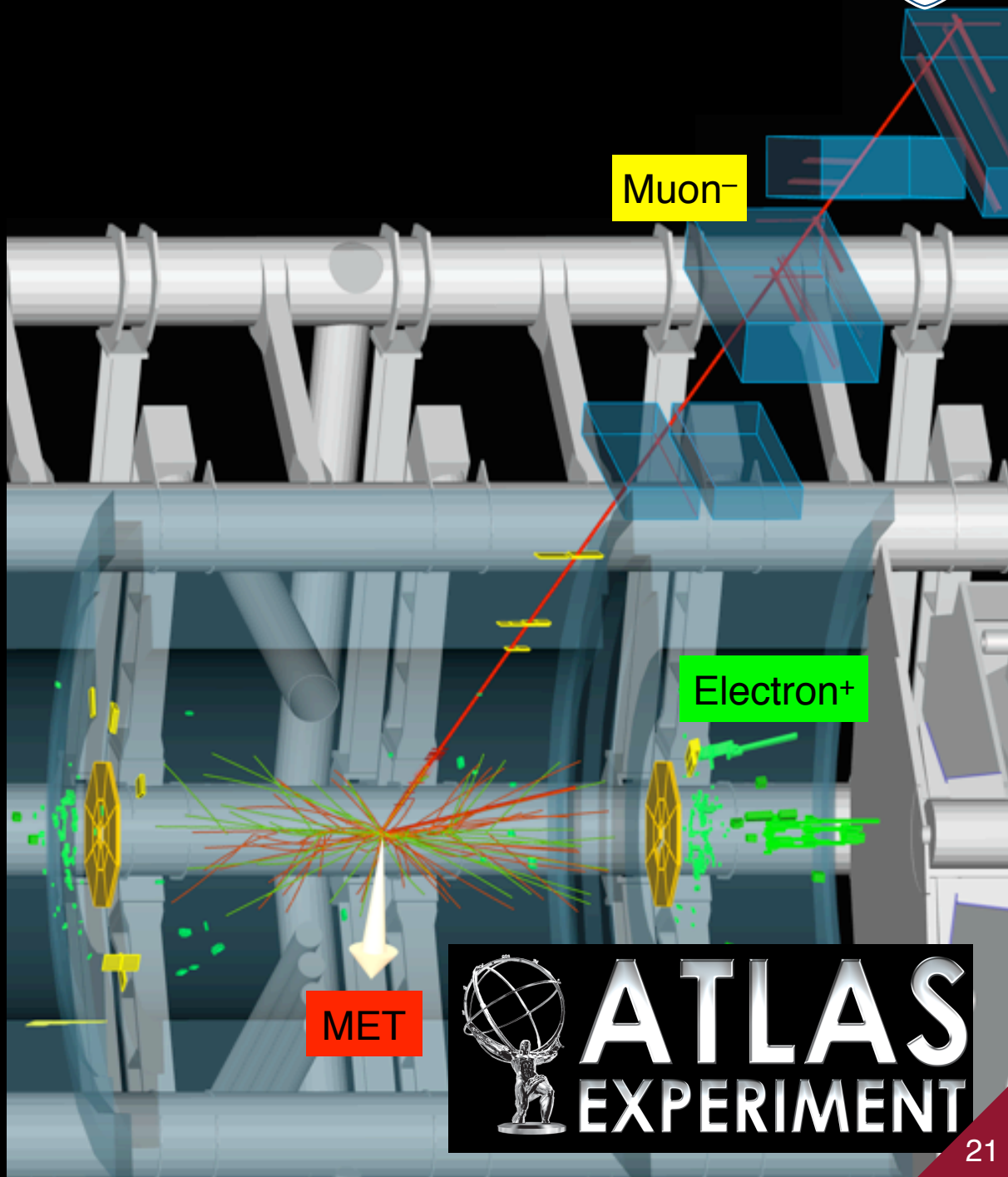

eμ + 0 jet in 2011 passing all cuts [10] Hong

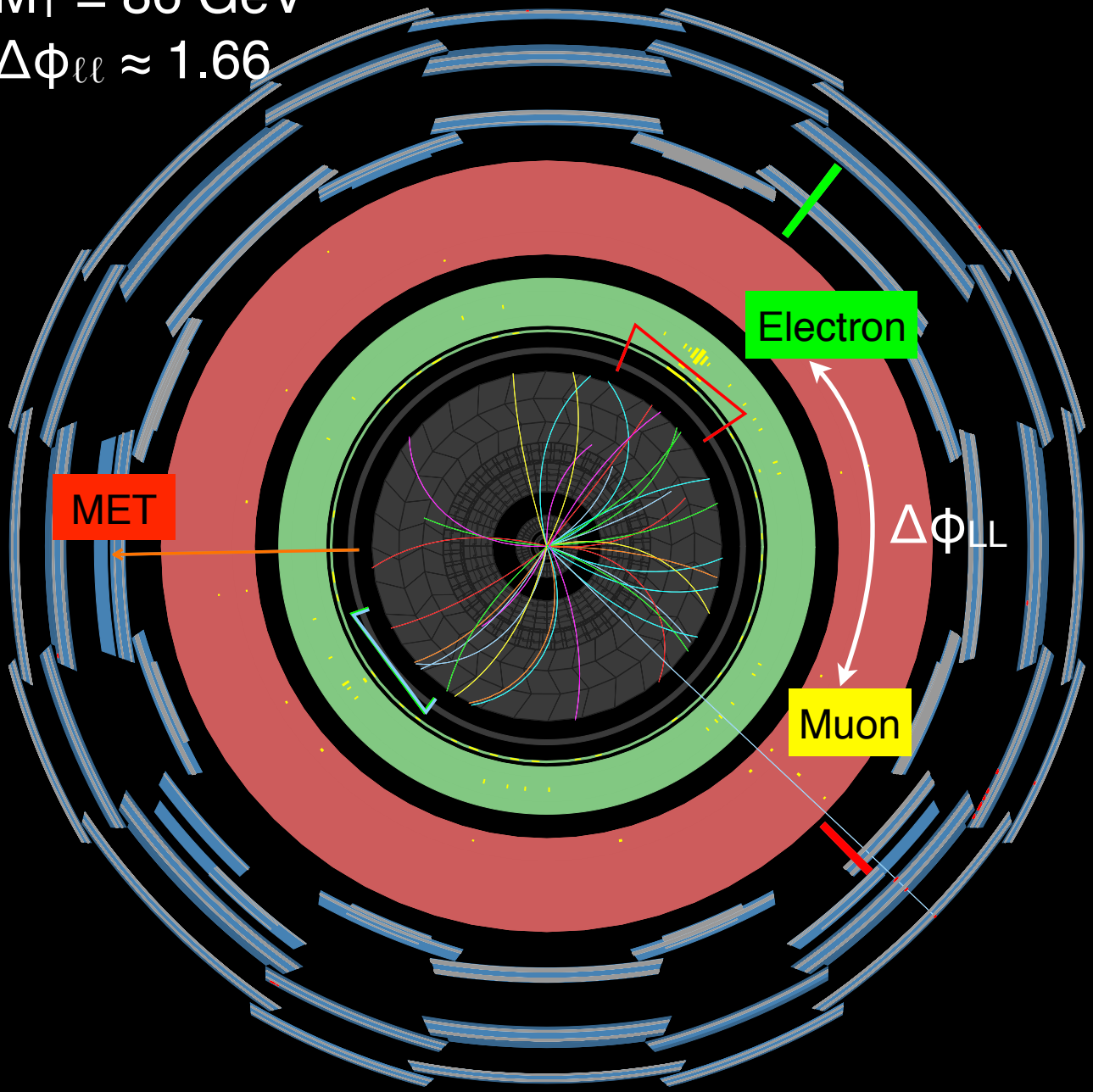

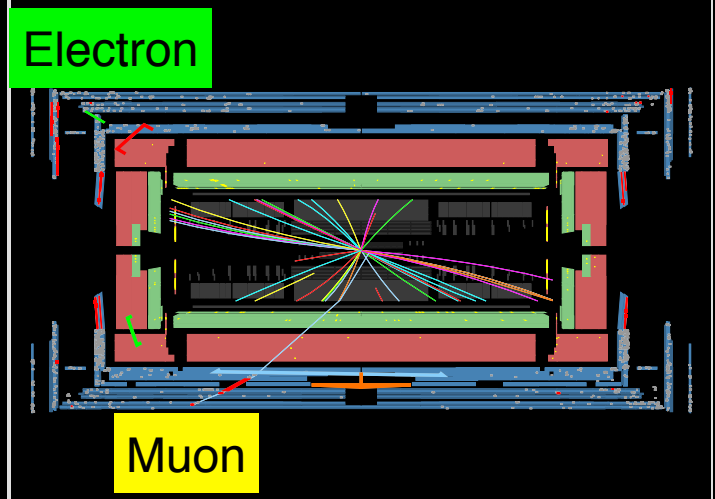

ATLAS EXPERIMENT

Run Number: 189483, Event Number: 90659667

Date: 2011-09-19 10:11:20 CEST

eμ + 0 jet in 2012 passing all cuts [11] Hong

M_T = 94 GeV

$\Delta\phi_{\ell\ell} \approx 0.29$

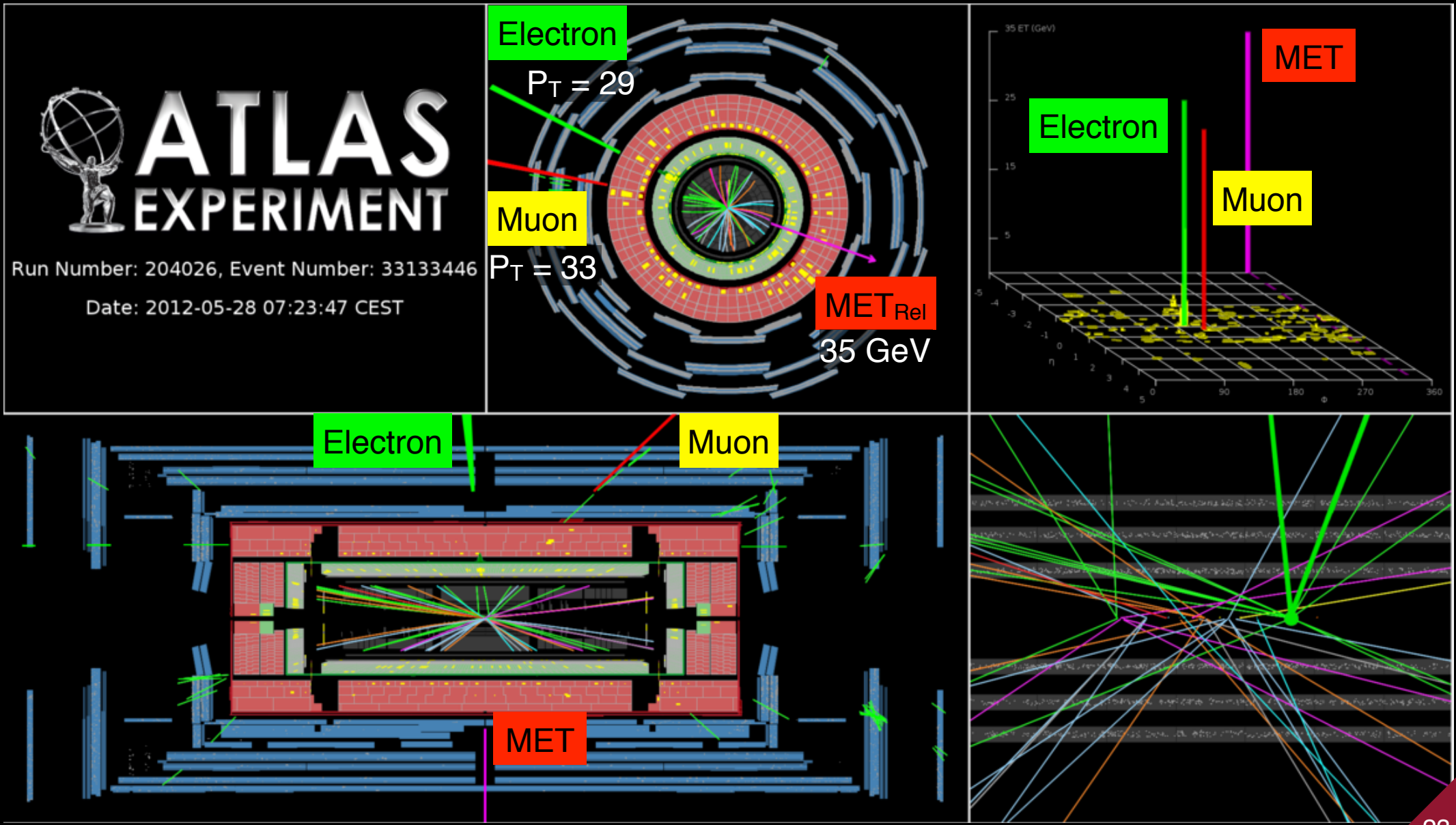

W+jets event (not related to HWW)

Hong

Here is a W→μν + 3 jets (one jet contains a μ) [9]

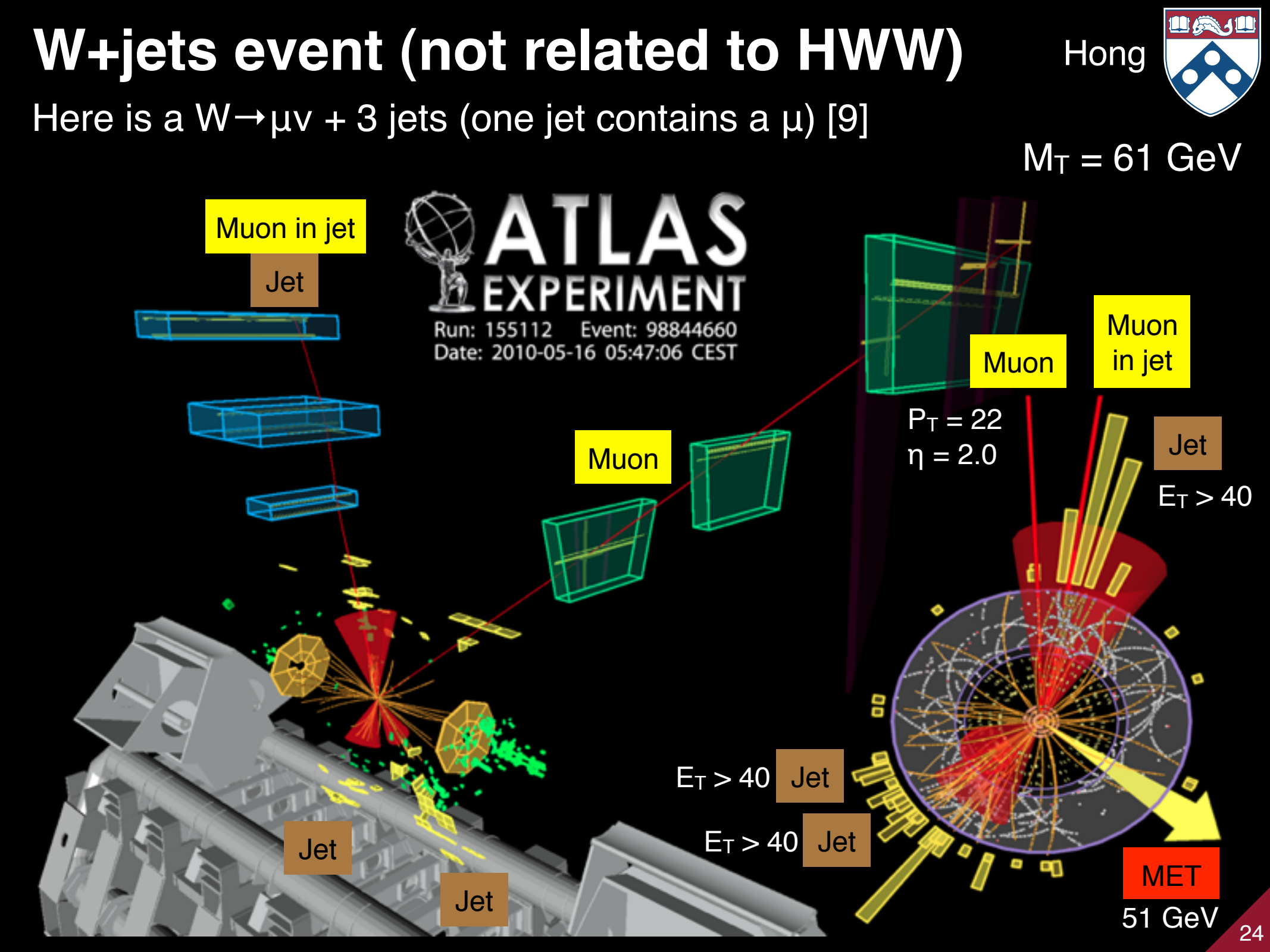

W+jet discussion

Hong

W+jet about 10^3 higher production than SM-WW. Rare, but deadly.

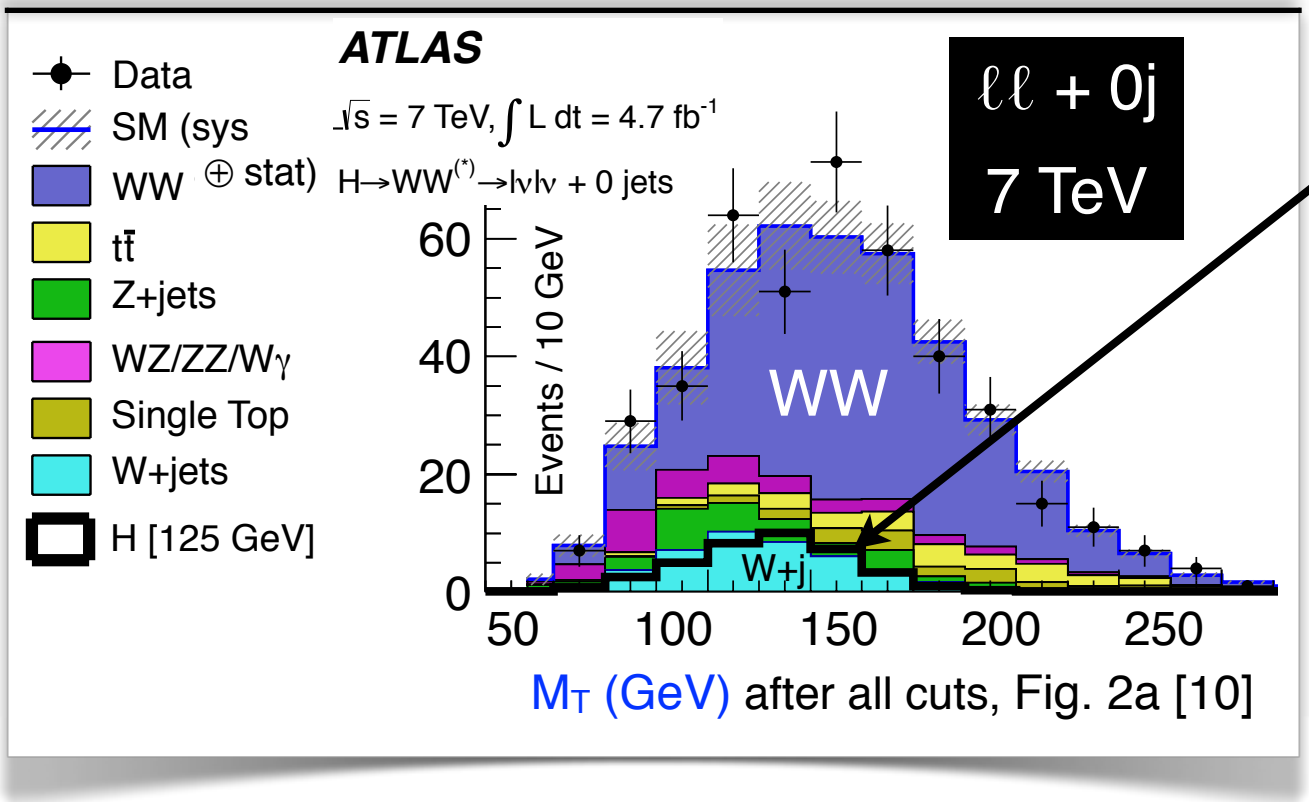

- Cuts sculpt the phase space such that HWW & W+jet magnitudes & shapes are identical.

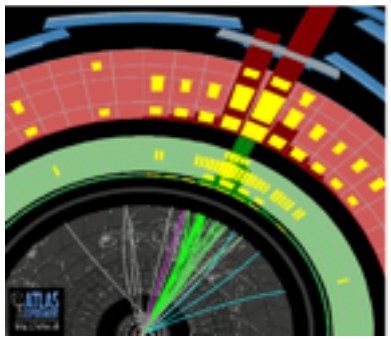

Jet [9]

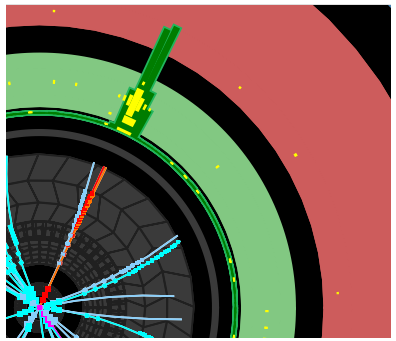

Electron [9]

- Check W+jets & di-jet in MC difference in extrapolation is within 40% → syst.
- $N_{\text{fail ID}}$ means e fails medium++, but passes loose iso & IP cut; μ passes StacoCombined, loose iso & IP cut.

DY rejection in ee & μμ in $N_{Jet} \leq 1$

Hong

Look at soft hadronic recoil opposite $\ell\ell$ (add jet to system for $N_{jet}=1$)

- Compare events with MET like $WW \to \ell\nu\ell\nu$ v. without MET ($Z \to \ell\ell$). See cartoon on right.
- If it passes our MET selection, then it is due to soft hadronic recoil that did not form a jet.
- Use jets $P_T>10$ in ±45° opposite $\ell\ell$ to define

$$f_{\mathrm{Recoil}} = \frac{\left|\sum_j f_{\mathrm{JVF}} \cdot \vec{P}_{T,j}\right|}{\left|\vec{P}_{T,\ell\ell}\right|}$$

- Cut on f_{Recoil} & estimate N_{DY} (see next slide)

$WW \to \ell\nu\ell\nu$ or any non-DY

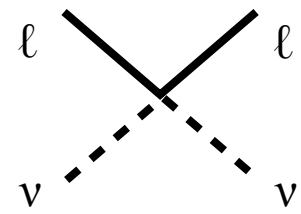

$Z \to \ell\ell$ with soft hadronic recoil

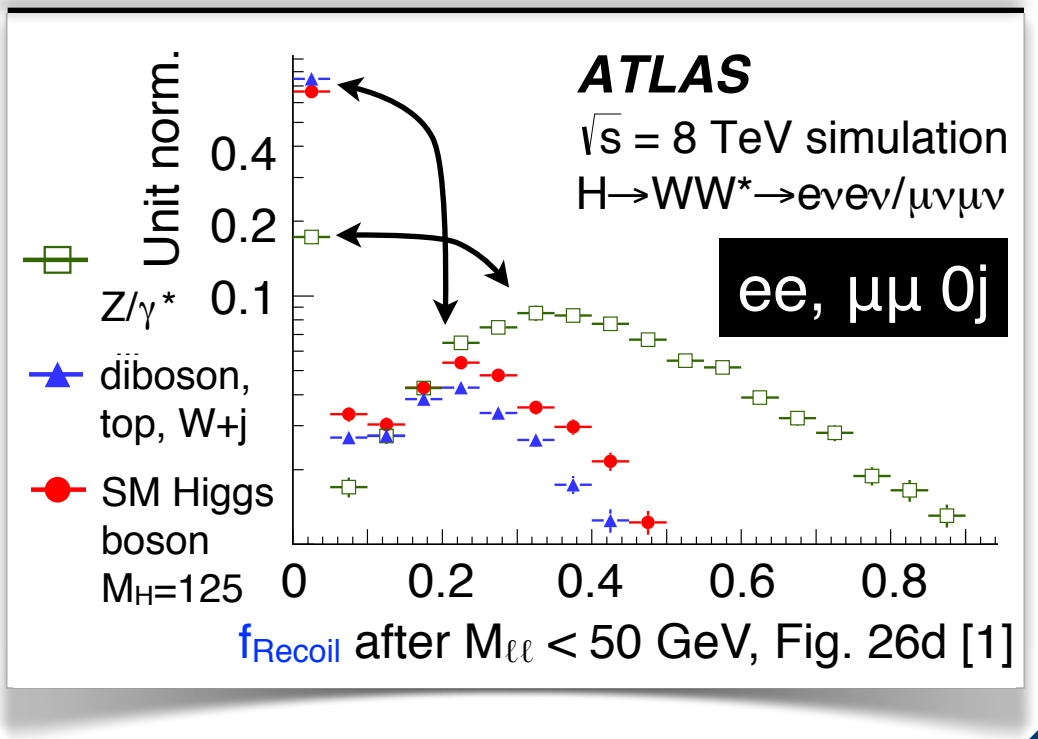

DY algebra

Hong

For $N_{Jet} \leq 1$, N_{DY} is fully data-driven using C.R.s.

- C.R.s are used to determine the non-DY & DY efficiencies in data.

  ε_{DY} = In $Z \rightarrow \ell\ell$ peak with nonDY subtraction

  ε_{nonDY} = In SR eμ w/ $M_{\ell\ell} < 50$ GeV

- Reject DY by a cut on f_{Recoil} (vertical line; see top right).
- Use algebra to find N_{DY} (see right).
- Largest syst. from ε_{DY} (~30%) from low-MET data & low-$M_{\ell\ell}$ DY MC.
- N_{DY} uncertainty ~60% for 0-jet
  ~80% for 1-jet

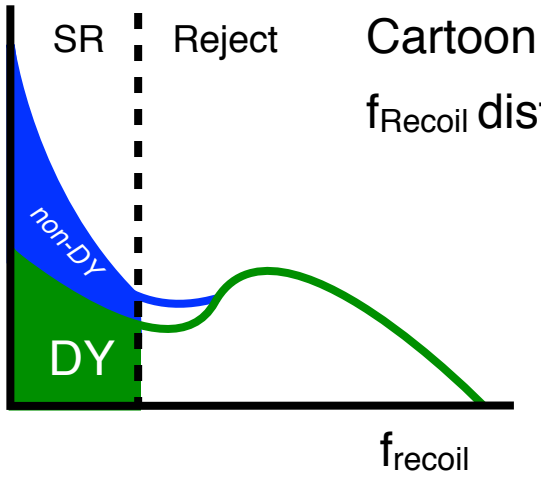

Cartoon of the f_{Recoil} distribution

$$N_{DY} = \frac{N_{data,\ after\ cut} - \left(N_{data,\ no\ cut} \cdot \varepsilon_{nonDY}\right)}{\varepsilon_{DY} - \varepsilon_{nonDY}} \cdot \varepsilon_{DY}$$

DY estimation in VBF

Hong

Use $M_{\ell\ell}$ v. MET plane in data to extrapolate into S.R.

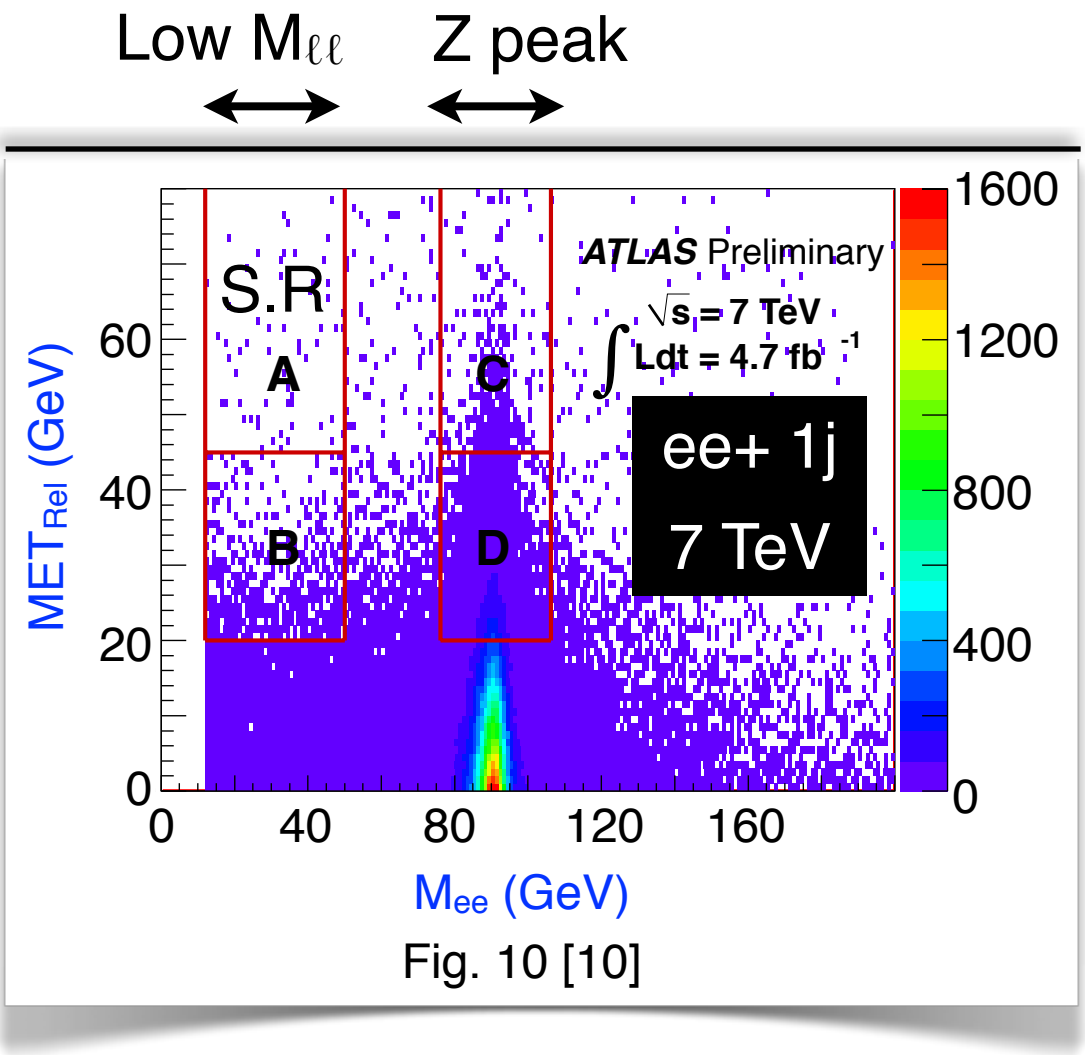

Fig. 10 [10]

Normalization found by using Z peak (w/o VBF cuts)

- $N_{DY} = N_A = N_B \cdot N_C / N_D$
- Shown for 1j to illustrate the method; not used for 1j but for VBF channel
- Apply $M_{\ell\ell}$-MET small correlation in MC $(3 \pm 10)\%_{stat}$

VBF modeling evaluated separately with low MET data

- Uncertainty is 15% on yield

ttbar background in VBF

Hong

If extrapolation is dependable, then normalization doesn't matter

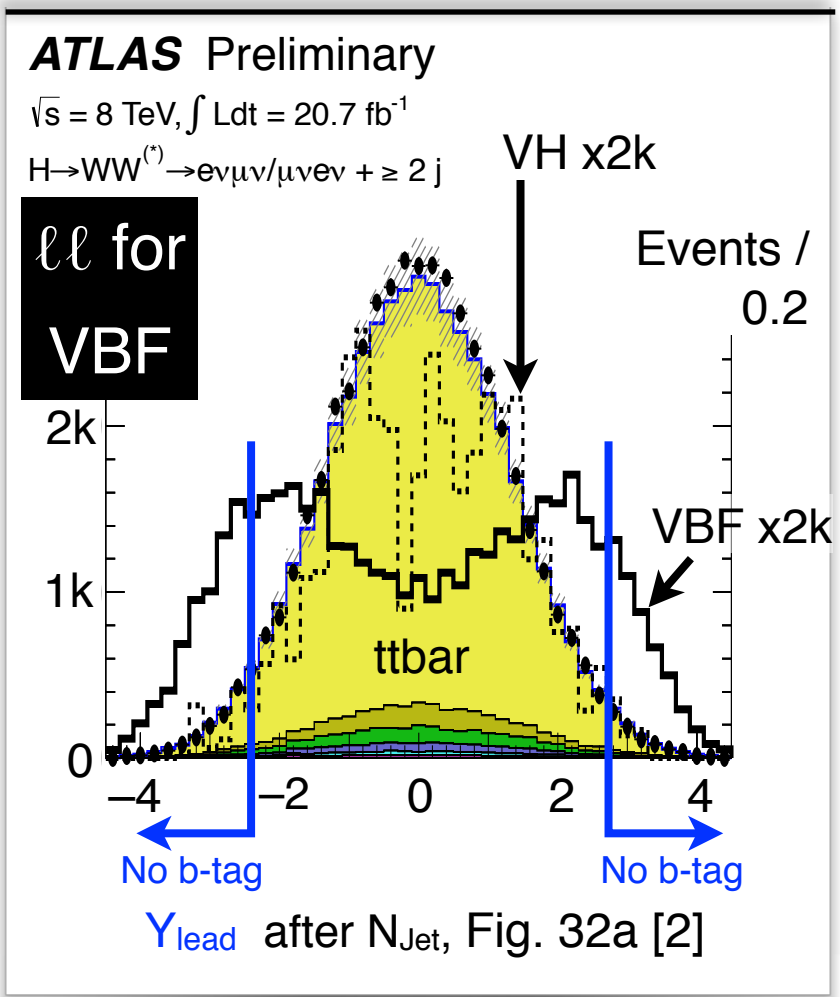

C.R. requires $N_{b\text{-tag}} = 1$

- S.R. with ≥ 1 forward jet ($\Delta Y_{JJ} > 2.8$)
- Cannot b-tag outside tracking vol.
- Limited modeling for ISR / FSR

ttbar using MC@NLO

- Difficult to model high M_{JJ}; check that the syst. covers extrapolation
- Good modeling for $\ell\ell$ etc., so M_T fine

$$N_{\text{top}}^{\text{SR, est.}} = N_{\text{top}}^{\text{SR, MC}} \cdot \underbrace{\frac{N_{\text{data}}^{\text{CR}} - N_{\text{other}}^{\text{CR}}}{N_{\text{top}}^{\text{CR, MC}}}}_{\text{NF}_{\text{top}}} = \underbrace{\frac{N_{\text{top}}^{\text{SR, MC}}}{N_{\text{top}}^{\text{CR, MC}}}}_{\text{CR to SR extrap'n}} \cdot \left(N_{\text{data}}^{\text{CR}} - N_{\text{other}}^{\text{CR}}\right)$$

= 0.59 ± 0.07 (stat) = 15% systematic v. multi-leg generators

Higgs spin

Hong

For details, see “Higgs spin & couplings in ATLAS,” T. Doyle

- Follow HWW cuts for eμ 0j w/ loosened cuts on MET_{Rel}, M_T, $P_{T,\ell\ell}$, $M_{\ell\ell}$, $\Delta\phi_{\ell\ell}$
- Train separate BDT on the latter 4 variables for $J=0^+$, 1^+, 1^-, 2^+ bosons
- Study test statistic of $J=0^+$ v. others

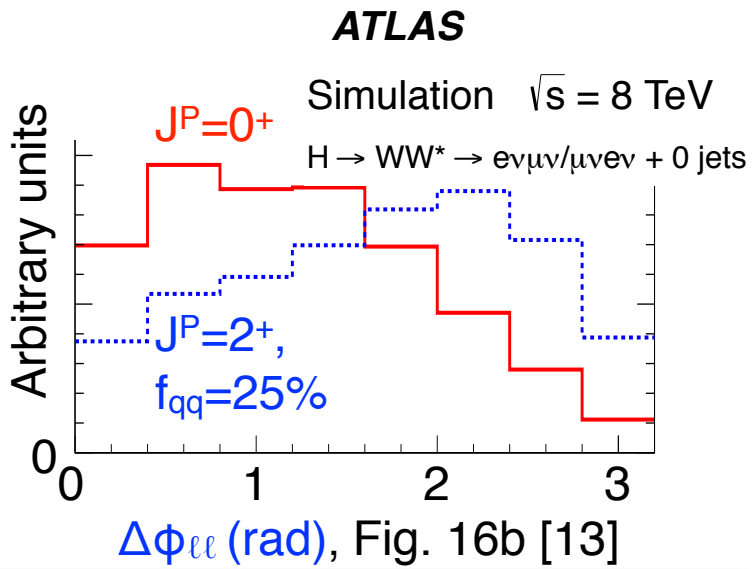

Exclusion limits

- 1^+ at 92% C.L.
- 1^- at 98% C.L.
- 2^+ at 95 - 99% C.L.
  gg qq production

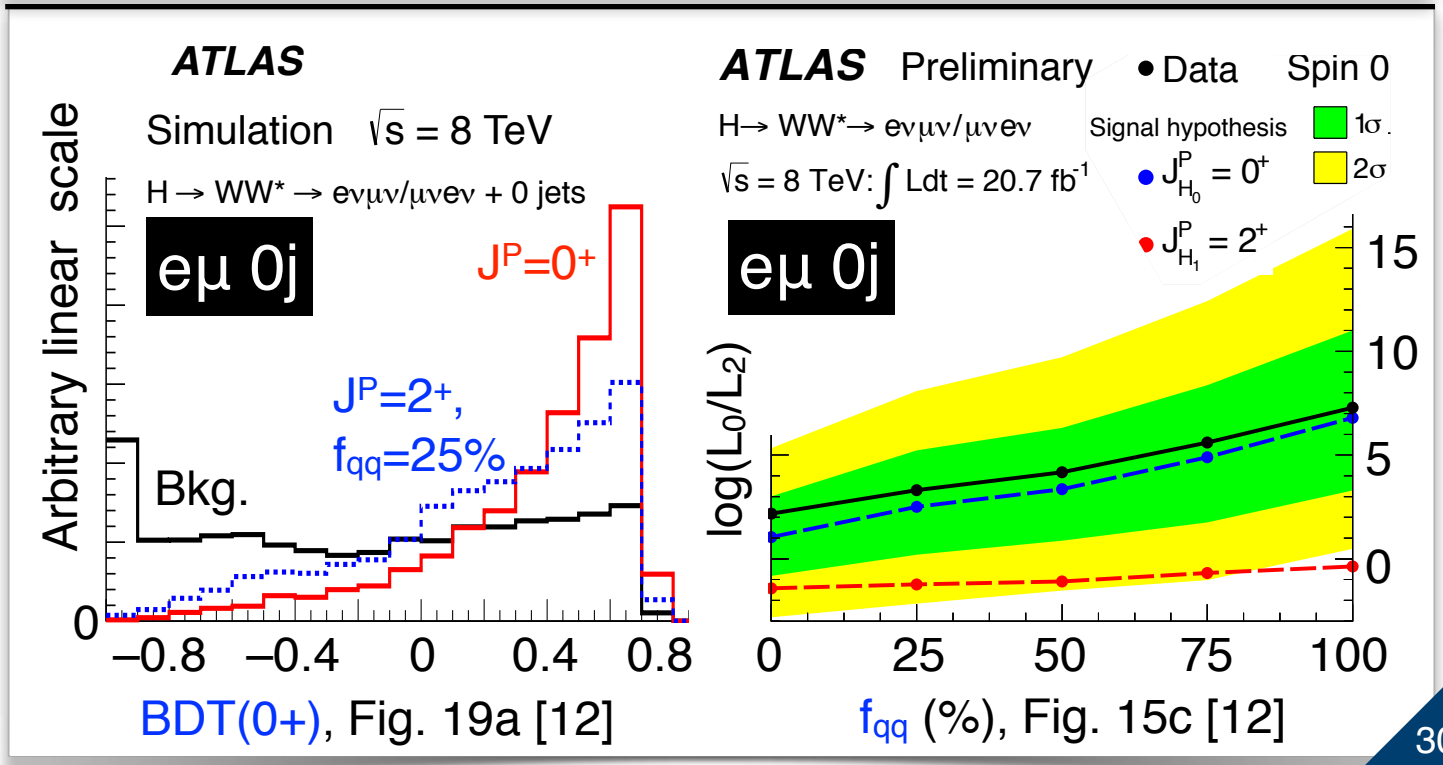

High M_H searches

Hong

For high M_H, see "LHC high mass WW & ZZ," J. Wang

Analysis

- HWW cuts w/ mods for 260< M_H <1000

M_H (GeV)	σ_{ggF} (fb)	σ_{VBF} (fb)
300	262	32
600	31	6

Higgs decay width

- M_H < 400 GeV Breit-Wigner lineshape
- M_H ≥ 400 GeV Complex pole scheme
- Also Narrow Width Approx. Γ = 1 GeV

Limits

- SM excludes 260 < M_H < 642 GeV
- NWA excludes 300 < M_H < 1000 GeV
- 95% CL upper limit set on σ • BR (fb)

95% CL UL on σ • BR (fb)

Prod-uction	Width	M_H = 300	= 600	= 1000
ggF	SM	250	34	19
ggF	NWA	230	32	29
VBF	SM	40	16	10
VBF	NWA	39	12	10

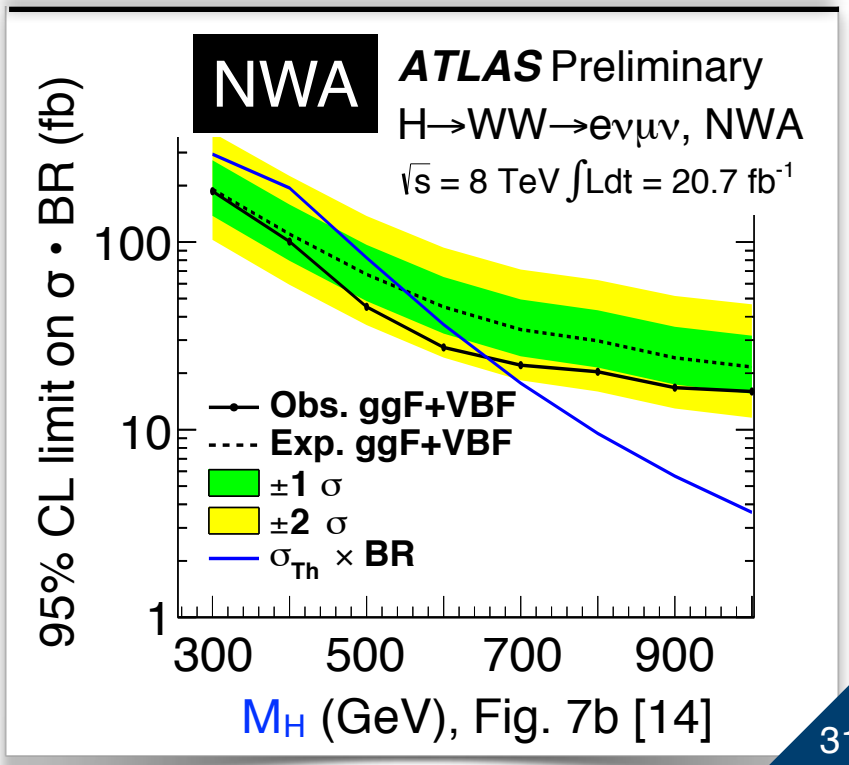

WH, ZH production in 3ℓ & 4ℓ

Hong

New preliminary result in July 2013 [15]

Analysis has leptons with MET

- Divide into # of same-flavor opposite-sign (SFOS) lepton combinations
- C.R. normalization of backgrounds

Composition of C.R. for 3ℓ

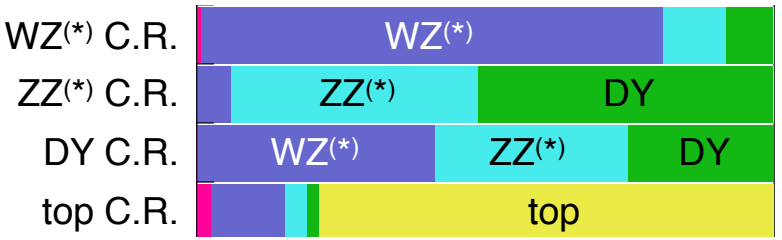

Fig. 7 [15]

Yields for 3ℓ & 4ℓ

SFOS	All SF
0	-
1	No
1	Yes
2	-

Data	Bkg	WH
9	2.7	0.9
16	12	1.0
8	14	0.4
-	-	-

Data	Bkg	ZH
-	-	-
-	-	-
2	0.3	0.2
0	0.8	0.2

Signal significance

	VH	HWW [2]	Combined
Expected	0.7σ	3.7σ	3.8σ
Observed	2.0σ	3.8σ	4.0σ

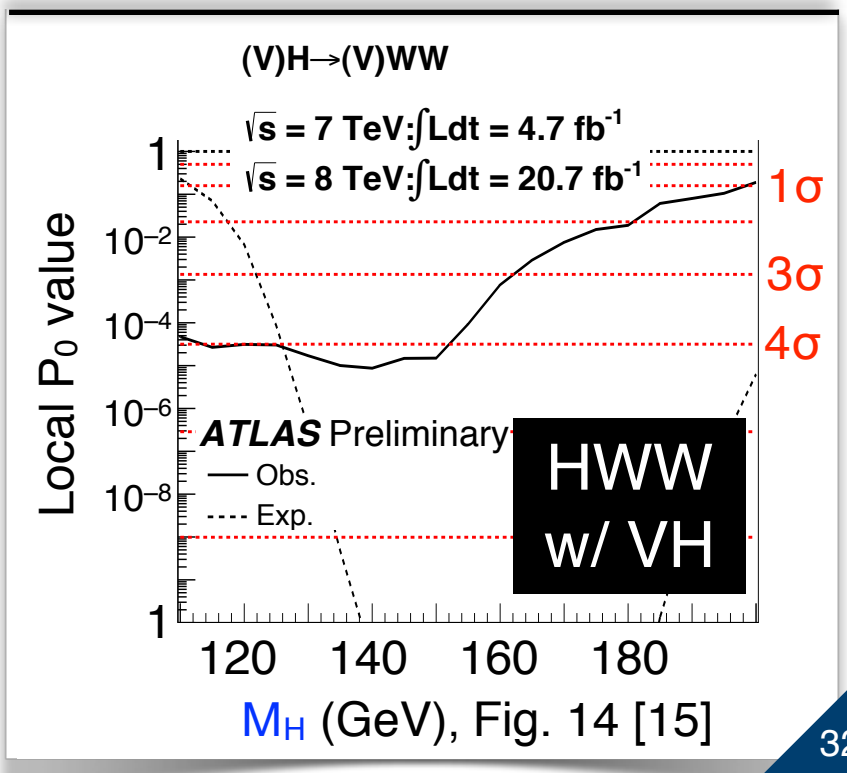

ATLAS data

Hong

22 fb^{-1} of data at ~7•10^{33} peak luminosity with higher pile-up.

Integrated luminosity [7]

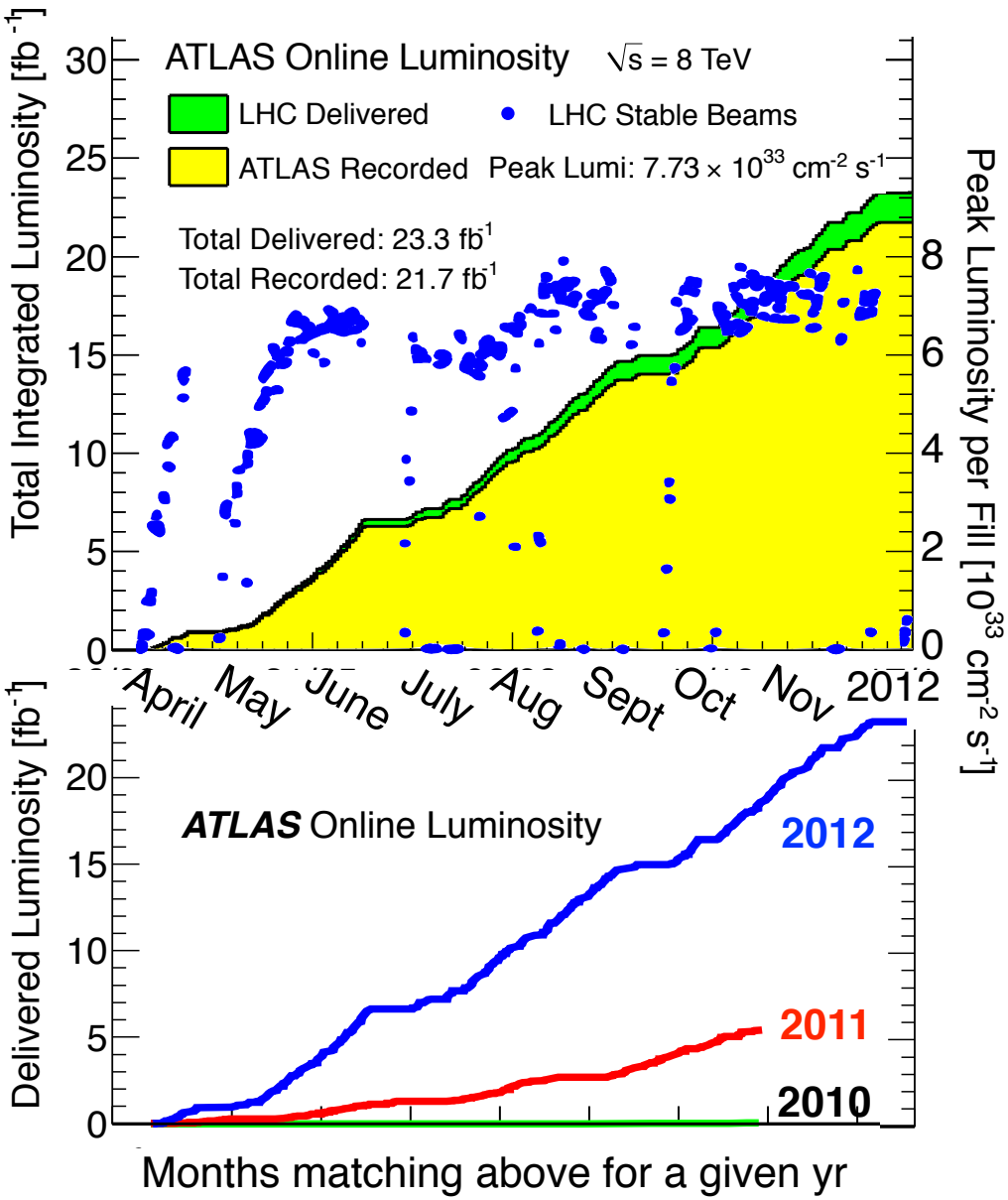

Pile-up [7]

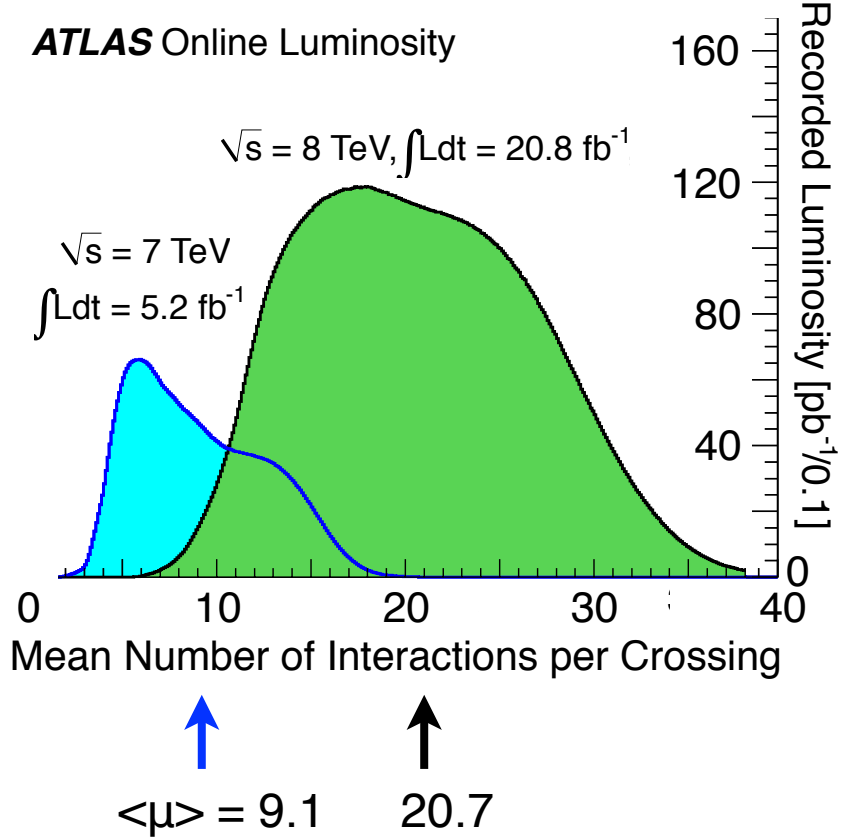

ATLAS detector

Hong

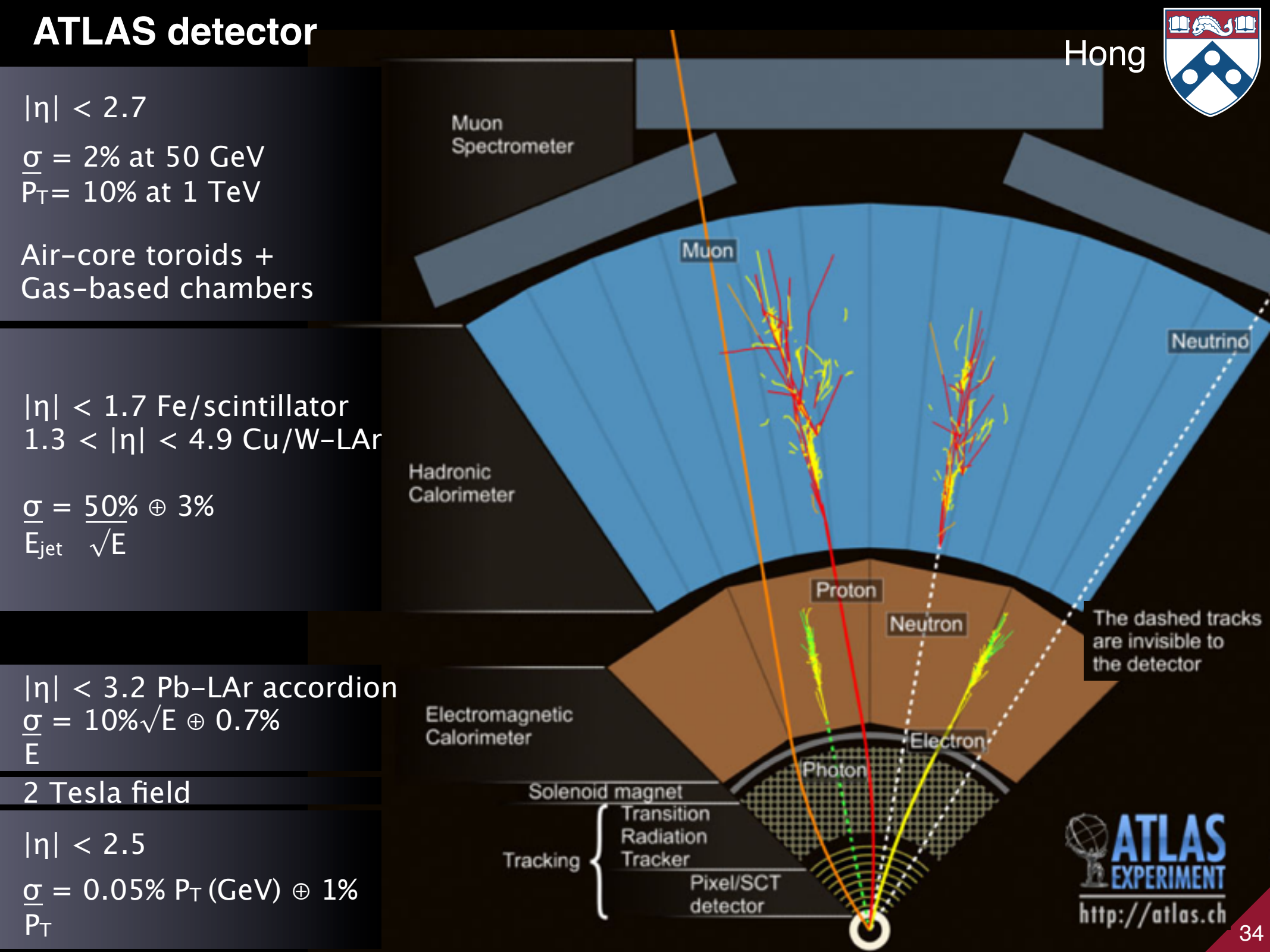

$|\eta| < 2.7$

$\frac{\sigma}{P_T} = 2\%$ at 50 GeV
$\frac{\sigma}{P_T} = 10\%$ at 1 TeV

Air-core toroids +
Gas-based chambers

$|\eta| < 1.7$ Fe/scintillator
$1.3 < |\eta| < 4.9$ Cu/W-LAr

$\frac{\sigma}{E_{jet}} = \frac{50\%}{\sqrt{E}} \oplus 3\%$

$|\eta| < 3.2$ Pb-LAr accordion
$\frac{\sigma}{E} = 10\%\sqrt{E} \oplus 0.7\%$

2 Tesla field

$|\eta| < 2.5$

$\frac{\sigma}{P_T} = 0.05\% P_T\,(\text{GeV}) \oplus 1\%$

Higgs cross sections

Hong

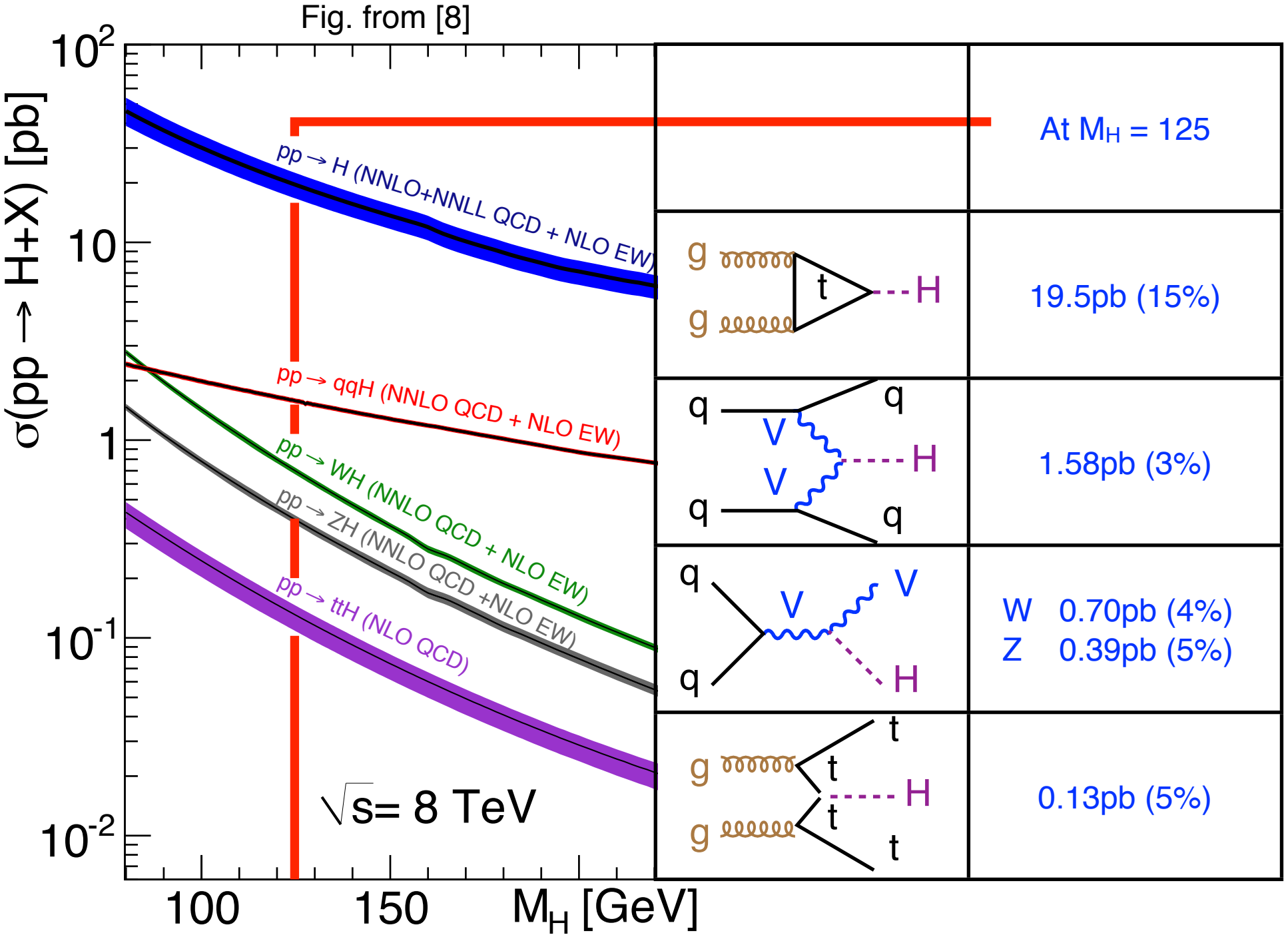

Final selection

Hong

After MET cuts; see Back-up Tables

Motivation	$N_{Jet} = 0$	$N_{Jet} = 1$	$N_{Jet} \geq 2$
Remove top	$N_{Bjet} = 0$		
No potential pathological evts	$\Delta\phi_{\ell\ell,MET} > \pi / 2$		-
Remove DY	$P_{T,\ell\ell} > 30$ GeV	$Z \rightarrow \tau\tau$ veto	$Z \rightarrow \tau\tau$ veto
Higgs decay J=0, W→lν	$M_{\ell\ell} < 50$ GeV		$M_{\ell\ell} < 60$ GeV
	$MET_{Trk,Rel,Cl} > 45$ GeV		
	$\Delta\phi_{\ell\ell} < 1.8$		
	$f_{Recoil} < 0.05$	$f_{Recoil} < 0.2$	
	Split $M_{\ell\ell}$ at 30 for eμ bin in M_T		bin in M_T

VBF topology

$M_{JJ} > 500$ GeV

$\Delta Y_{JJ} > 2.8$

No central jets

No lep outside fwd jets' η-vol

ee+μμ cuts

Object selection

Hong

Leptons

- Single lepton trig. $P_T > 24$ GeV
- Leading lepton $P_T > 25$ GeV
- Sub-leading lepton $P_T > 15$ GeV
- Electrons $|\eta| < 2.47$ (excl. barrel-endcap gap)
- Muons $|\eta| < 2.5$
- Tracks Isolation & impact parameter cuts

Jets

- Jets Anti-K_T R = 0.4 (see p5)
- Central jets in VBF Same as jets, but with $P_T > 20$
- B-jet tagging Neural Network at 85% eff. operating point

MET

- MET = E_T^{miss} Calorimeter-based
- MET_{STVF} Calo; weight the unassociated clusters by f_{JVF}
- $MET_{Trk} = P_T^{miss}$ Track-based

Outlook

- ggF HWW measurement starting to be dominated by systematics. Improve bkg. syst., e.g., W+jet. Expect improvements with more data and better understanding.
- VBF HWW precision at 50%; is limited by statistics. Theory is 3% for VBF v. 10% ggF. Tree-level relation to κ_W. Expect large improvements with more data.
- Rarer productions still to be seen. WH, ZH at 1-2σ now (see p36).

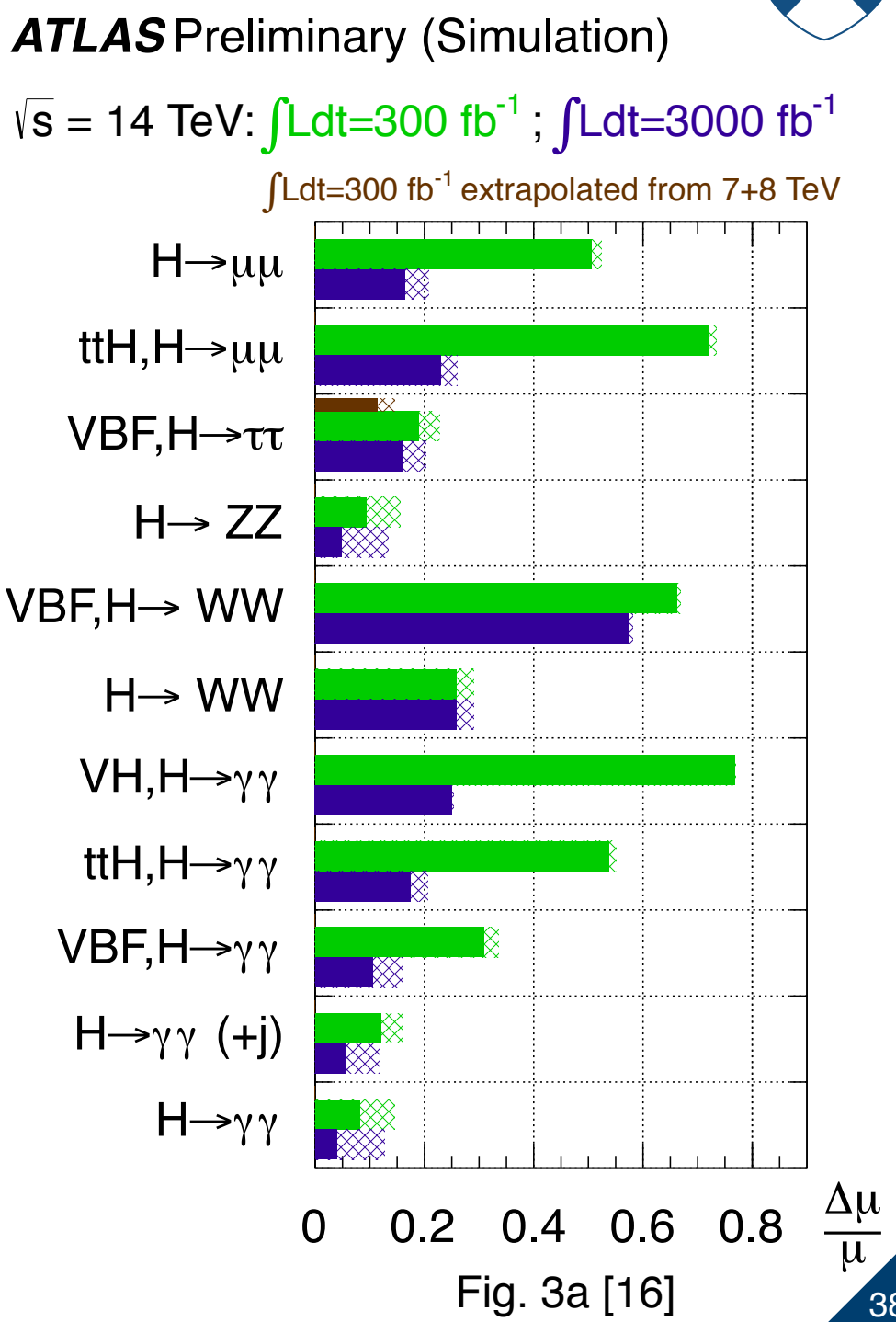

Fig. 3a [16]

Acknowledgements

Thanks to ATLAS & LHC for excellent operations. I'd also like to acknowledge colleagues who helped me prepare this talk:

Doug Schaefer (Penn)

Brig Williams (Penn)

Keisuke Yoshihara (Tokyo)

Philip Chang (Illinois)

Olivier Arnaez (Mainz)

Joana Machado Miguens (Lisbon)

Lashkar Kashif (Wisconsin)

Tatjana Lenz (NIKHEF)

Domizia Orestano (Rome 3)

Takashi Kubota (Melbourne)

Tom LeCompte (Argonne)

More tables from [1, 2]

- p41 - 50

List of MC generators [2]

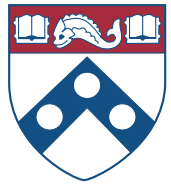

Table 1: Monte Carlo generators used to model the signal and background processes in which all of the W and Z decay channels are included in the corresponding product of the cross section (σ) and branching fraction ($\mathcal{B}$) at $\sqrt{s} = 8$ TeV. Masses are given in units of GeV. Details are given in the text.

Signal	MC generator	$\sigma \cdot \mathcal{B}$ (pb)
ggF	POWHEG [30]+PYTHIA8 [31]	0.44
VBF	POWHEG+PYTHIA8	0.035
VH	PYTHIA8	0.13

Background	MC generator	$\sigma \cdot \mathcal{B}$ (pb)
$q\bar{q}, gq \to WW$	POWHEG+PYTHIA6 [32]	5.7
$q\bar{q}, gq \to WW+2j$	Sherpa [33] with no $\mathcal{O}(\alpha_s)$ terms	0.039
$gg \to WW$	GG2WW 3.1.2 [34, 35]+HERWIG [36]	0.16
$t\bar{t}$	MC@NLO [37]+HERWIG	240
Single top: tW, tb	MC@NLO+HERWIG	28
Single top: tqb	AcerMC [38]+PYTHIA6	88
Z/γ^*, inclusive	ALPGEN+HERWIG	16000
$Z^{(*)} \to \ell\ell + 2j$	Sherpa processes up to $\mathcal{O}(\alpha_s)$	1.2
$Z^{(*)}Z^{(*)} \to 4\ell$	POWHEG+PYTHIA8	0.73
$WZ/W\gamma^*, m_{Z/\gamma^*}>7$	POWHEG+PYTHIA8	0.83
$W\gamma^*, m_{\gamma^*} \leq 7$	MadGraph [39–41]+PYTHIA6	11
$W\gamma$	ALPGEN+HERWIG	370

List of cuts [2]

Table 2: Selection listing for 8 TeV data. The criteria specific to $e\mu + \mu e$ and $ee + \mu\mu$ are noted as such; otherwise, they apply to both. Pre-selection applies to all N_{jet} modes. The rapidity gap is the y range spanned by the two leading jets. The $m_{\ell\ell}$ split is at 30 GeV. The modifications for the 7 TeV analysis are given in Section 6 and are not listed here. Energies, masses, and momenta are in units of GeV.

Category	$N_{\text{jet}} = 0$	$N_{\text{jet}} = 1$	$N_{\text{jet}} \geq 2$
Pre-selection	Two isolated leptons ($\ell = e, \mu$) with opposite charge Leptons with $p_{\text{T}}^{\text{lead}} > 25$ and $p_{\text{T}}^{\text{sublead}} > 15$ $e\mu + \mu e$: $m_{\ell\ell} > 10$ $ee + \mu\mu$: $m_{\ell\ell} > 12$, $\lvert m_{\ell\ell} - m_Z \rvert > 15$		
Missing transverse momentum and hadronic recoil	$e\mu + \mu e$: $E_{\text{T,rel}}^{\text{miss}} > 25$ $ee + \mu\mu$: $E_{\text{T,rel}}^{\text{miss}} > 45$ $ee + \mu\mu$: $p_{\text{T,rel}}^{\text{miss}} > 45$ $ee + \mu\mu$: $f_{\text{recoil}} < 0.05$	$e\mu + \mu e$: $E_{\text{T,rel}}^{\text{miss}} > 25$ $ee + \mu\mu$: $E_{\text{T,rel}}^{\text{miss}} > 45$ $ee + \mu\mu$: $p_{\text{T,rel}}^{\text{miss}} > 45$ $ee + \mu\mu$: $f_{\text{recoil}} < 0.2$	$e\mu + \mu e$: $E_{\text{T}}^{\text{miss}} > 20$ $ee + \mu\mu$: $E_{\text{T}}^{\text{miss}} > 45$ $ee + \mu\mu$: $E_{\text{T,STVF}}^{\text{miss}} > 35$ -
General selection	- $\lvert \Delta\phi_{\ell\ell,MET} \rvert > \pi/2$ $p_{\text{T}}^{\ell\ell} > 30$	$N_{b\text{-jet}} = 0$ - $e\mu + \mu e$: $Z/\gamma^* \to \tau\tau$ veto	$N_{b\text{-jet}} = 0$ $p_{\text{T}}^{\text{tot}} < 45$ $e\mu + \mu e$: $Z/\gamma^* \to \tau\tau$ veto
VBF topology	- - - -	- - - -	$m_{jj} > 500$ $\lvert \Delta y_{jj} \rvert > 2.8$ No jets ($p_{\text{T}} > 20$) in rapidity gap Require both ℓ in rapidity gap
$H \to WW^{(*)} \to \ell\nu\ell\nu$ topology	$m_{\ell\ell} < 50$ $\lvert \Delta\phi_{\ell\ell} \rvert < 1.8$ $e\mu + \mu e$: split $m_{\ell\ell}$ Fit m_{T}	$m_{\ell\ell} < 50$ $\lvert \Delta\phi_{\ell\ell} \rvert < 1.8$ $e\mu + \mu e$: split $m_{\ell\ell}$ Fit m_{T}	$m_{\ell\ell} < 60$ $\lvert \Delta\phi_{\ell\ell} \rvert < 1.8$ - Fit m_{T}

Summary of systematics & yield [2]

Hong

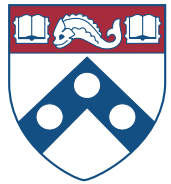

Table 8: For $m_H = 125$ GeV, the leading systematic uncertainties for the 8 TeV $H \to WW^* \to \ell\nu\ell\nu$ analysis. All numbers are summed over lepton flavours. Sources contributing less than 4% are omitted, and individual entries below 1% are indicated with a '-'. Relative signs indicate correlation and anticorrelation (migration) between the N_{jet} categories represented by adjacent columns, and a ± indicates an uncorrelated uncertainty. The exception is the jet energy scale and resolution, which includes multiple sources of uncertainty treated as correlated across categories but uncorrelated with each other. All rows are uncorrelated.

Source	$N_{\text{jet}} = 0$	$N_{\text{jet}} = 1$	$N_{\text{jet}} \geq 2$
Theoretical uncertainties on total signal yield (%)			
QCD scale for ggF, $N_{\text{jet}} \geq 0$	+13	-	-
QCD scale for ggF, $N_{\text{jet}} \geq 1$	+10	−27	-
QCD scale for ggF, $N_{\text{jet}} \geq 2$	-	−15	+4
QCD scale for ggF, $N_{\text{jet}} \geq 3$	-	-	+4
Parton shower and underlying event	+3	−10	±5
QCD scale (acceptance)	+4	+4	±3
Experimental uncertainties on total signal yield (%)			
Jet energy scale and resolution	5	2	6
Uncertainties on total background yield (%)			
WW transfer factors (theory)	±1	±2	±4
Jet energy scale and resolution	2	3	7
b-tagging efficiency	-	+7	+2
f_{recoil} efficiency	±4	±2	-

Table 9: For the $H \to WW^* \to \ell\nu\ell\nu$ analysis of the 8 TeV data, the numbers of events observed in the data and expected from signal ($m_H = 125.5$ GeV) and backgrounds inside the transverse mass regions $0.75\,m_H < m_{\text{T}} < m_H$ for $N_{\text{jet}} \leq 1$ and $m_{\text{T}} < 1.2\,m_H$ for $N_{\text{jet}} \geq 2$. All lepton flavours are combined. The total background as well as its main components are shown. The quoted uncertainties include the statistical and systematic contributions, and account for anticorrelations between the background predictions.

	$N_{\text{jet}} = 0$	$N_{\text{jet}} = 1$	$N_{\text{jet}} \geq 2$
Observed	831	309	55
Signal	100 ± 21	41 ± 14	10.9 ± 1.4
Total background	739 ± 39	261 ± 28	36 ± 4
WW	551 ± 41	108 ± 40	4.1 ± 1.5
Other VV	58 ± 8	27 ± 6	1.9 ± 0.4
Top-quark	39 ± 5	95 ± 28	5.4 ± 2.1
Z+jets	30 ± 10	12 ± 6	22 ± 3
W+jets	61 ± 21	20 ± 5	0.7 ± 0.2

Summary of bkg. treatment [2]

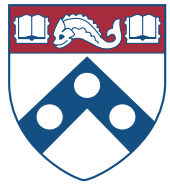

Table 3: Background treatment listing. The estimation procedures for various background processes are given in four categories: normalised using a control region (CR); data-derived estimate (Data); normalised using the MC (MC); and normalised using the MC, but validated in a control region (MC + VR). The "$(e\mu + \mu e)$" terms denote that for the $ee + \mu\mu$ channel in the same N_{jet} mode, the $e\mu + \mu e$ region is used instead, for reasons of purity and/or statistics. The "(merged)" terms indicate that the fully combined $e\mu + \mu e + ee + \mu\mu$ control region is used for all channels.

Channel	WW	Top	$Z/\gamma^* \to \tau\tau$	$Z/\gamma^* \to \ell\ell$	W+jets	VV
$N_{\text{jet}} = 0$						
$e\mu + \mu e$	CR	CR	CR	MC	Data	MC + VR
$ee + \mu\mu$	CR $(e\mu + \mu e)$	CR $(e\mu + \mu e)$	CR $(e\mu + \mu e)$	Data	Data	MC + VR
$N_{\text{jet}} = 1$						
$e\mu + \mu e$	CR	CR	CR	MC	Data	MC + VR
$ee + \mu\mu$	CR $(e\mu + \mu e)$	CR $(e\mu + \mu e)$	CR $(e\mu + \mu e)$	Data	Data	MC + VR
$N_{\text{jet}} \geq 2$						
$e\mu + \mu e$	MC	CR (merged)	CR	MC	Data	MC
$ee + \mu\mu$	MC	CR (merged)	CR $(e\mu + \mu e)$	Data	Data	MC

Summary of CR yields [2]

Table 4: Control region yields for 8 TeV data. The observed (N_{obs}) and expected (N_{exp}) yields for the signal (N_{sig}) and background (N_{bkg}) processes are given. The composition of N_{bkg} is given on the right. For $N_{\text{jet}} \geq 2$, $N_{\text{sig,ggF}}$ is added to N_{bkg}. In general, no normalisation factors are applied with the following exception: the top and $Z/\gamma^* \to \tau\tau$ normalisation factors are applied for the corresponding estimates in the WW CRs. All uncertainties are statistical.

Estimate	N_{obs}	N_{bkg}	N_{sig}	N_{WW}	N_{VV}	$N_{t\bar{t}}$	N_t	N_{Z/γ^*}	$N_{W+\text{jets}}$
WW									
$N_{\text{jet}} = 0$	2224	1970 ± 17	31 ± 0.7	1383 ± 9.3	100 ± 6.8	152 ± 4.4	107 ± 4.3	68 ± 10	160 ± 3.6
$N_{\text{jet}} = 1$	1897	1893 ± 17	1.9 ± 0.3	752 ± 6.8	88 ± 5.5	717 ± 9.5	243 ± 6.7	37 ± 7.5	56 ± 2.5
$Z/\gamma^* \to \tau\tau$									
$N_{\text{jet}} = 0$	1935	2251 ± 31	2.5 ± 0.2	61 ± 1.9	8.5 ± 1.1	4.5 ± 0.8	2.7 ± 0.6	2113 ± 31	61 ± 3.8
$N_{\text{jet}} = 1$	2884	3226 ± 34	7.5 ± 0.3	117 ± 2.7	22 ± 3.1	570 ± 8.4	50 ± 3	2379 ± 32	88 ± 4.3
$N_{\text{jet}} \geq 2$	212	224 ± 7	0.6 ± 0.1	13 ± 1	4 ± 1	44 ± 3	5 ± 1	148 ± 6	9 ± 1
Top									
$N_{\text{jet}} = 1$	4926	4781 ± 26	12 ± 0.5	184 ± 3.7	43 ± 9.5	3399 ± 20	1049 ± 13	72 ± 3.1	35 ± 2.2
$N_{\text{jet}} \geq 2$	126	201 ± 5	1.6 ± 0.1	6.4 ± 0.4	1.0 ± 0.3	157 ± 4	26 ± 2	9 ± 1	0.3 ± 0.4

Summary of extrapolation unc. [2]

Table 5: Uncertainties on the extrapolation parameters α for the WW background in the $N_{\text{jet}} = 0$ and $= 1$ channels. Uncertainties due to the QCD scale, PDF, parton shower (PS), underlying event (UE), and modelling of the NLO qq, $gq \to WW$ processes are given. Each source, represented by a column, is assumed to be uncorrelated, but for a given source the uncertainties are assumed to be fully correlated among all signal regions with $N_{\text{jet}} = 0$ and $= 1$. A relative sign between two entries in a column indicates anti-correlation between those signal regions for that source of uncertainty.

Channel	Range (GeV)	QCD scale (%)	PS, UE (%)	PDF (%)	Modelling (%)
$N_{\text{jet}} = 0$					
$e\mu + \mu e$	$10 < m_{\ell\ell} < 30$	0.9	0.2	1.5	−1.2
$e\mu + \mu e$	$30 \leq m_{\ell\ell} < 50$	0.9	0.8	1.1	−1.4
$ee + \mu\mu$	$12 < m_{\ell\ell} < 50$	1.0	0.3	1.1	1.7
$N_{\text{jet}} = 1$					
$e\mu + \mu e$	$10 < m_{\ell\ell} < 30$	1.6	0.5	2.0	−5.1
$e\mu + \mu e$	$30 \leq m_{\ell\ell} < 50$	1.5	0.5	1.8	−5.0
$ee + \mu\mu$	$12 < m_{\ell\ell} < 50$	1.4	0.6	1.7	−3.1

Summary of background unc. [2]

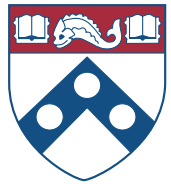

Table 6: Total relative uncertainties on backgrounds that are normalised using control regions (CR). The statistical component (Stat.) is from the CR yields; the theoretical uncertainties (Theory) are from the α extrapolation parameter; the experimental (Expt.) uncertainties are given. The approximate uncertainties on the normalisation of other processes in the CR (Crosstalk) are given. The WW and top in $N_{\text{jet}} = 1$ are anti-correlated due to the b-jet selection, so that the uncertainties partially cancel.

Estimate	Stat. (%)	Theory (%)	Expt. (%)	Crosstalk (%)	Total (%)
WW					
$N_{\text{jet}} = 0$	2.9	1.6	4.4	5.0	7.4
$N_{\text{jet}} = 1$	6	5	4	36	37
Top					
$N_{\text{jet}} = 1$	2	8	22	16	29
$N_{\text{jet}} \geq 2$	10	15	29	19	39

Cutflow table for $N_{Jet} = 0$ [2]

Hong

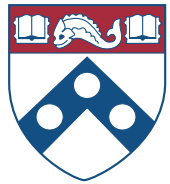

Table 8: Selection table for $N_{\text{jet}} = 0$ in 8 TeV data. The observed (N_{obs}) and expected (N_{exp}) yields for the signal (N_{sig}) and background (N_{bkg}) processes are shown for the (a) $e\mu + \mu e$ and (b) $ee + \mu\mu$ channels. The composition of N_{bkg} is given on the right. The requirements are imposed sequentially from top to bottom. Energies, masses, and momenta are in units of GeV. All uncertainties are statistical.

(a) $e\mu + \mu e$ channel

Selection	N_{obs}	N_{bkg}	N_{sig}	N_{WW}	N_{VV}	$N_{t\bar{t}}$	N_t	N_{Z/γ^*}	$N_{W+\text{jets}}$
$N_{\text{jet}} = 0$	9024	9000 ± 40	172 ± 2	4900 ± 20	370 ± 10	510 ± 10	310 ± 10	2440 ± 30	470 ± 10
$\lvert\Delta\phi_{\ell\ell,MET}\rvert > \frac{\pi}{2}$	8100	8120 ± 40	170 ± 2	4840 ± 20	360 ± 10	490 ± 10	310 ± 10	1690 ± 30	440 ± 10
$p_{\text{T}}^{\ell\ell} > 30$	5497	5490 ± 30	156 ± 2	4050 ± 20	290 ± 10	450 ± 10	280 ± 10	100 ± 10	320 ± 5
$m_{\ell\ell} < 50$	1453	1310 ± 10	124 ± 1	960 ± 10	110 ± 6	69 ± 3	46 ± 3	18 ± 7	100 ± 2
$\lvert\Delta\phi_{\ell\ell}\rvert < 1.8$	1399	1240 ± 10	119 ± 1	930 ± 10	107 ± 6	67 ± 3	44 ± 3	13 ± 7	88 ± 2

(b) $ee + \mu\mu$ channel

Selection	N_{obs}	N_{bkg}	N_{sig}	N_{WW}	N_{VV}	$N_{t\bar{t}}$	N_t	N_{Z/γ^*}	$N_{W+\text{jets}}$
$N_{\text{jet}} = 0$	16446	15600 ± 200	104 ± 1	2440 ± 10	190 ± 5	280 ± 6	175 ± 6	12300 ± 160	170 ± 10
$\lvert\Delta\phi_{\ell\ell,MET}\rvert > \frac{\pi}{2}$	13697	12970 ± 140	103 ± 1	2430 ± 10	190 ± 5	280 ± 6	174 ± 6	9740 ± 140	160 ± 10
$p_{\text{T}}^{\ell\ell} > 30$	5670	5650 ± 70	99 ± 1	2300 ± 10	170 ± 5	260 ± 6	167 ± 5	2610 ± 70	134 ± 4
$m_{\ell\ell} < 50$	2314	2390 ± 20	84 ± 1	760 ± 10	64 ± 3	53 ± 3	42 ± 3	1410 ± 20	62 ± 3
$p_{\text{T,rel}}^{\text{miss}} > 45$	1032	993 ± 10	63 ± 1	650 ± 10	42 ± 2	47 ± 3	39 ± 3	200 ± 5	19 ± 2
$\lvert\Delta\phi_{\ell\ell}\rvert < 1.8$	1026	983 ± 10	63 ± 1	640 ± 10	41 ± 2	46 ± 3	39 ± 3	195 ± 5	18 ± 2
$f_{\text{recoil}} < 0.05$	671	647 ± 7	42 ± 1	520 ± 10	30 ± 2	19 ± 2	22 ± 2	49 ± 3	12 ± 1

Cutflow table for $N_{Jet} = 1$ [2]

Table 9: Selection table for $N_{\text{jet}} = 1$ in 8 TeV data. More details are given in the caption of Table 8.

(a) $e\mu + \mu e$ channel

Selection	N_{obs}	N_{bkg}	N_{sig}	N_{WW}	N_{VV}	$N_{t\bar{t}}$	N_t	N_{Z/γ^*}	$N_{W+\text{jets}}$
$N_{\text{jet}} = 1$	9527	9460 ± 40	97 ± 1	1660 ± 10	270 ± 10	4980 ± 30	1600 ± 20	760 ± 20	195 ± 5
$N_{b\text{-jet}} = 0$	4320	4240 ± 30	85 ± 1	1460 ± 10	220 ± 10	1270 ± 10	460 ± 10	670 ± 10	160 ± 4
$Z \to \tau\tau$ veto	4138	4020 ± 30	84 ± 1	1420 ± 10	220 ± 10	1220 ± 10	440 ± 10	580 ± 10	155 ± 4
$m_{\ell\ell} < 50$	886	830 ± 10	63 ± 1	270 ± 4	69 ± 5	216 ± 6	80 ± 4	149 ± 5	46 ± 2
$\lvert\Delta\phi_{\ell\ell}\rvert < 1.8$	728	650 ± 10	59 ± 1	250 ± 4	60 ± 4	204 ± 6	76 ± 4	28 ± 3	34 ± 2

(b) $ee + \mu\mu$ channel

Selection	N_{obs}	N_{bkg}	N_{sig}	N_{WW}	N_{VV}	$N_{t\bar{t}}$	N_t	N_{Z/γ^*}	$N_{W+\text{jets}}$
$N_{\text{jet}} = 1$	8354	8120 ± 90	54 ± 1	820 ± 10	140 ± 10	2740 ± 20	890 ± 10	3470 ± 80	60 ± 10
$N_{b\text{-jet}} = 0$	5192	4800 ± 80	48 ± 1	720 ± 10	120 ± 10	720 ± 10	260 ± 10	2940 ± 70	40 ± 10
$m_{\ell\ell} < 50$	1773	1540 ± 20	38 ± 1	195 ± 4	35 ± 2	166 ± 5	65 ± 3	1060 ± 10	20 ± 2
$p_{\text{T,rel}}^{\text{miss}} > 45$	440	420 ± 10	21 ± 1	148 ± 3	21 ± 1	128 ± 5	52 ± 3	64 ± 4	5.1 ± 0.8
$\lvert\Delta\phi_{\ell\ell}\rvert < 1.8$	430	410 ± 10	20 ± 1	143 ± 3	20 ± 1	125 ± 5	51 ± 3	63 ± 4	4.5 ± 0.7
$f_{\text{recoil}} < 0.2$	346	320 ± 10	16 ± 1	128 ± 3	17 ± 1	97 ± 4	44 ± 3	25 ± 2	3.1 ± 0.6

Cutflow table for $N_{Jet} \geq 2$ [2]

Hong

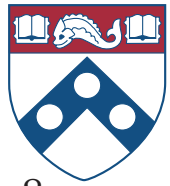

Table 10: Selection table for $N_{\text{jet}} \geq 2$ in 8 TeV data. More details are given in the caption of Table 8. In this table, the $N_{\text{sig,ggF}}$ is included in N_{bkg}; the $N_{\text{sig},VH}$ is included in $N_{\text{sig,VBF}}$, but the contributions are negligible after the VBF-related criteria. The y gap is described in Table 2.

(a) $e\mu + \mu e$ channel

Selection	N_{obs}	N_{bkg}	$N_{\text{sig,VBF}}$	$N_{\text{sig,ggF}}$	N_{WW}	N_{VV}	$N_{t\bar{t}}$	N_t	N_{Z/γ^*}	$N_{W+\text{jets}}$
$N_{\text{jet}} \geq 2$	48723	47740 ± 80	43 ± 1	67 ± 1	940 ± 10	300 ± 20	41800 ± 70	2370 ± 20	1800 ± 30	440 ± 10
$N_{b\text{-jet}} = 0$	5852	5690 ± 30	31 ± 1	49 ± 1	690 ± 10	200 ± 10	2930 ± 20	350 ± 10	1300 ± 20	171 ± 5
$p_{\text{T}}^{\text{tot}} < 45$	4790	4620 ± 30	27 ± 1	41 ± 1	590 ± 10	160 ± 10	2320 ± 20	290 ± 10	1100 ± 20	126 ± 4
$Z \to \tau\tau$ veto	4007	3840 ± 30	25 ± 1	38 ± 1	540 ± 10	140 ± 10	2150 ± 20	260 ± 10	600 ± 20	108 ± 4
$\lvert\Delta y_{jj}\rvert > 2.8$	696	680 ± 10	12 ± 0.2	9.5 ± 0.3	100 ± 2	25 ± 3	380 ± 10	55 ± 3	95 ± 5	19 ± 2
$m_{jj} > 500$	198	170 ± 4	7.5 ± 0.1	2.9 ± 0.2	34 ± 1	5.6 ± 0.6	93 ± 3	11 ± 1	19 ± 2	4.4 ± 0.7
No jets in y gap	92	77 ± 2	6.3 ± 0.1	1.7 ± 0.2	25 ± 1	2.8 ± 0.4	30 ± 2	5.2 ± 0.8	9 ± 1	3.1 ± 0.6
Both ℓ in y gap	78	59 ± 2	6.1 ± 0.1	1.6 ± 0.1	19 ± 1	2.1 ± 0.3	22 ± 1	4.3 ± 0.7	7 ± 1	2.4 ± 0.5
$m_{\ell\ell} < 60$	31	16 ± 1	5.5 ± 0.1	1.5 ± 0.1	3.8 ± 0.4	0.7 ± 0.2	4.5 ± 0.7	0.7 ± 0.3	4.4 ± 0.8	1.0 ± 0.4
$\lvert\Delta\phi_{\ell\ell}\rvert < 1.8$	23	12 ± 1	5.1 ± 0.1	1.3 ± 0.1	3.5 ± 0.4	0.6 ± 0.2	3.7 ± 0.7	0.7 ± 0.3	1.9 ± 0.5	0.6 ± 0.3

(b) $ee + \mu\mu$ channel

Selection	N_{obs}	N_{bkg}	$N_{\text{sig,VBF}}$	$N_{\text{sig,ggF}}$	N_{WW}	N_{VV}	$N_{t\bar{t}}$	N_t	N_{Z/γ^*}	$N_{W+\text{jets}}$
$N_{\text{jet}} \geq 2$	32877	32300 ± 100	26 ± 0.7	40 ± 1	540 ± 6	180 ± 10	24540 ± 60	1390 ± 20	5420 ± 90	190 ± 10
$N_{b\text{-jet}} = 0$	65388	6370 ± 80	19 ± 0.6	30 ± 1	390 ± 5	130 ± 10	1750 ± 20	200 ± 10	3810 ± 80	58 ± 4
$p_{\text{T}}^{\text{tot}} < 45$	4903	4830 ± 70	17 ± 0.5	24 ± 1	340 ± 4	92 ± 5	1370 ± 10	170 ± 10	2790 ± 70	43 ± 3
$\lvert\Delta y_{jj}\rvert > 2.8$	958	930 ± 30	8.1 ± 0.2	6.2 ± 0.3	61 ± 2	12 ± 1.3	252 ± 6	35 ± 2	560 ± 30	6 ± 1
$m_{jj} > 500$	298	245 ± 6	5.5 ± 0.1	2.1 ± 0.2	23 ± 1	4.1 ± 1.1	62 ± 3	9 ± 1	142 ± 5	1.4 ± 0.6
No jets in y gap	147	119 ± 4	4.7 ± 0.1	1.1 ± 0.1	17 ± 1	2.8 ± 1.1	19 ± 1	4.1 ± 0.7	74 ± 3	0.7 ± 0.4
Both ℓ in y gap	108	85 ± 3	4.5 ± 0.1	0.9 ± 0.1	12 ± 1	2.3 ± 1.1	14 ± 1	3.1 ± 0.6	51 ± 3	0.3 ± 0.3
$m_{\ell\ell} < 60$	52	40 ± 2	4.0 ± 0.1	0.8 ± 0.1	3.2 ± 0.3	1.6 ± 1.1	3.7 ± 0.6	0.8 ± 0.3	30 ± 2	0.1 ± 0.2
$\lvert\Delta\phi_{\ell\ell}\rvert < 1.8$	42	34 ± 2	3.7 ± 0.1	0.7 ± 0.1	2.8 ± 0.3	1.6 ± 1.1	3.3 ± 0.5	0.7 ± 0.3	25 ± 2	0.1 ± 0.2

More plots from [1, 2]

- p52 - 104

Table of contents

Hong

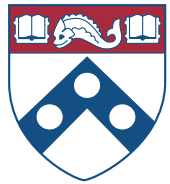

Source	Fig.	Plot	Channel	Njet	Comment
[1]	4	mll	eμ	0	SR w/o Δφll
[1]	5a	mT	eμ	0+1	SR
[1]	5b	mT	eμ	VBF	SR
[1]	6	μ	Breakdown for Hγγ, HZZ, HWW		
[1]	7	μggF v. μVBF	Breakdown for Hγγ, HZZ, HWW		
[1]	8	μVBF / μggF	Breakdown for Hγγ, HZZ, HWW		
[1]	10	kV v. kF	Breakdown for Hγγ, HZZ, HWW		
[2]	12a	p0	all	VBF	-
[2]	12c	μ	all	VBF	-
[2]	14a	μggF v. μVBF	all	VBF	-
[1]	26a	ETmiss	eμ	0+1	dilepton
[1]	26b	pTmiss	ee+μμ	0+1	dilepton
[1]	26c	ETmiss,STVF	ee+μμ	VBF	dilepton
[1]	26d	frecoil	ee+μμ	0 simulation	mll
[1]	27a	Njet	eμ	all	Etmiss
[1]	27b	Njet	ee+μμ	all	Etmiss
[1]	28	mT	eμ	0	same-sign after pTll
[1]	29a	mT	eμ	0	before mll split
[1]	29b	mT	ee+μμ	0	before mll split
[1]	29c	mT	eμ	1	before mll split
[1]	29d	mT	ee+μμ	1	before mll split
[1]	29e	mT	eμ	VBF	before mll split
[1]	29f	mT	ee+μμ	VBF	before mll split
[1]	30a	mT	eμ	1	top CR
[1]	30b	mT	ee+μμ	VBF	top CR
[2]	34a	Δφll	eμ	VBF	Nbtag=1 after pttot
[2]	34b	mT	eμ	VBF	Nbtag=1 after pttot
[2]	34c	mll	eμ	vBF	Nbtag=1 after pttot
[1]	31a	mT	eμ	0	WW CR
[1]	31b	mT	ee+μμ	1	WW CR
[1]	32a	mT	eμ	0	7 TeV SR
[1]	32b	mT	ee+μμ	0	7 TeV SR
[1]	32c	mT	eμ	1	7 TeV SR
[1]	32d	mT	ee+μμ	1	7 TeV SR
[1]	33	p0	all	all	-
[1]	34	Event display	eμ	VBF	-
[2]	32a	y lead	eμ	VBF	after Njet
[2]	32b	y sublead	eμ	VBF	after Njet
[1]	35a	dy jj	eμ	VBF	after pttot
[1]	35b	dy jj	ee+μμ	VBF	after pttot
[1]	35c	mjj	eμ	VBF	after dy jj
[1]	35d	mjj	ee+μμ	VBF	after dy jj
[1]	36a	mll	eμ	VBF	after olv
[1]	36b	mll	ee+μμ	VBF	after olv
[1]	36c	Δφll	eμ	VBF	after mll
[1]	36d	Δφll	ee+μμ	VBF	after mll
[1]	37	μ	Breakdown for Hγγ, HZZ, HWW		
[1]	41a	μ v. mH	Breakdown for Hγγ, HZZ, HWW		
[1]	41b	μ v. mH	Breakdown for Hγγ, HZZ, HWW		
[1]	42	μVBF / μggF	Breakdown for Hγγ, HZZ, HWW		
[2]	16a	Zμμ fraction	Shows pile-up dependence as a fn. of Nvtx		
[2]	16b	Zμμ fraction	Shows pile-up dependence as a fn. of Nvtx		

Fig. 4 [1]

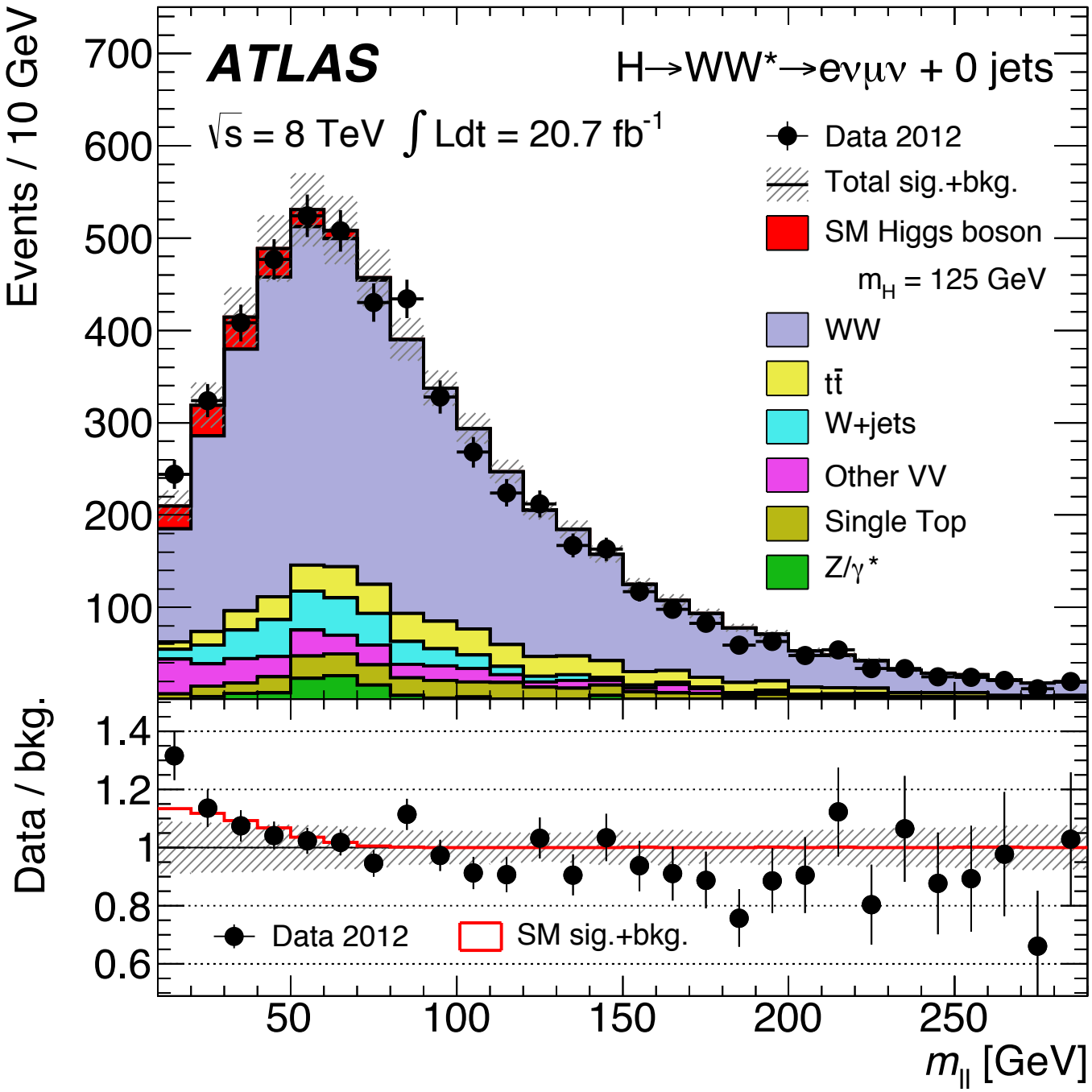

Caption

The **mll** distribution of **eμ** events with **Njet = 0** for the 8 TeV H→WW*→lνlν analysis.The events with mll <50 GeV correspond to the signal region except that the **Δϕll < 1.8 requirement is not applied** here, and the events with 50 GeV < mll < 100 GeV correspond to the Njet =0 WW control region. The signal is stacked on top of the background. The hatched area represents the total uncertainty on the sum of the signal and background yields from statistical, experimental, and theoretical sources. The lower part of the figure shows the ratio of the data to the predicted background. For comparison, the expected ratio of the signal plus background to the background alone is also shown.

Fig. 5a [1]

Hong

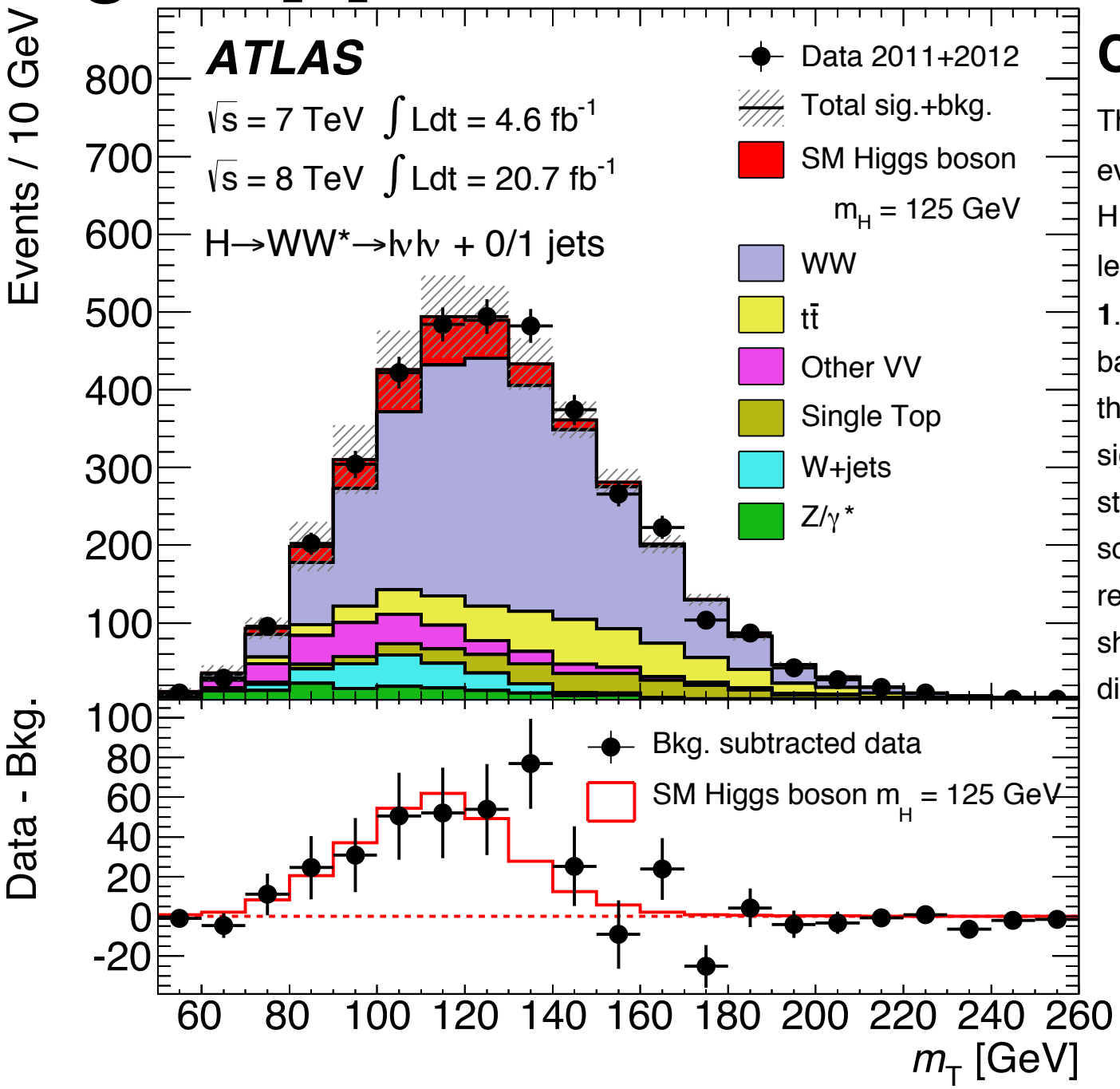

Caption

The **transverse mass** distributions for events **passing the full selection** of the H→WW∗→lνlν analysis summed over all lep- ton flavours for final states with **Njet ≤ 1**. The signal is stacked on top of the background. The hatched area represents the total uncertainty on the sum of the signal and background yields from statistical, experimental, and theoretical sources. The residuals of the data with respect to the estimated background are shown, compared to the expected mT distribution of a SM Higgs boson.

Fig. 5b [1]

Hong

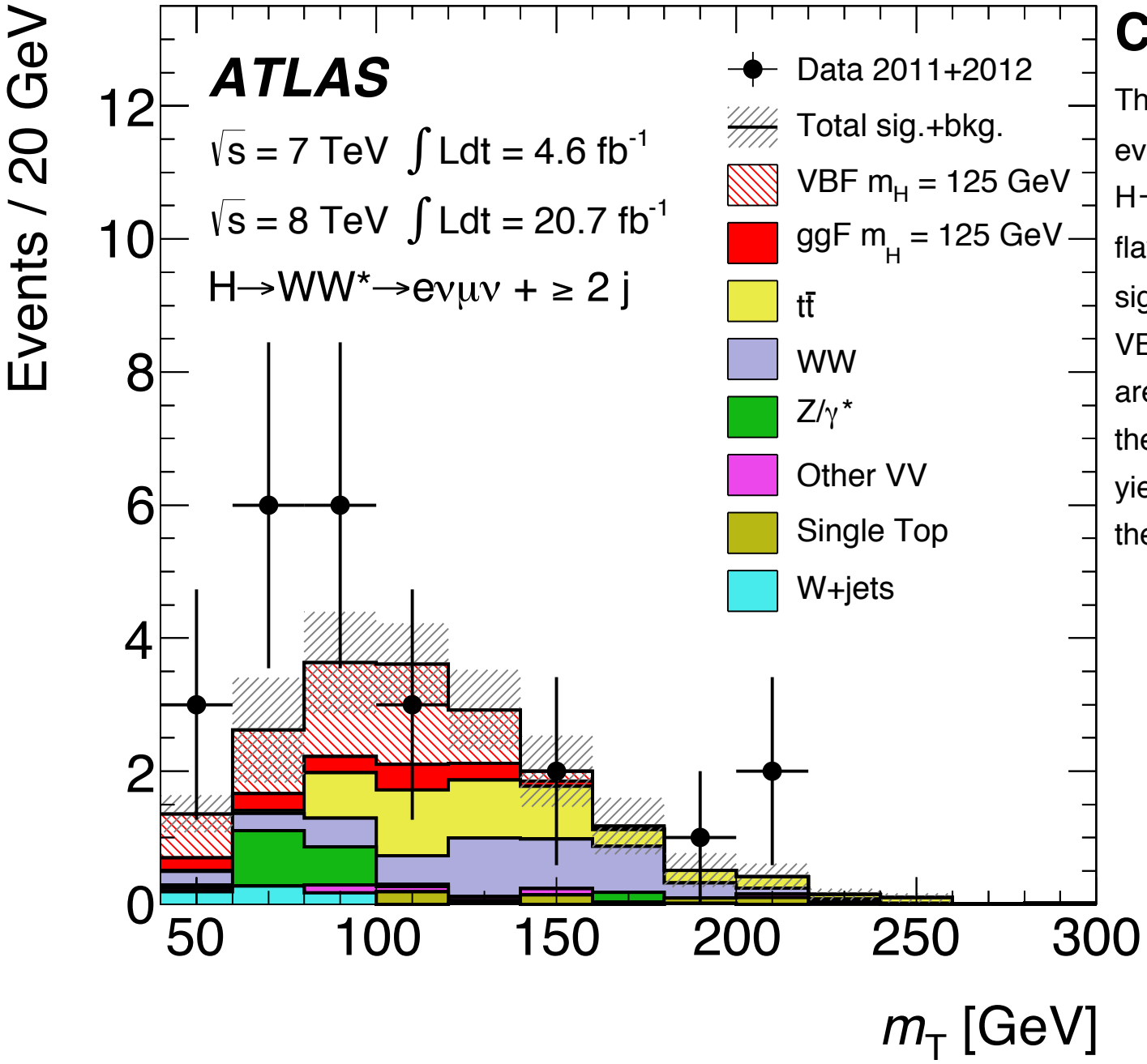

Caption

The **transverse mass** distributions for events **passing the full selection** of the H→WW*→lνlν analysis for different-flavour final states with **Njet ≥ 2**. The signal is shown separately for the ggF and VBF production processes. The hatched area represents the total uncertainty on the sum of the signal and background yields from statistical, experimental, and theoretical sources.

Fig. 6 [1]

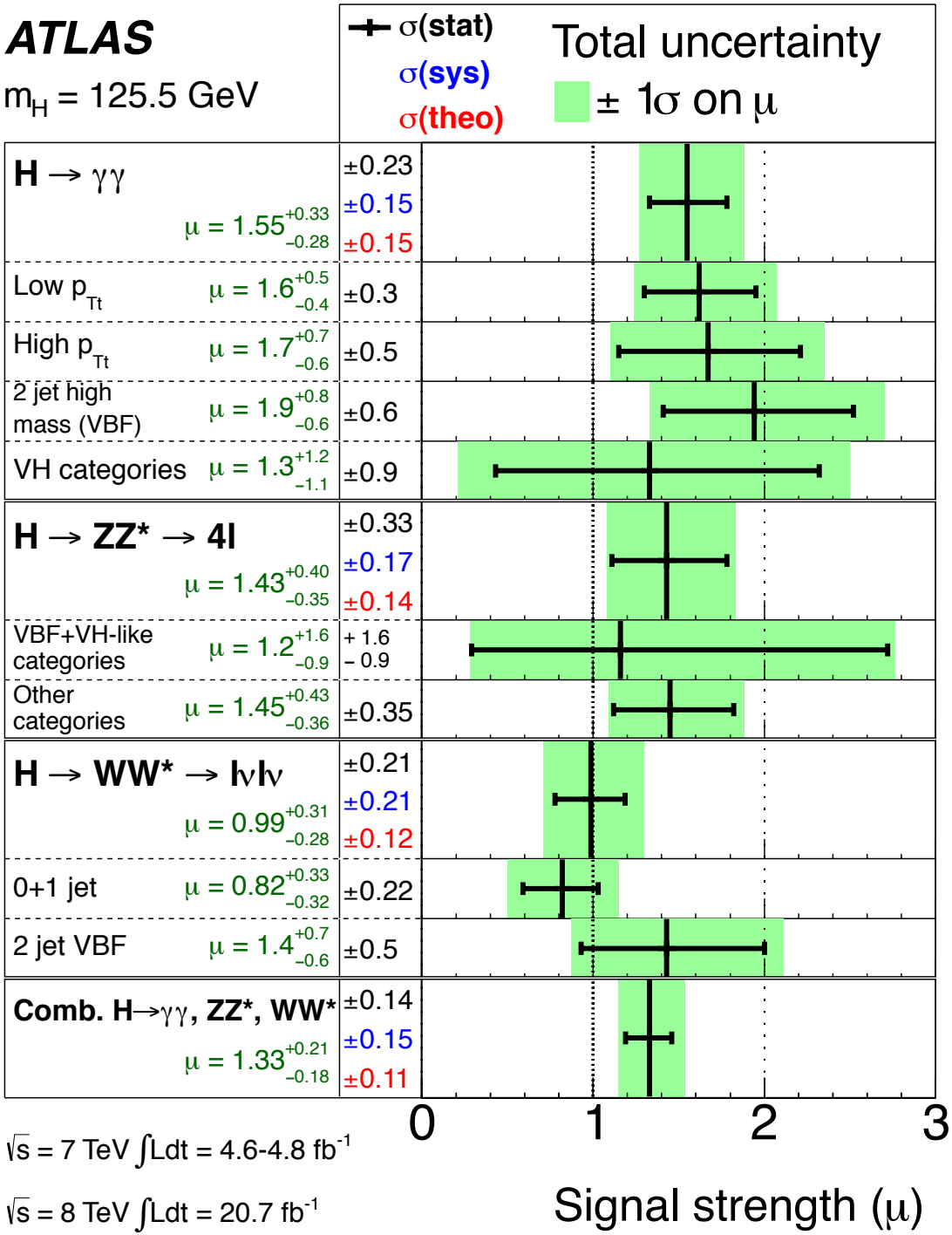

Caption

The **measured production strengths** for a Higgs boson of mass **mH =125.5 GeV**, normalised to the SM expectations, for diboson final states and their combination. Results are also given for the main categories of each analysis (described in Sections 4.2, 5.2 and 6.2). The best-fit values are shown by the solid vertical lines, with the total ±1σ uncertainty indicated by the shaded band, and the statistical uncertainty by the superimposed horizontal error bars. The numbers in the second column specify the contributions of the (symmetrised) statistical uncertainty (top), the total (experimental and theoretical) systematic uncertainty (middle), and the theory uncertainty (bottom) on the signal cross section (from QCD scale, PDF, and branching ratios) alone; for the individual categories only the statistical uncertainty is given.

Fig. 7 [1]

Hong

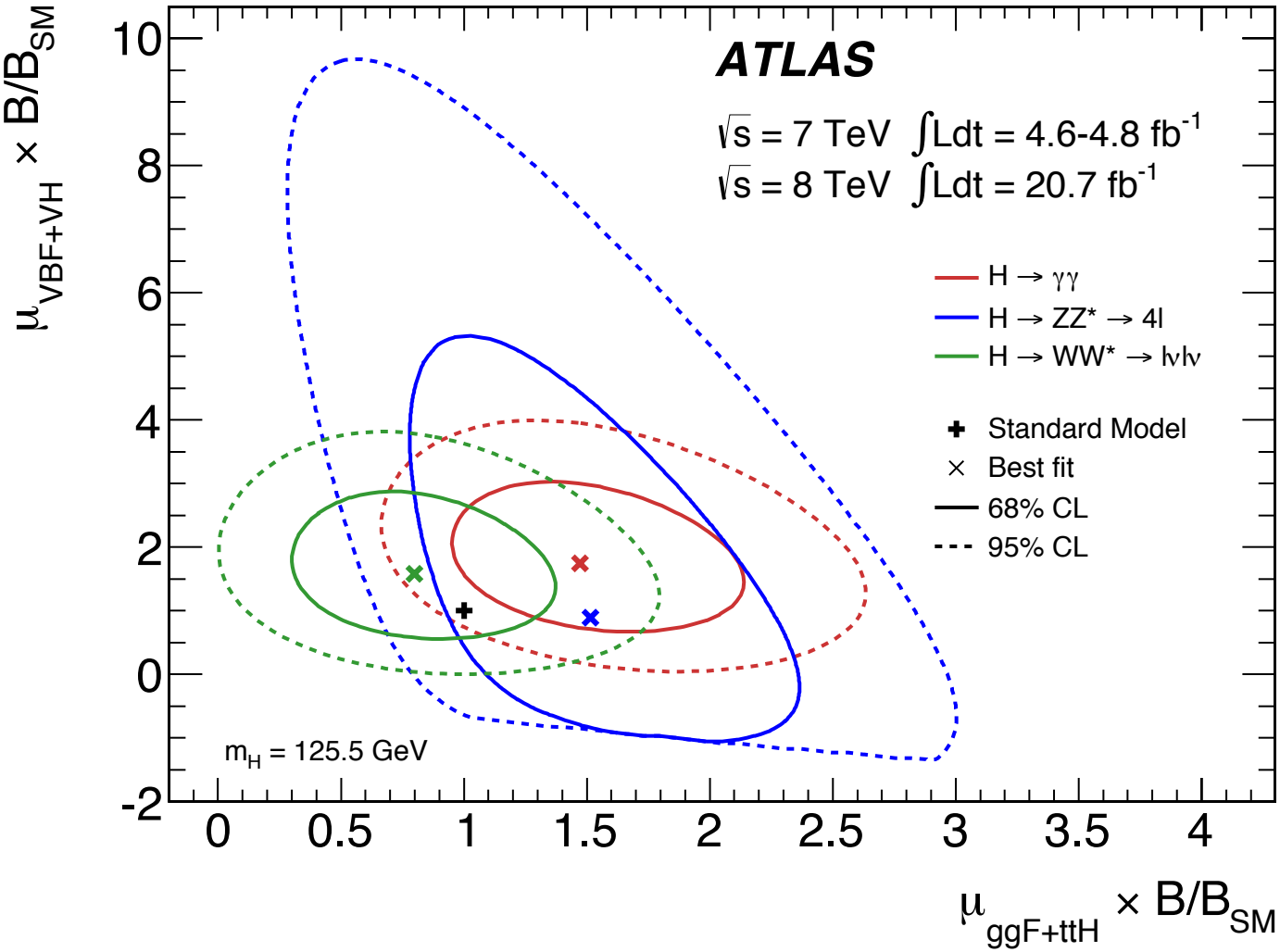

Caption

Likelihood contours for the H→γγ, H→ZZ*→4l and H→WW*→lνlν channels in the (μggF+ttH × B/BSM, μVBF+VH × B/BSM) plane for a Higgs boson mass mH = 125.5 GeV. **The branching-ratio scale factors B/BSM can a priori be different for the different final states.** The sharp lower edge of the H→ ZZ*→ 4l contours is due to the small number of events in this channel and the requirement of a positive pdf. The best fits to the data (×) and the 68% (full) and 95% (dashed) CL contours are indicated, as well as the SM expectation (+).

Fig. 8 [1]

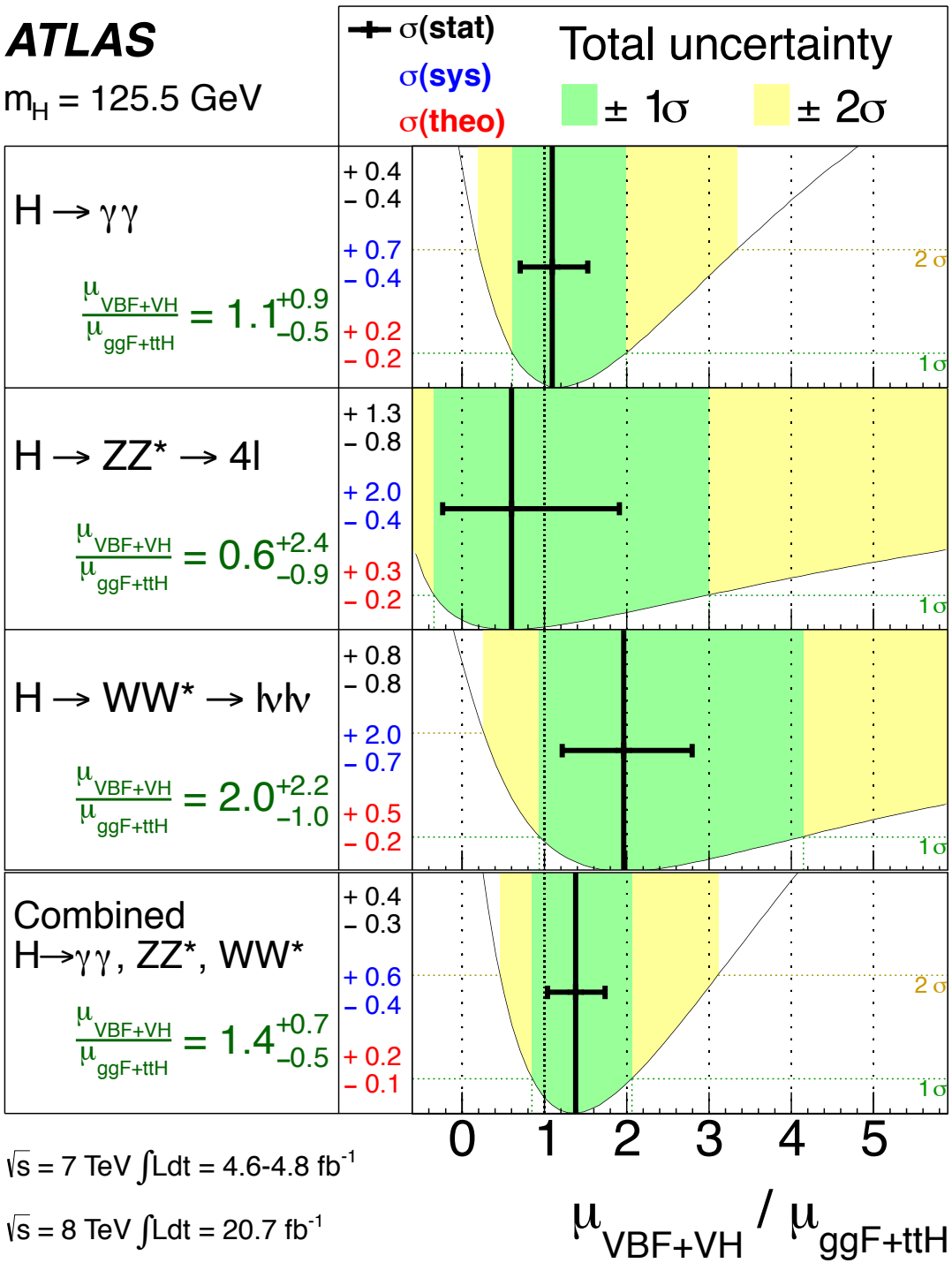

Caption

Measurements of the **μVBF+VH/μggF+ttH ratios** for diboson final states and their combination, for a Higgs boson mass mH =125.5 GeV. The best-fit values are represented by the solid vertical lines, with the total ±1σ and ±2σ uncertainties indicated by the dark- and light-shaded band, respectively, and the statistical uncertainties by the superimposed horizontal error bars. The numbers in the second column specify the contributions of the statistical uncertainty (top), the total (experimental and theoretical) systematic uncertainty (middle), and the theoretical uncertainty (bottom) on the signal cross section (from QCD scale, PDF, and branching ratios) alone. For a more complete illustration, the distributions of the likelihood ratios from which the total uncertainties are extracted are overlaid.

Fig. 10 [1]

Hong

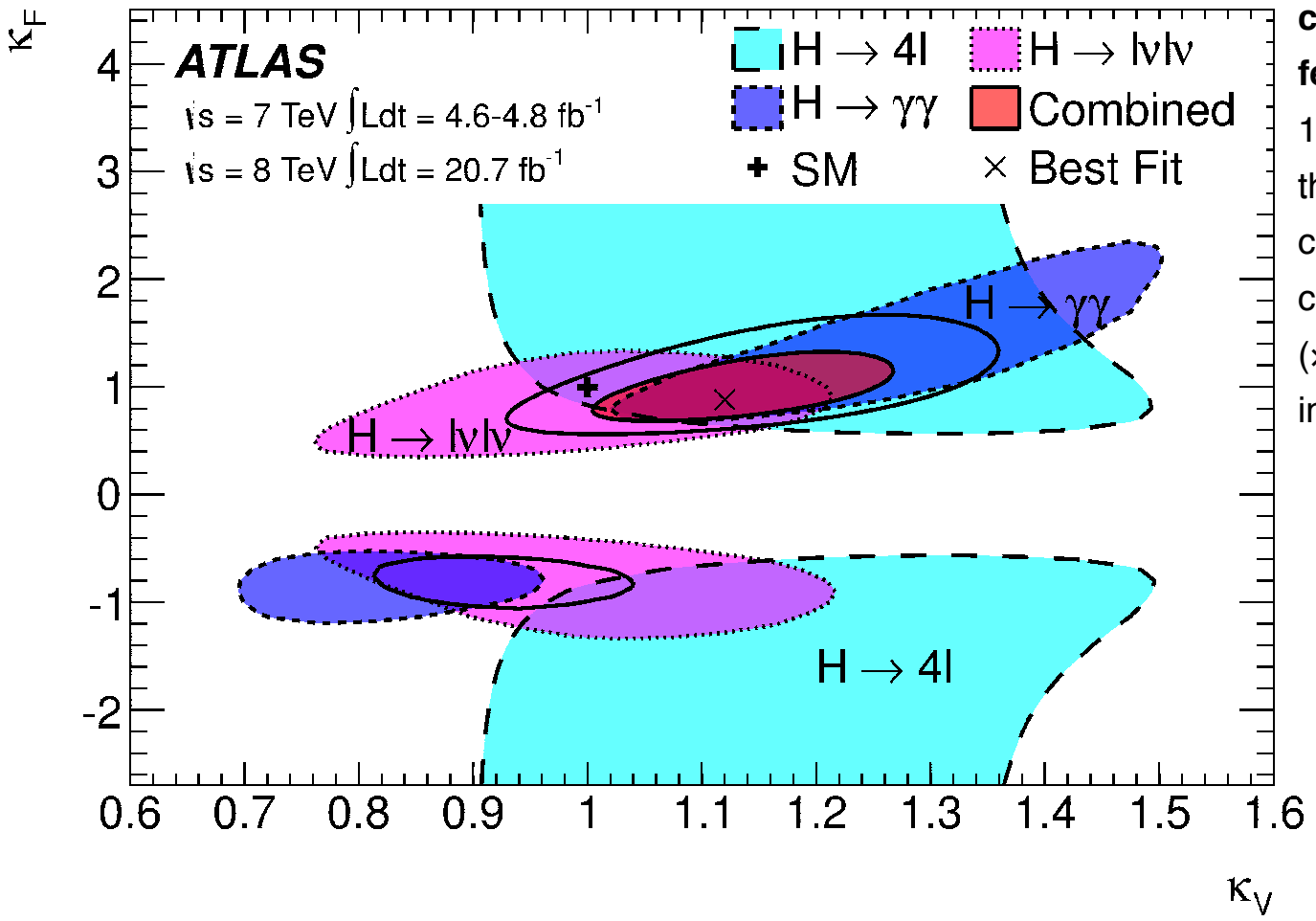

Caption

Likelihood contours (68% CL) of the **coupling scale factors κF and κV for fermions and bosons** (benchmark model 1 in Table 10), as obtained from fits to the three individual channels and their combination (for the latter, the 95% CL contour is also shown). The best-fit result (×) and the SM expectation (+) are also indicated.

Fig. 12a [2]

Hong

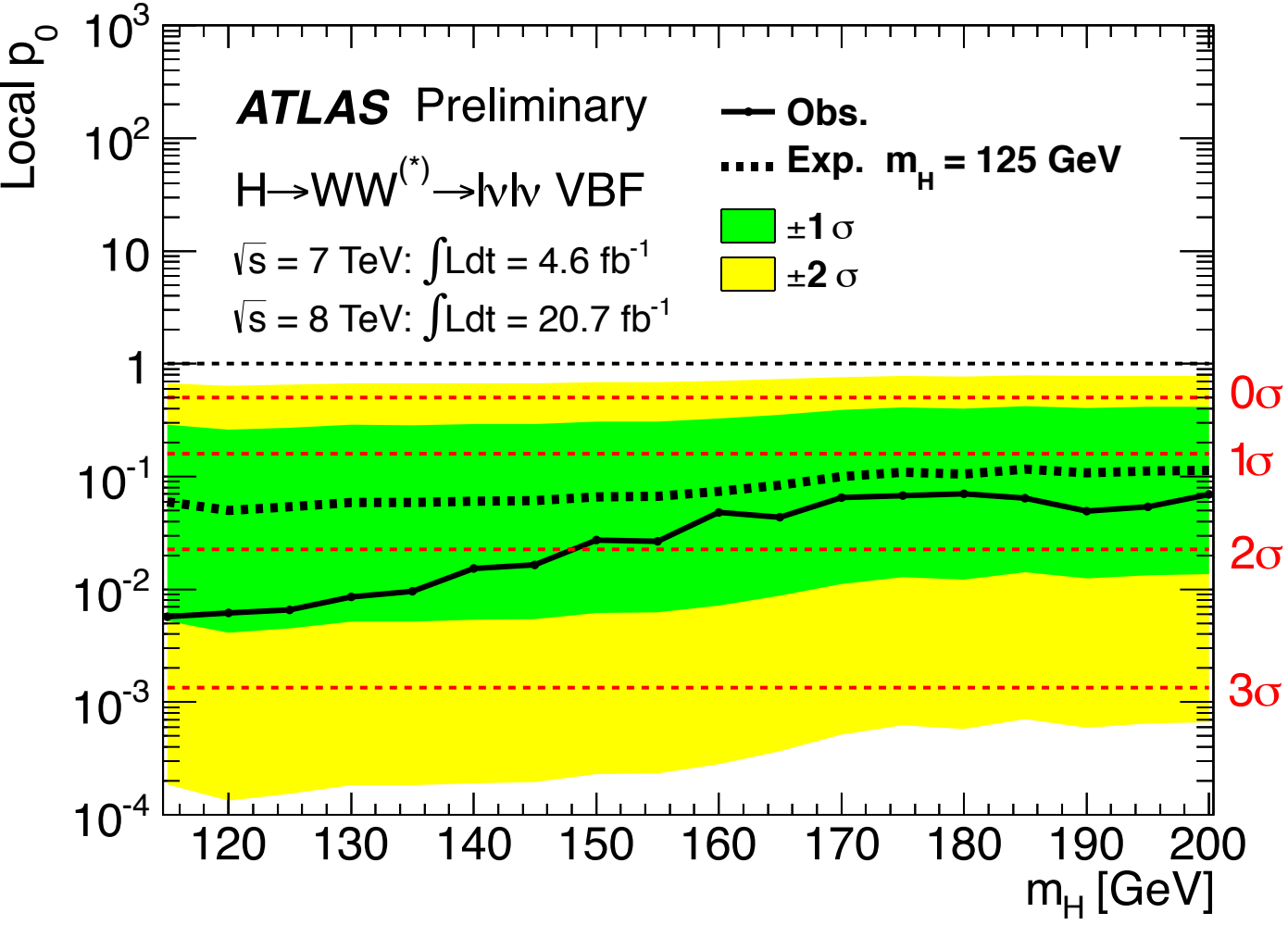

Caption

VBF results for **p0** using 8 TeV data considering VBF as signal and ggF as part of the background. Details are given in the caption of Fig. 10.

Fig. 13 [2]

Hong

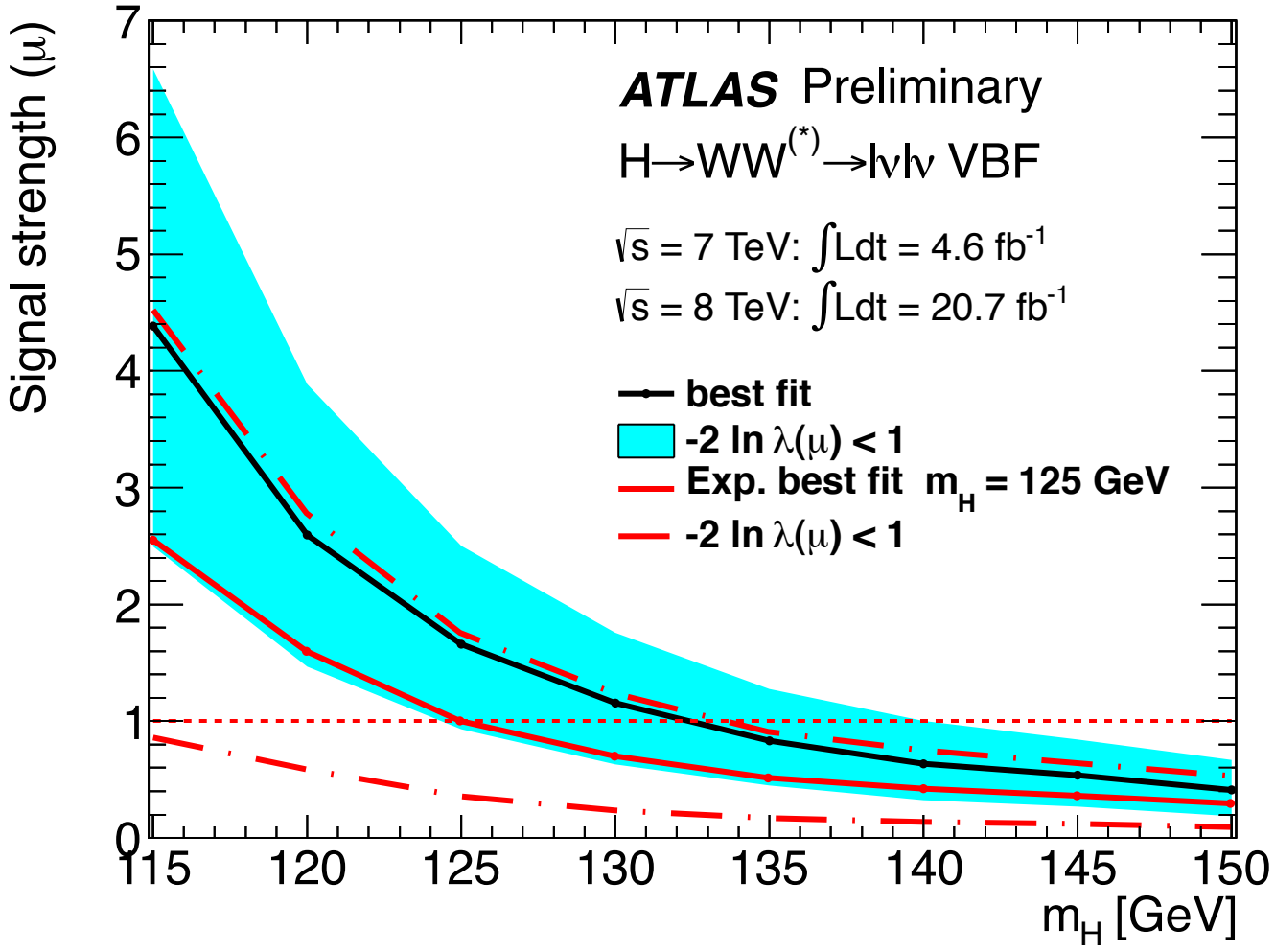

Caption

VBF signal strength parameter μ. The observed (solid black line with shaded cyan band) and the expected result (solid red line with dashed band) are shown.

Fig. 14a [2]

Hong

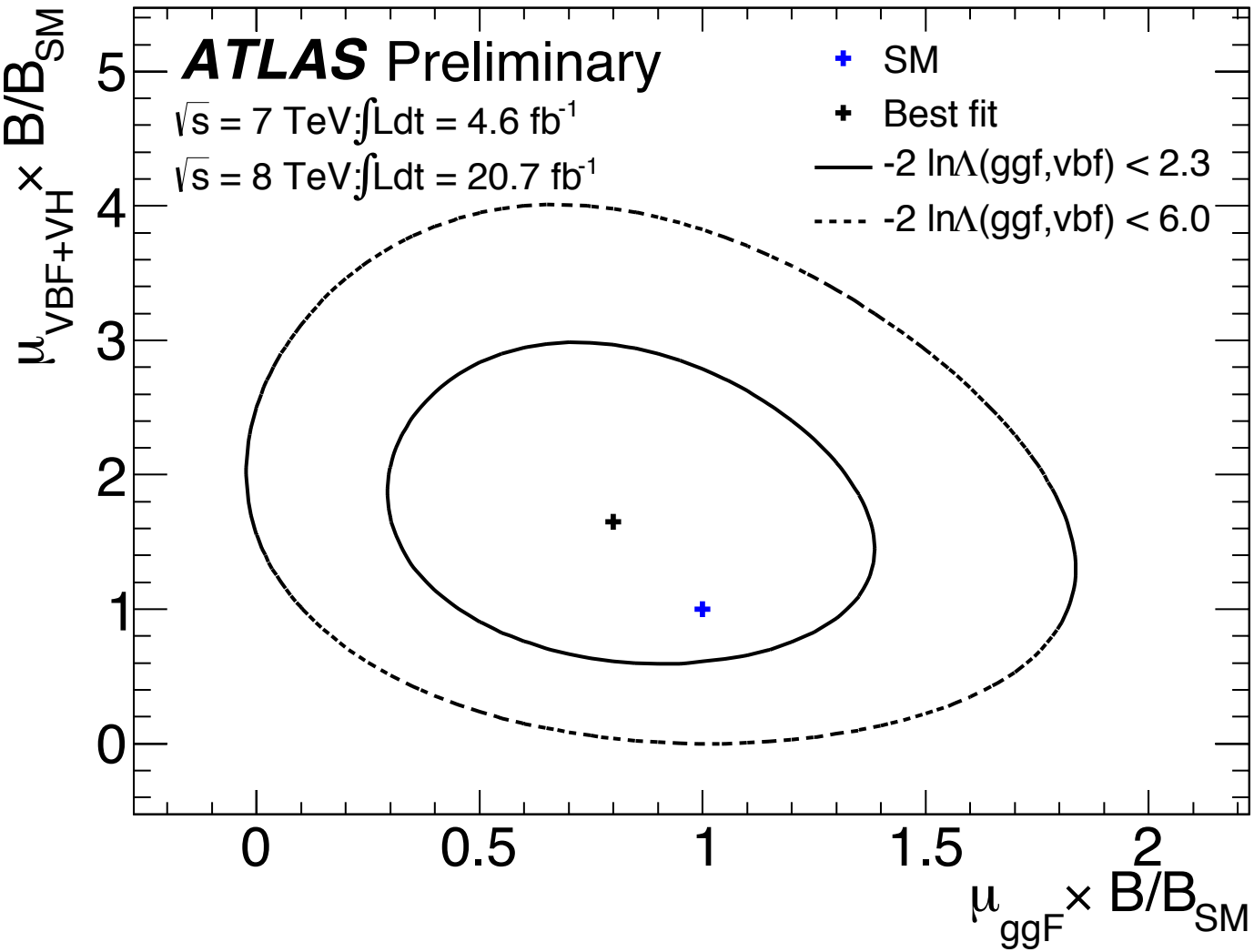

Caption

Likelihood contours for separate **ggF and VBF signal strength parameters**. HWW (*) →lvlv analysis uses the combined 7 and 8 TeV data.

Auxiliary Fig. 26a [1]

Hong

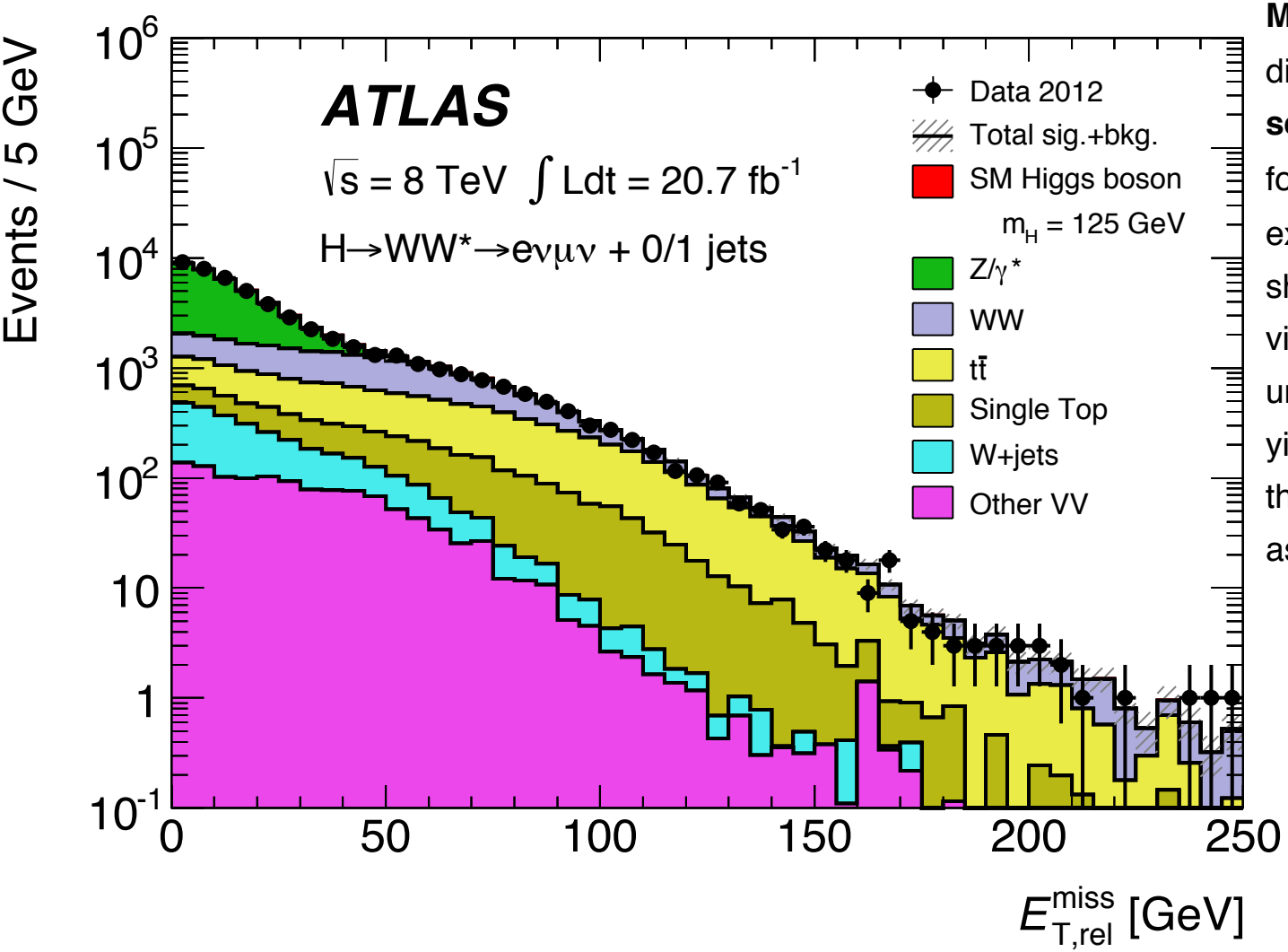

Caption

Missing transverse momentum distributions for events **after the dilepton selection** of the H→ WW∗→ lνlν analysis for **Etmiss for Njet ≤ 1**. The background expectation from the MC simulation is also shown. The hatched area (too small to be visible in these figures) represents the uncertainty on the signal and background yields from statistical, experimental, and theoretical sources. The signal is overlaid as a red curve in the top plots

Auxiliary Fig. 26b [1]

Hong

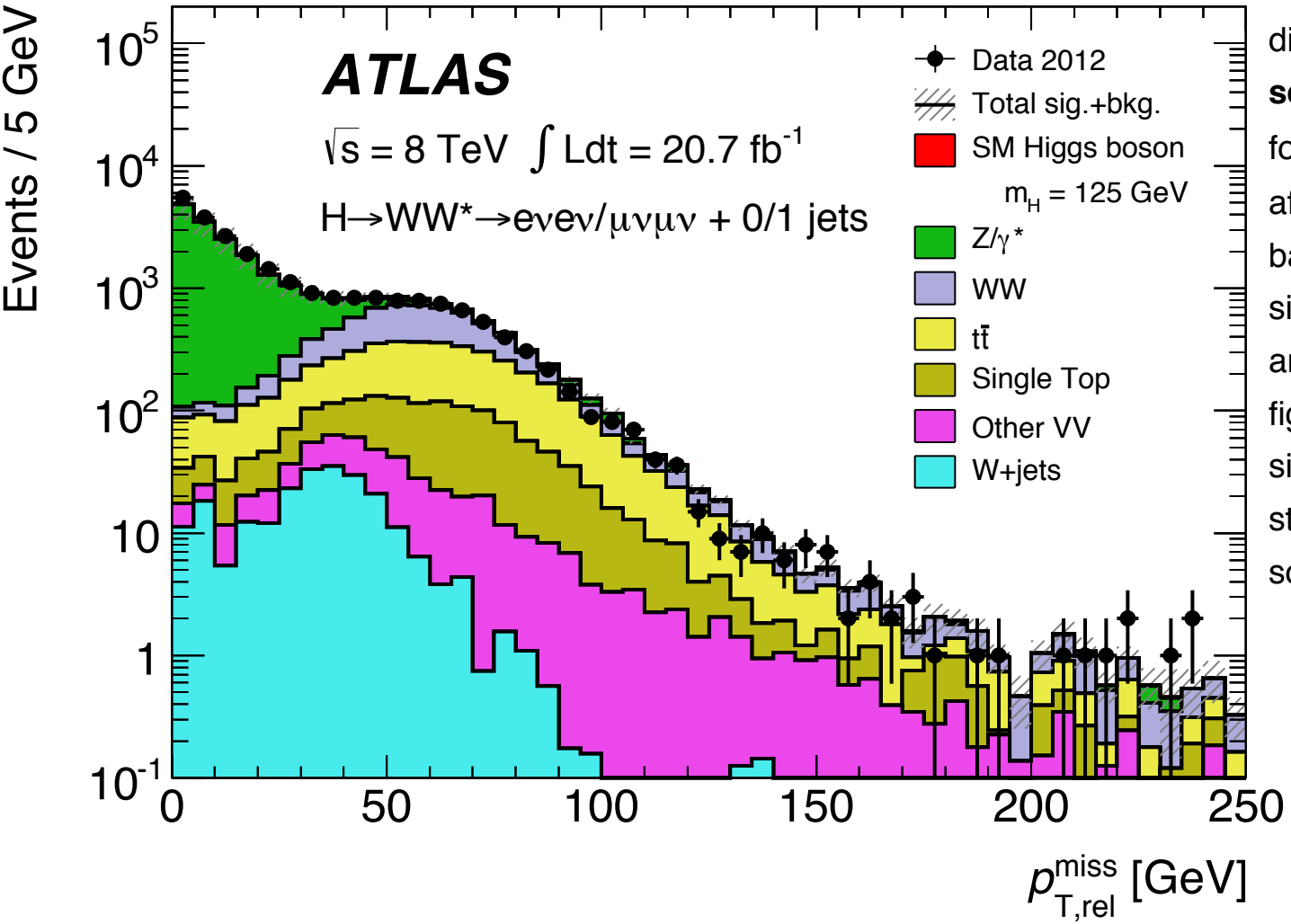

Caption

Missing transverse momentum distributions for events **after the dilepton selection** of the H→ WW∗→ lνlν analysis for **pmiss for Njet ≤ 1**. The plot is made after the requirement on $E_{T,rel}^{miss}$. The background expectation from the MC simulation is also shown. The hatched area (too small to be visible in these figures) represents the uncertainty on the signal and background yields from statistical, experimental, and theoretical sources.

Auxiliary Fig. 26c [1]

Hong

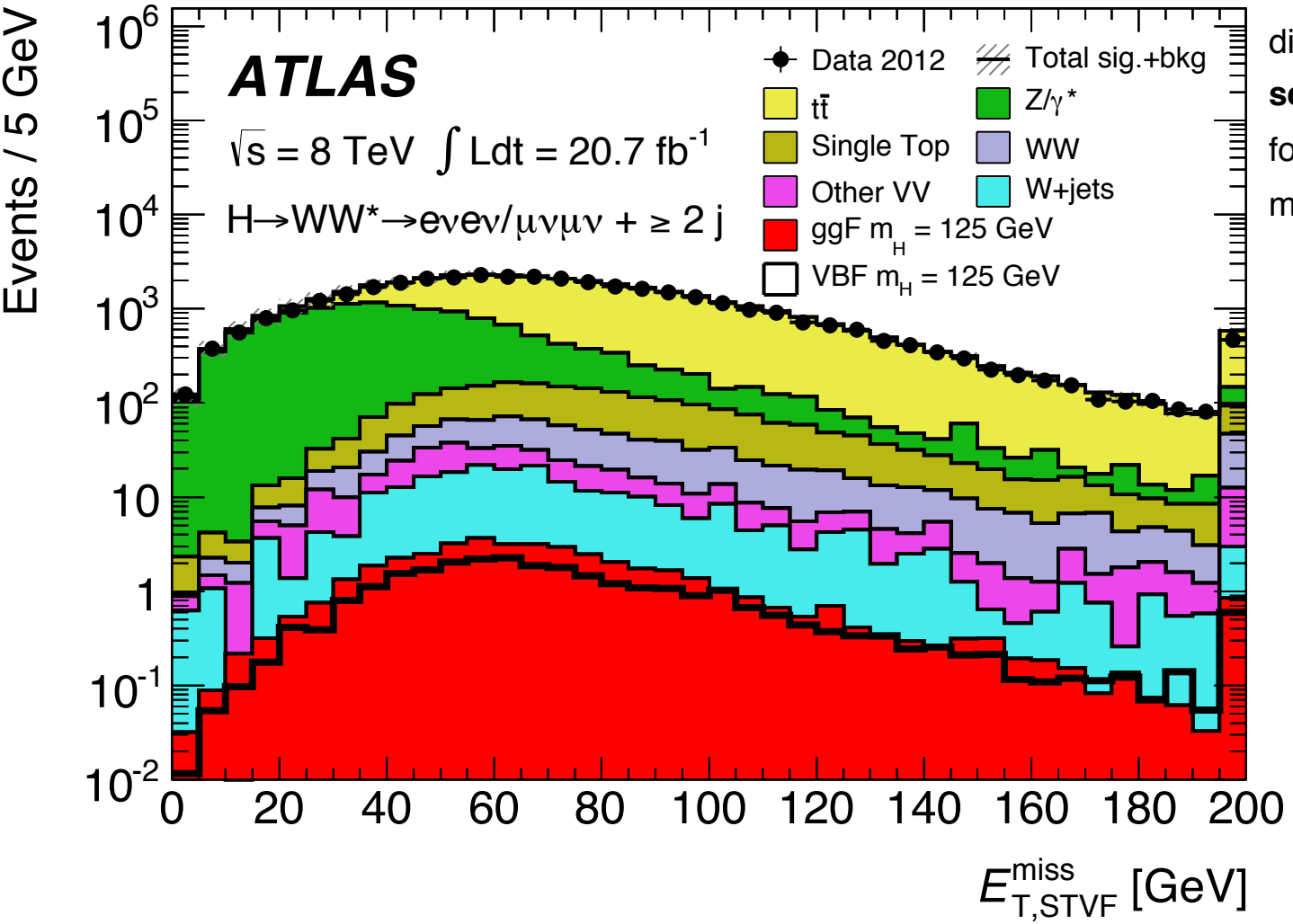

Caption

Missing transverse momentum distributions for events **after the dilepton selection** of the H→ WW∗→ lνlν analysis for **Emiss,STVF for Njet ≥ 2**. The plot is made after the requirement on E_T^{miss}.

Auxiliary Fig. 26d [1]

Hong

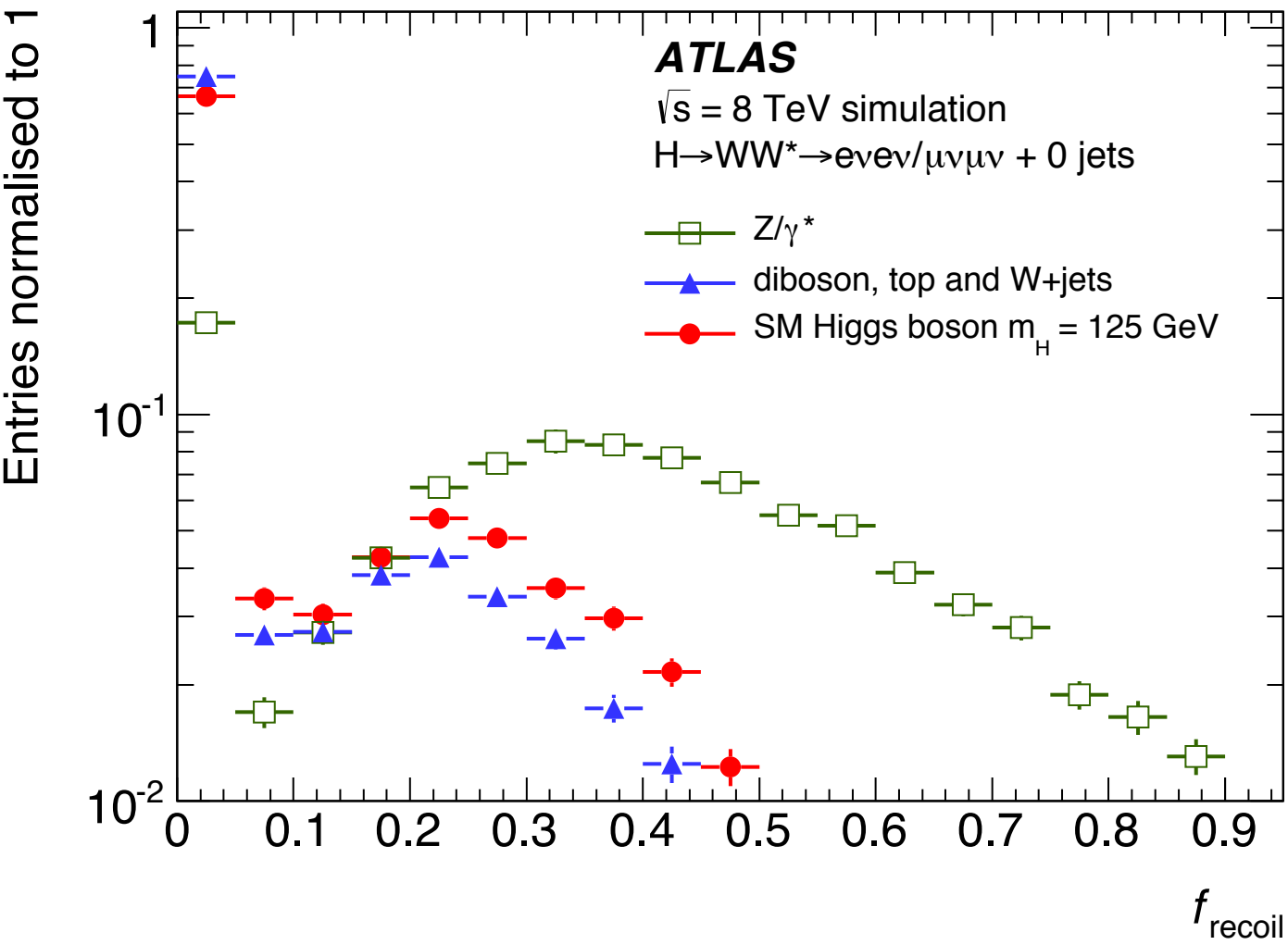

Caption

The **frecoil** distribution **for ee/μμ** events passing the **Njet = 0** selection **after the requirement mll < 50 GeV** for simulated DY, non-DY and signal processes.

Auxiliary Fig. 27a [1]

Hong

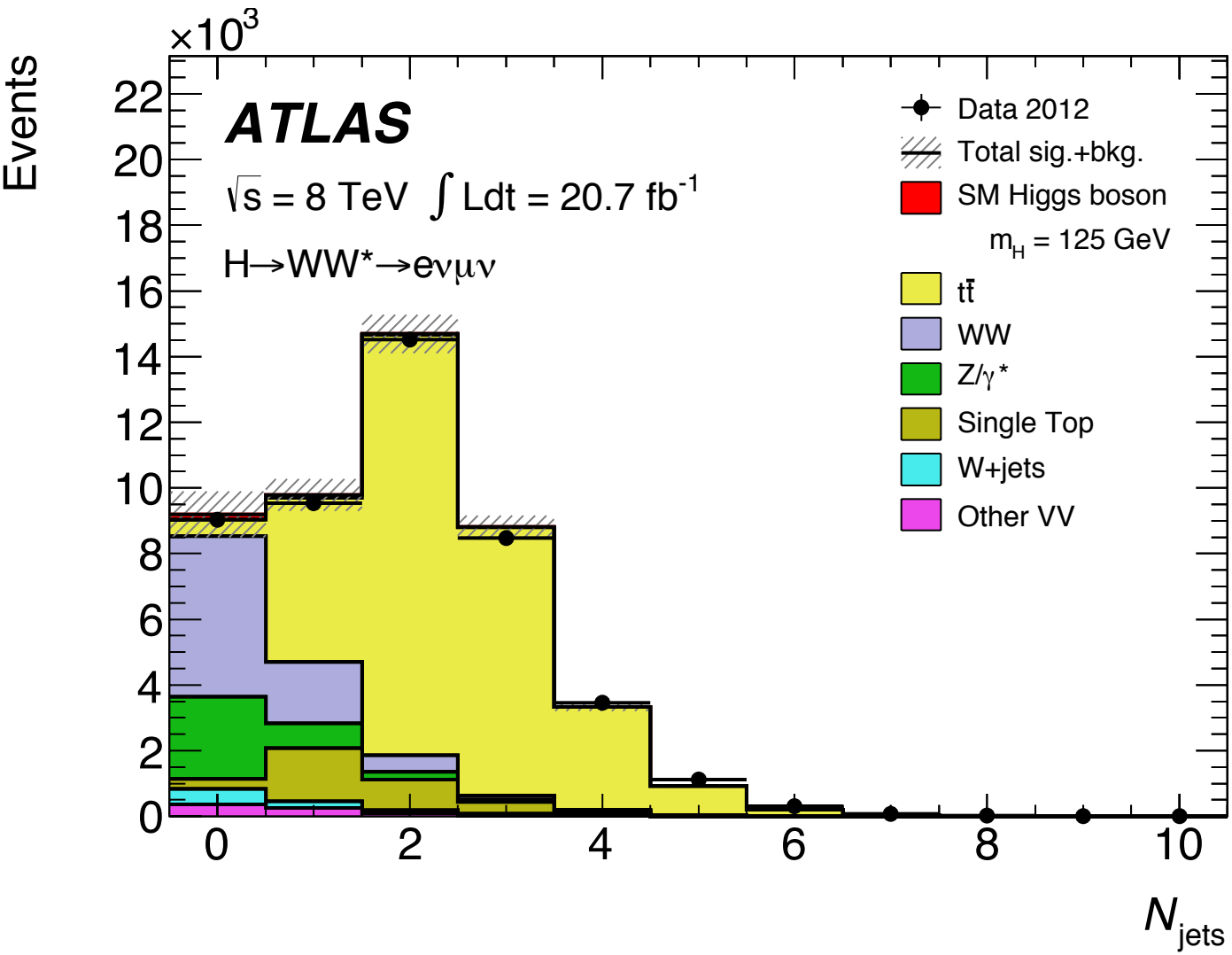

Caption

Jet multiplicity for eμ events from the 8 TeV data **after the dilepton selection** of the H→ WW∗→ lνlν analysis and **Emiss >25GeV and >45GeV requirements**, respectively. The background expectation from the MC simulation is also shown.The hatched area represents the uncertainty on the signal and background yields from statistical, experimental, and theoretical sources.

Auxiliary Fig. 27b [1]

Hong

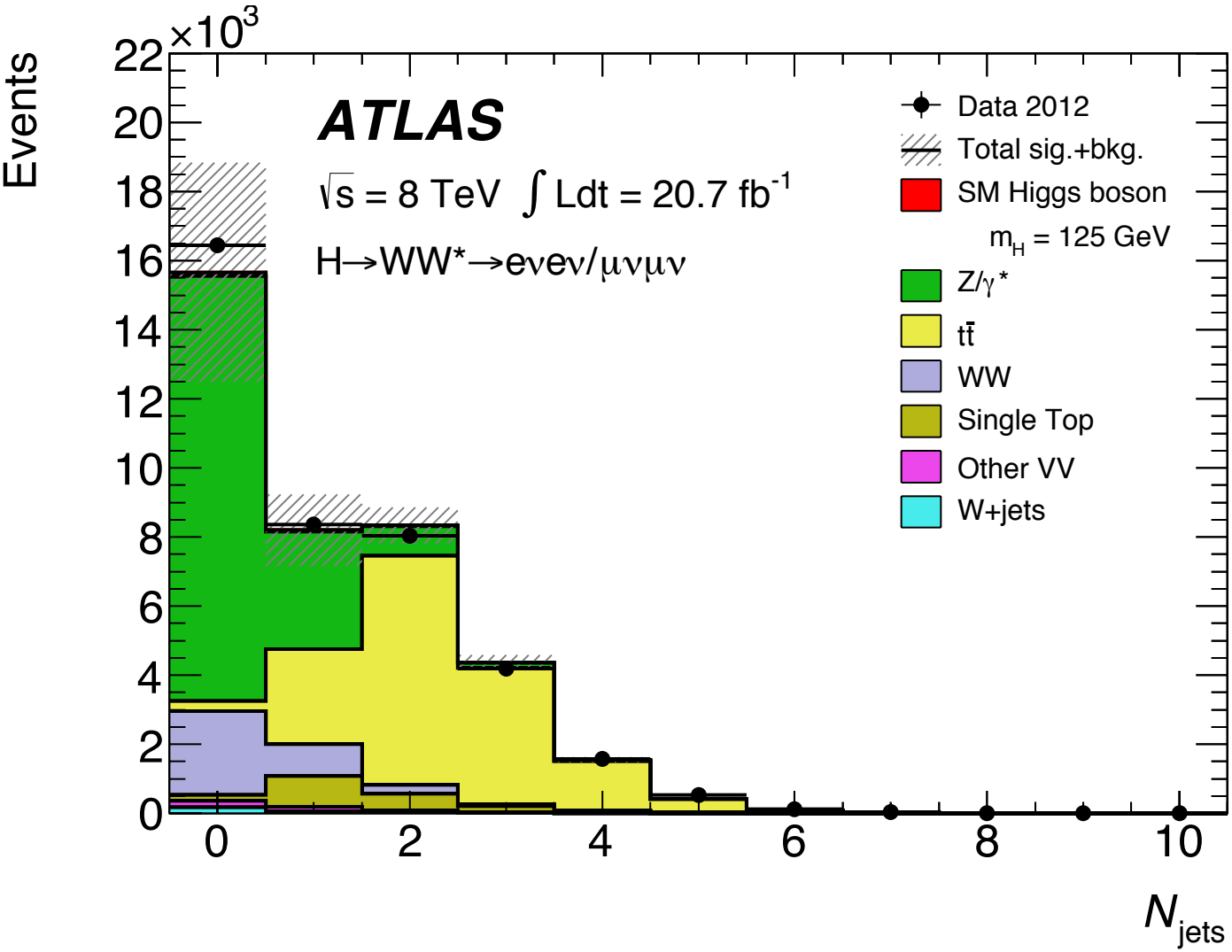

Caption

Jet multiplicity for ee/μμ events from the 8 TeV data **after the dilepton selection** of the H→ WW∗→ lνlν analysis and **Emiss >25GeV and >45GeV requirements**, respectively. The background expectation from the MC simulation is also shown.The hatched area represents the uncertainty on the signal and background yields from statistical, experimental, and theoretical sources.

Auxiliary Fig. 28 [1]

Hong

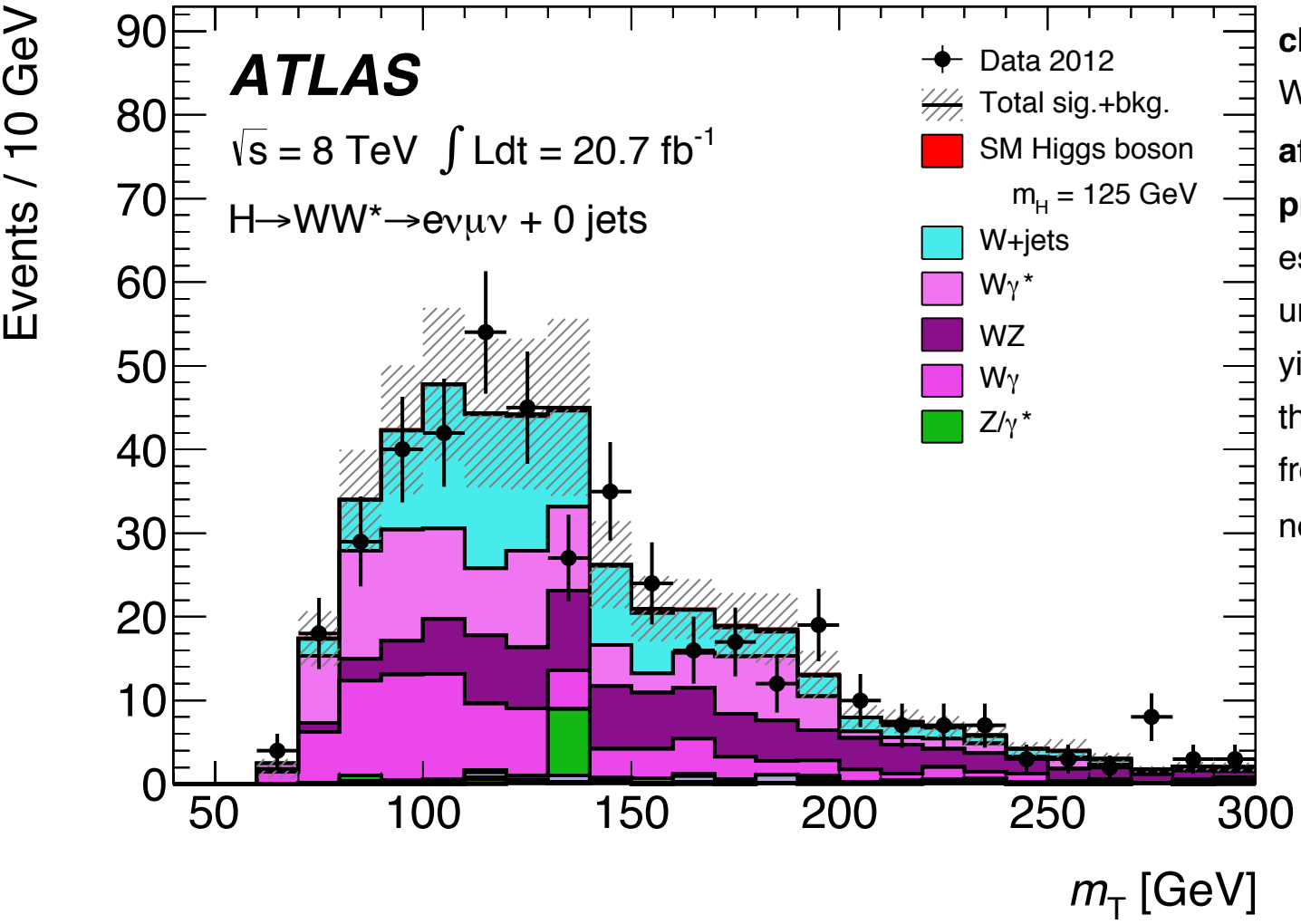

Caption

Distribution of **mT** in the **Njet = 0 same-charge validation region** of the H→ WW∗→ lνlν analysis for the 8 TeV data, **after the pTll selection**. The **W+jets prediction is from the data-driven** estimate. The hatched area represents the uncertainty on the signal and background yields from statistical, experimental, and theoretical sources. The contributions from WW, ZZ, tt, and single top are negligible and omitted from the legend.

Auxiliary Fig. 29a [1]

Hong

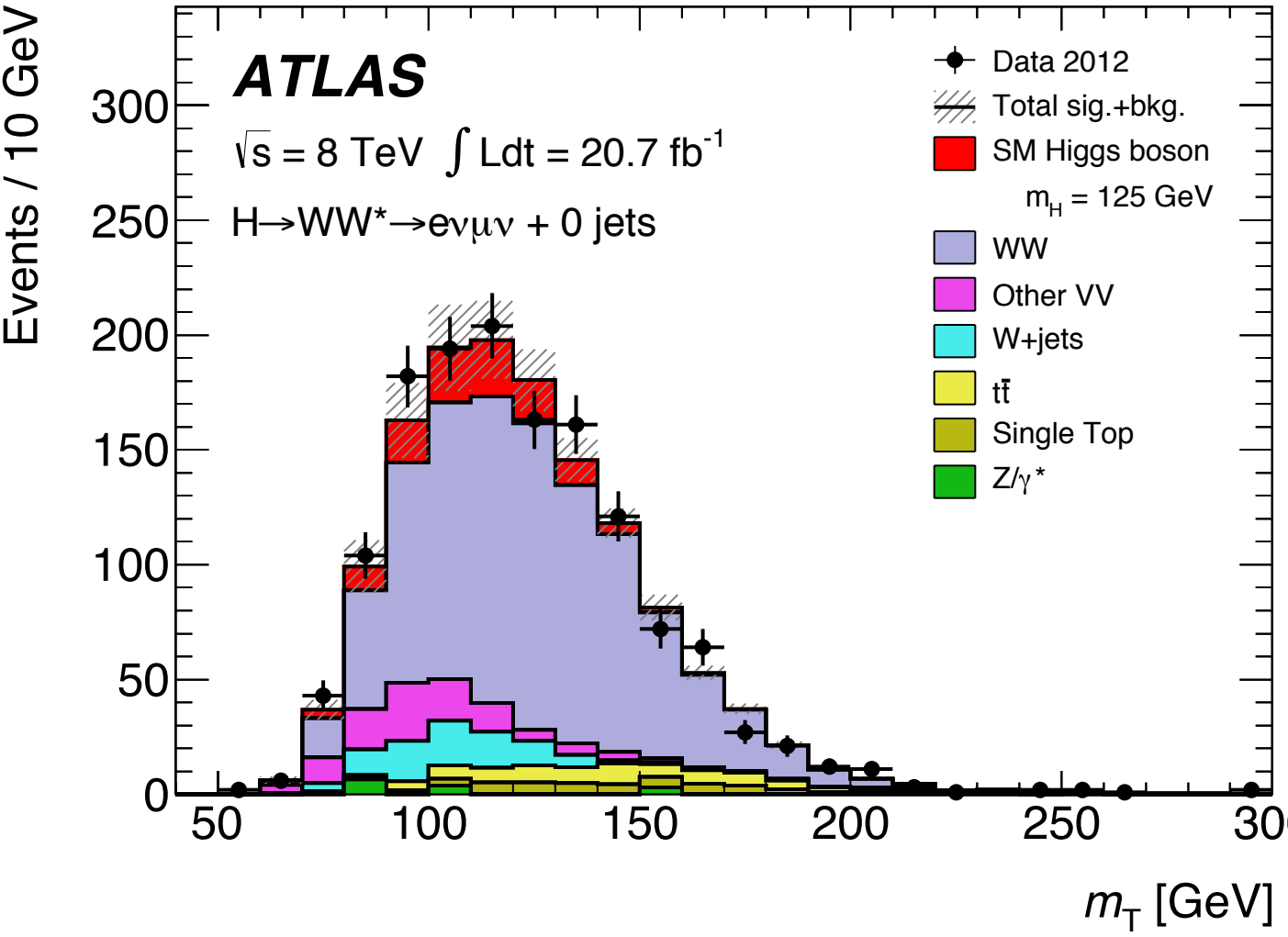

Caption

Distribution of the transverse mass, **mT**, for events in the H→WW*→lνlν signal regions in the 8 TeV data. The plot is shown for the **eμ** channel in **Njet = 0** final states. The distributions are shown **prior to splitting the samples into two mll regions** for the eμ channel in the Njet = 0 and = 1 cases. The WW, top-quark, and Z/γ* → ll backgrounds predicted by MC simulation are scaled using the normalisation from the corresponding control regions described in the text, and the W+jets prediction is from the data-driven estimate. The signal is stacked on top of the background. The hatched area represents the uncertainty on the signal and background yields from statistical, experimental, and theoretical sources.

Auxiliary Fig. 29b [1]

Hong

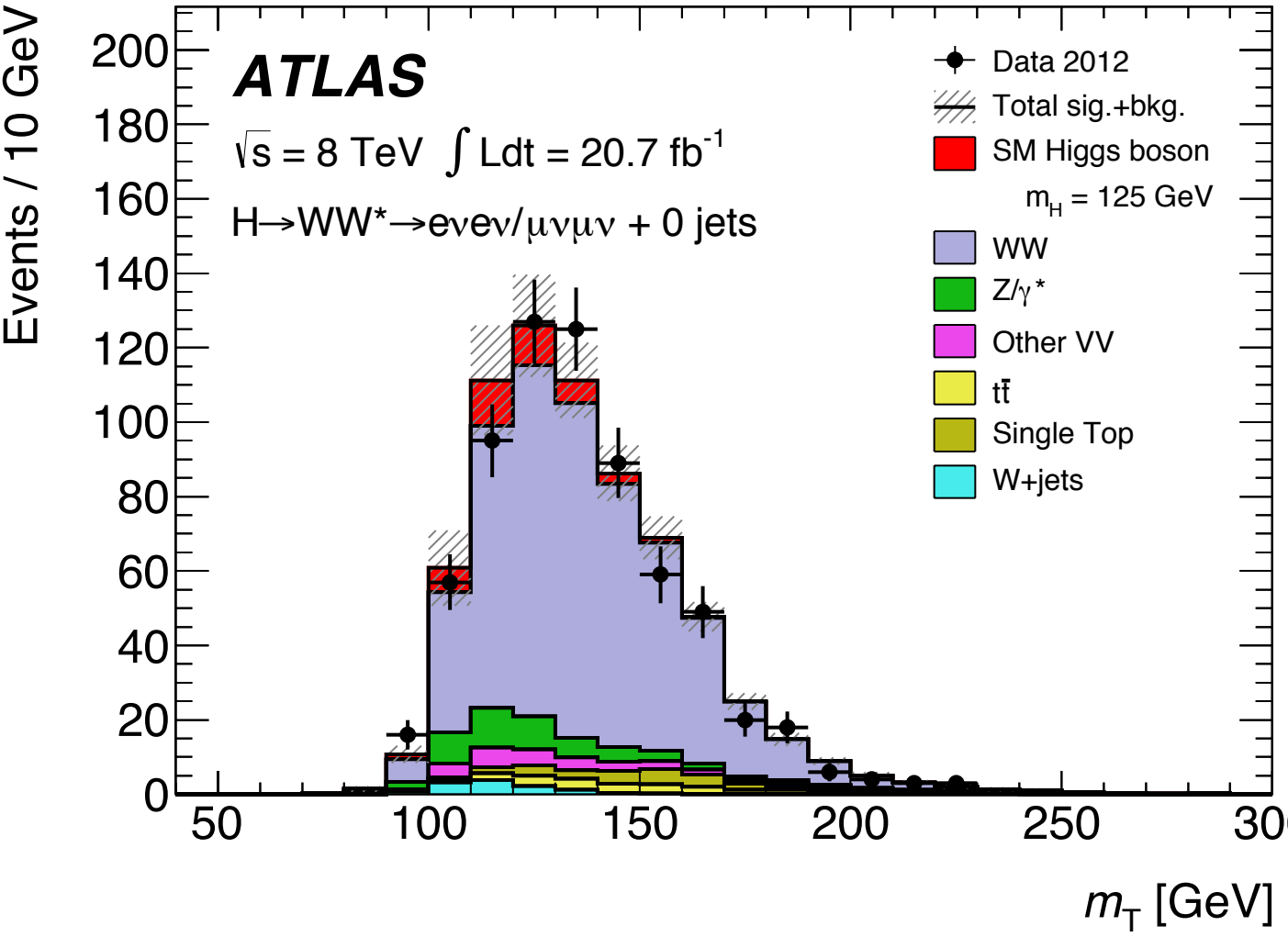

Caption

Distribution of the transverse mass, **mT**, for events in the H→WW*→lνlν signal regions in the 8 TeV data. The plot is shown for the **ee/μμ** channel in Njet = 0 final state. The distributions are **shown prior to splitting the samples into two mll regions** for the eμ channel in the Njet = 0 and = 1 cases. The WW, top-quark, and Z/γ* → ll backgrounds predicted by MC simulation are scaled using the normalisation from the corresponding control regions described in the text, and the W+jets prediction is from the data-driven estimate. The signal is stacked on top of the background. The hatched area represents the uncertainty on the signal and background yields from statistical, experimental, and theoretical sources.

Auxiliary Fig. 29c [1]

Hong

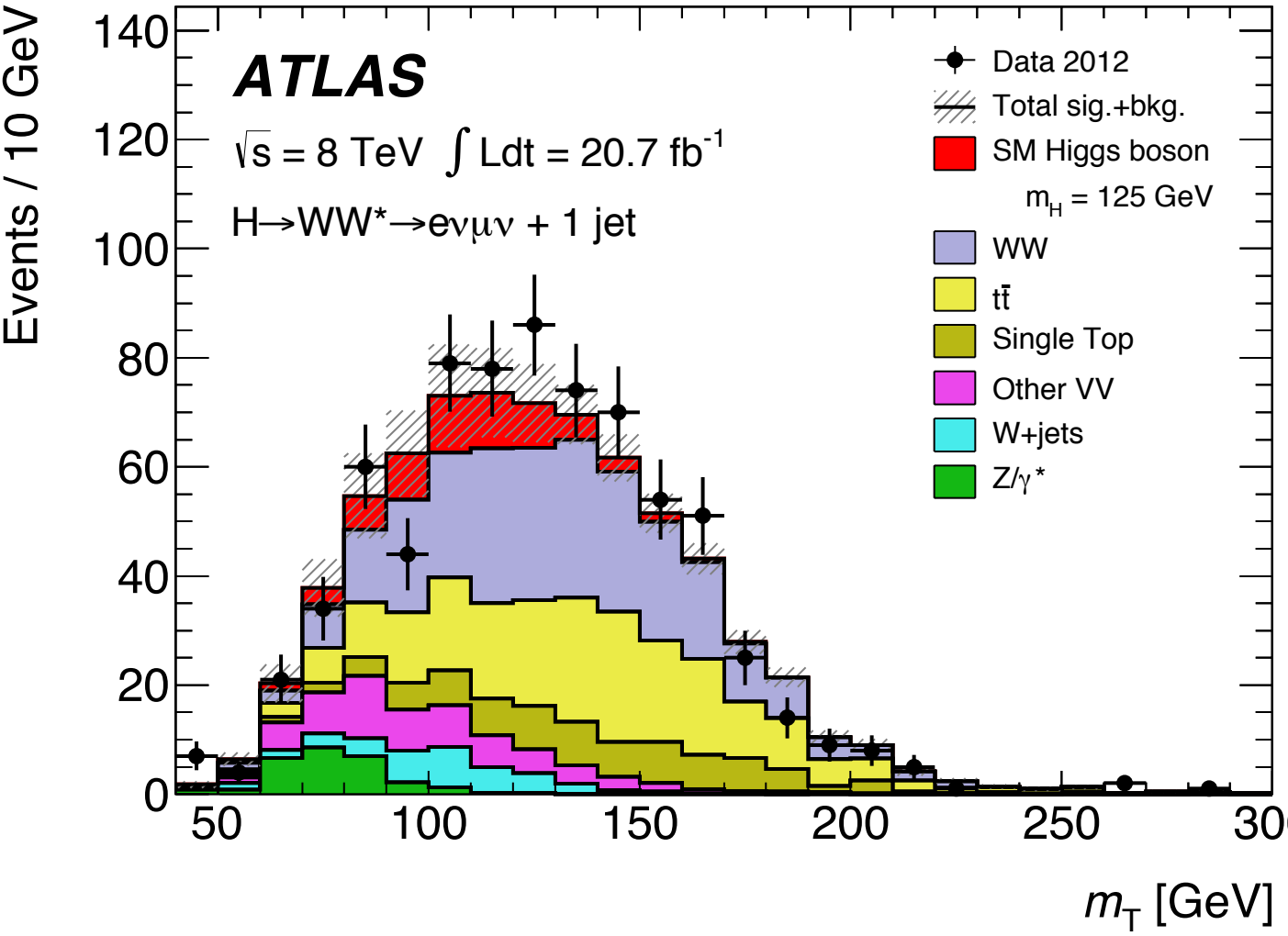

Caption

Distribution of the transverse mass, **mT**, for events in the H→WW*→lνlν signal regions in the 8 TeV data. The plot is shown for the **eμ** channel in **Njet = 1** final state. The distributions are **shown prior to splitting the samples into two mll regions** for the eμ channel in the Njet = 0 and = 1 cases. The WW, top-quark, and Z/γ* → ll backgrounds predicted by MC simulation are scaled using the normalisation from the corresponding control regions described in the text, and the W+jets prediction is from the data-driven estimate. The hatched area represents the uncertainty on the signal and background yields from statistical, experimental, and theoretical sources.

Auxiliary Fig. 29d [1]

Hong

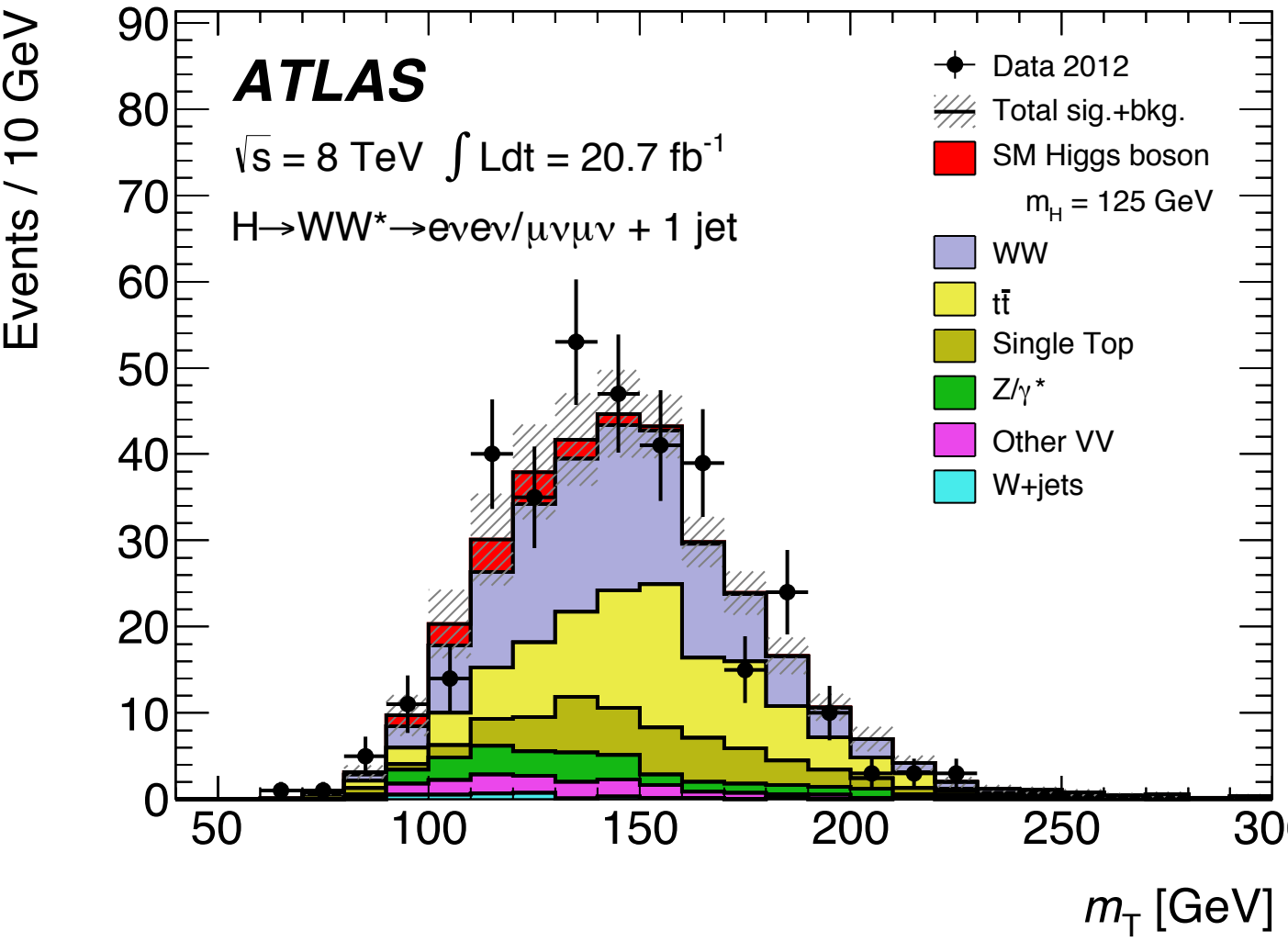

Caption

Distribution of the transverse mass, **mT**, for events in the H→WW*→lνlν signal regions in the 8 TeV data. The plot is shown for the **ee/μμ** channels in **Njet = 1** final state. The distributions are **shown prior to splitting the samples into two mll regions** for the eμ channel in the Njet = 0 and = 1 cases. The WW, top-quark, and $Z/\gamma^* \rightarrow ll$ backgrounds predicted by MC simulation are scaled using the normalisation from the corresponding control regions described in the text, and the W+jets prediction is from the data-driven estimate. The signal is stacked on top of the background. The hatched area represents the uncertainty on the signal and background yields from statistical, experimental, and theoretical sources.

Auxiliary Fig. 29e [1]

Hong

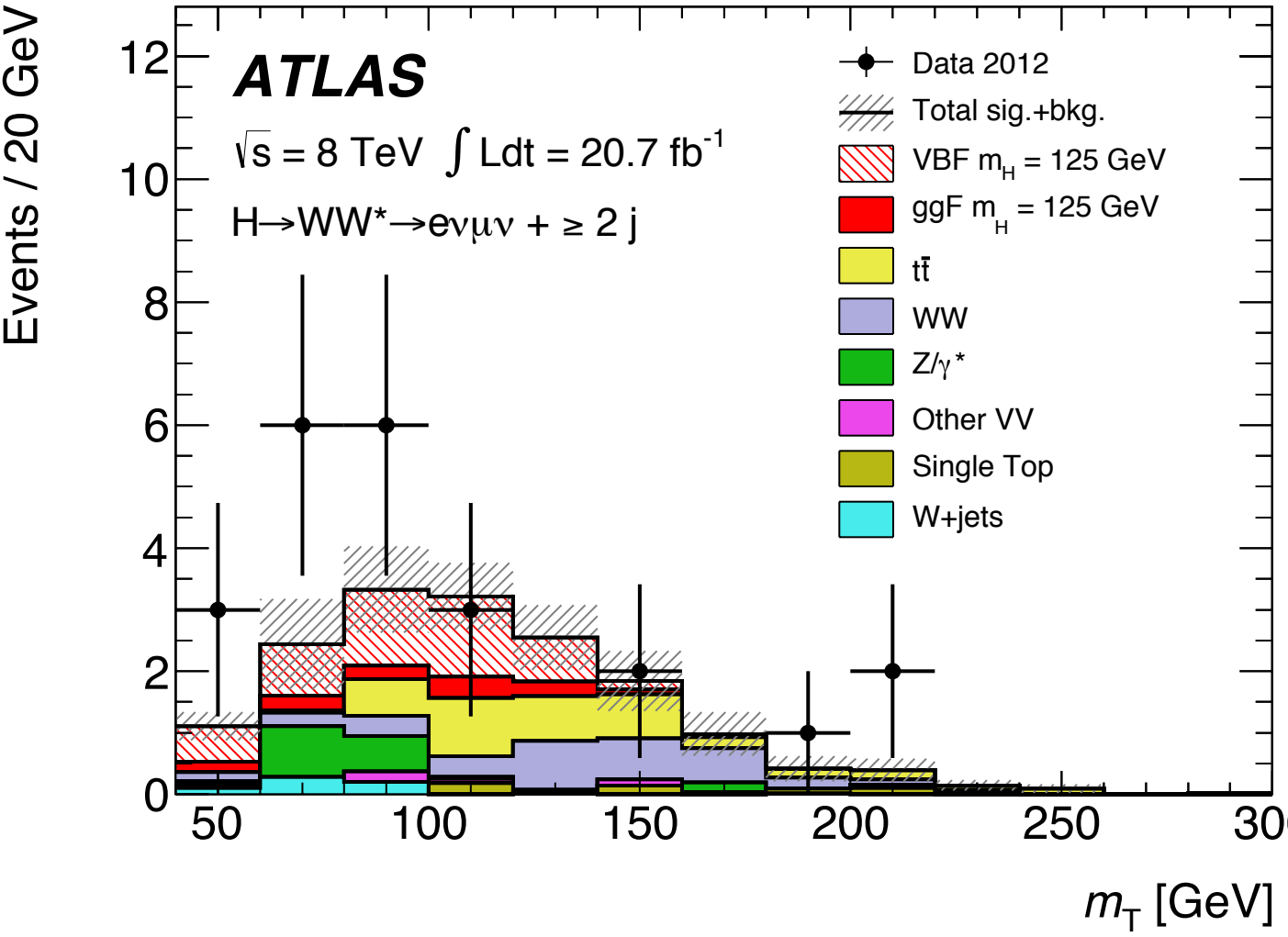

Caption

Distribution of the transverse mass, **mT**, for events in the H→WW*→lνlν signal regions in the 8 TeV data. The plot is shown for the **eμ** channel in **Njet ≥ 2** final state. The distributions are **shown prior to splitting the samples into two mll regions for the eμ** channel in the Njet = 0 and = 1 cases. The WW, top-quark, and Z/γ* → ll backgrounds predicted by MC simulation are scaled using the normalisation from the corresponding control regions described in the text, and the W+jets prediction is from the data-driven estimate. The signal is stacked on top of the background. For the Njet ≥ 2 final state, the signal is plotted separately for the ggF and VBF production processes. The hatched area represents the uncertainty on the signal and background yields from statistical, experimental, and theoretical sources.

Auxiliary Fig. 29f [1]

Hong

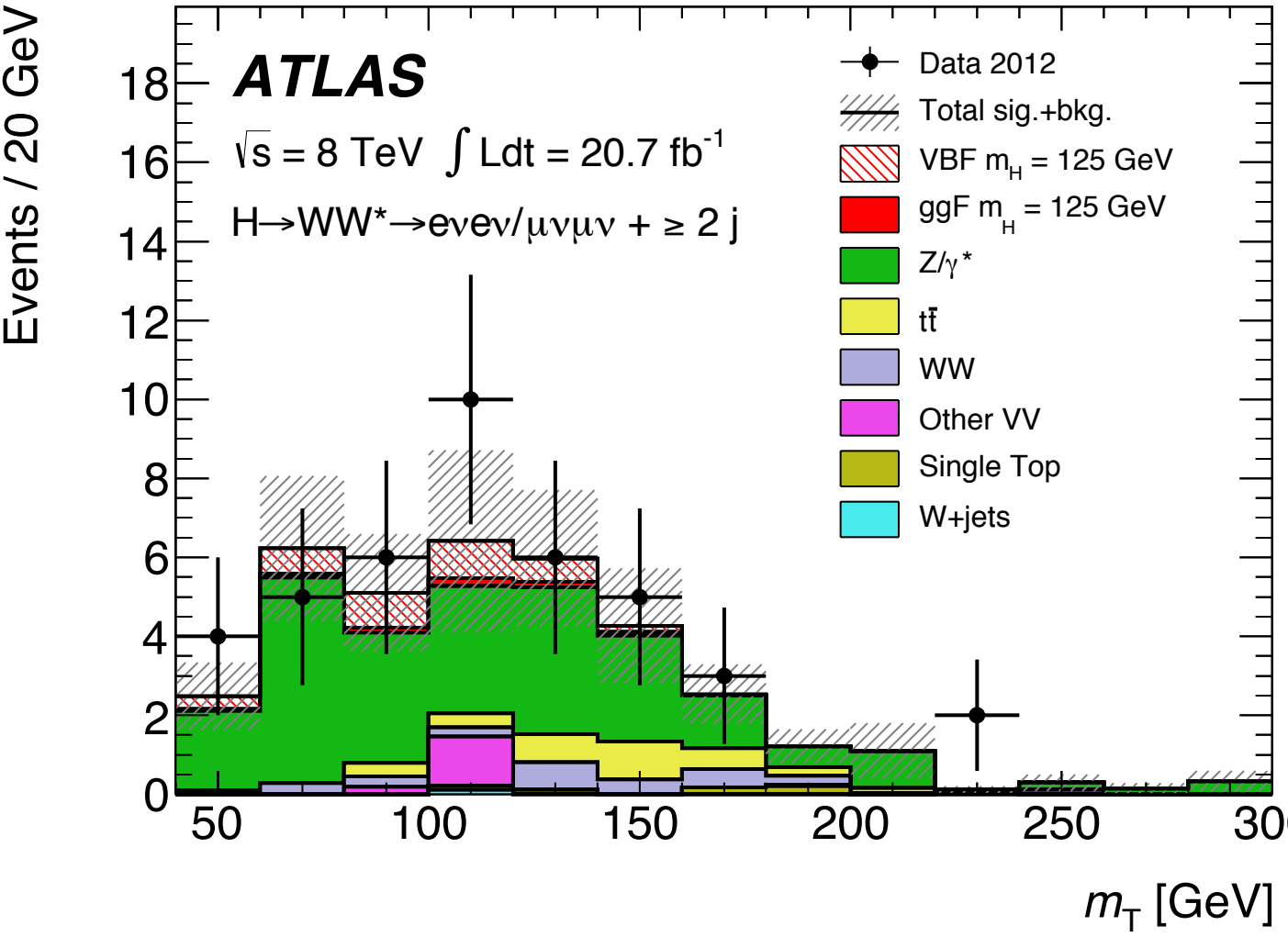

Caption

Distribution of the transverse mass, **mT**, for events in the H→WW∗→lνlν signal regions in the 8 TeV data. The plot is shown for the **ee/μμ** channel in **Njet ≥ 2** final state. The distributions are **shown prior to splitting the samples into two mll regions for the eμ** channel in the Njet = 0 and = 1 cases. The WW, top-quark, and Z/γ∗ → ll backgrounds predicted by MC simulation are scaled using the normalisation from the corresponding control regions described in the text, and the W+jets prediction is from the data-driven estimate. The signal is stacked on top of the background. For the Njet ≥ 2 final state, the signal is plotted separately for the ggF and VBF production processes. The hatched area represents the uncertainty on the signal and background yields from statistical, experimental, and theoretical sources.

Auxiliary Fig. 30a [1]

Hong

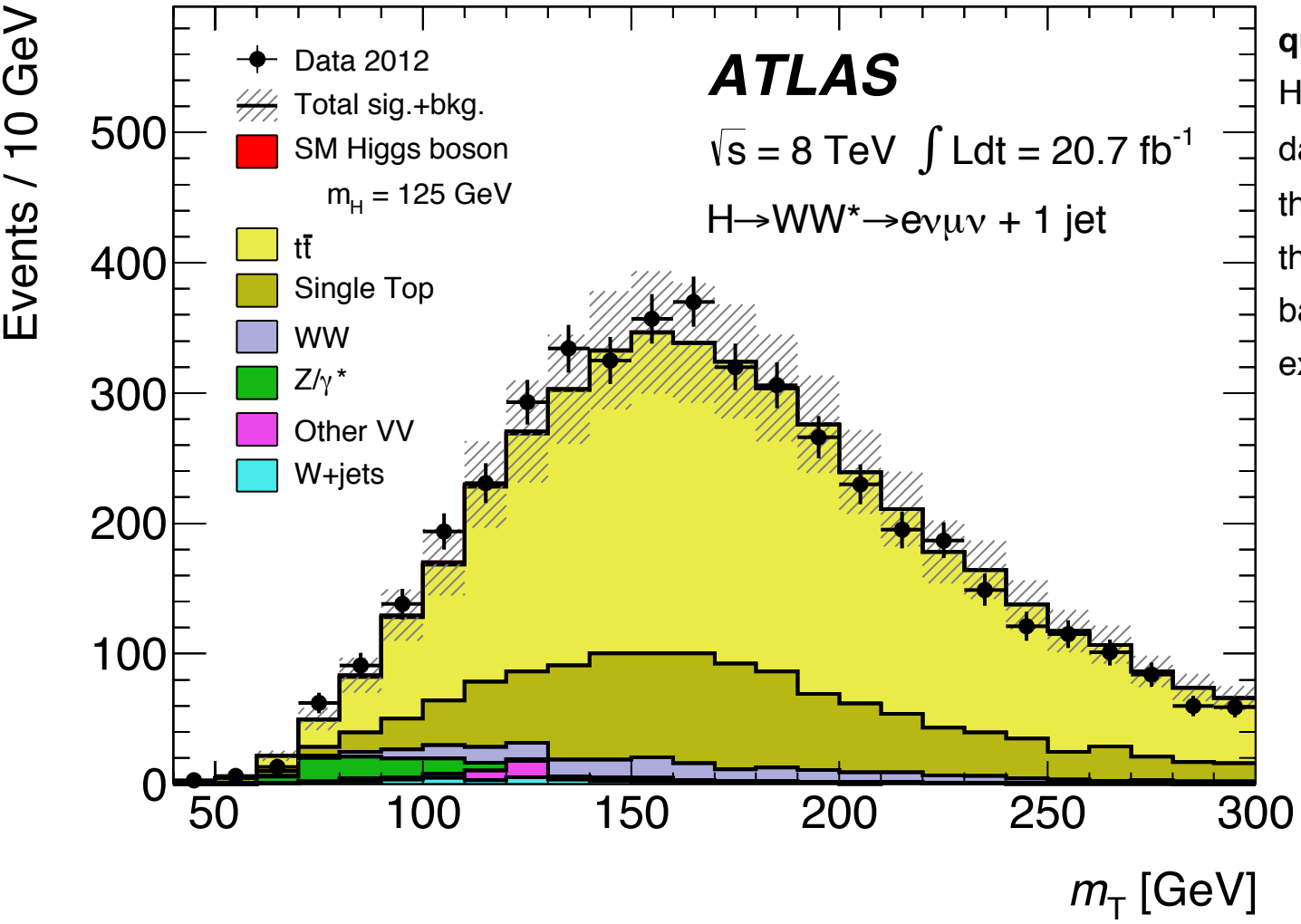

Caption

Distributions of **mT** in the **Njet = 1 top-quark background control region** for the H→ WW∗→ lνlν analysis of the 8 TeV data. The MC expectation is normalised to the data. The hatched area represents the uncertainty on the signal and background yields from statistical, experimental, and theoretical sources.

Auxiliary Fig. 30b [1]

Hong

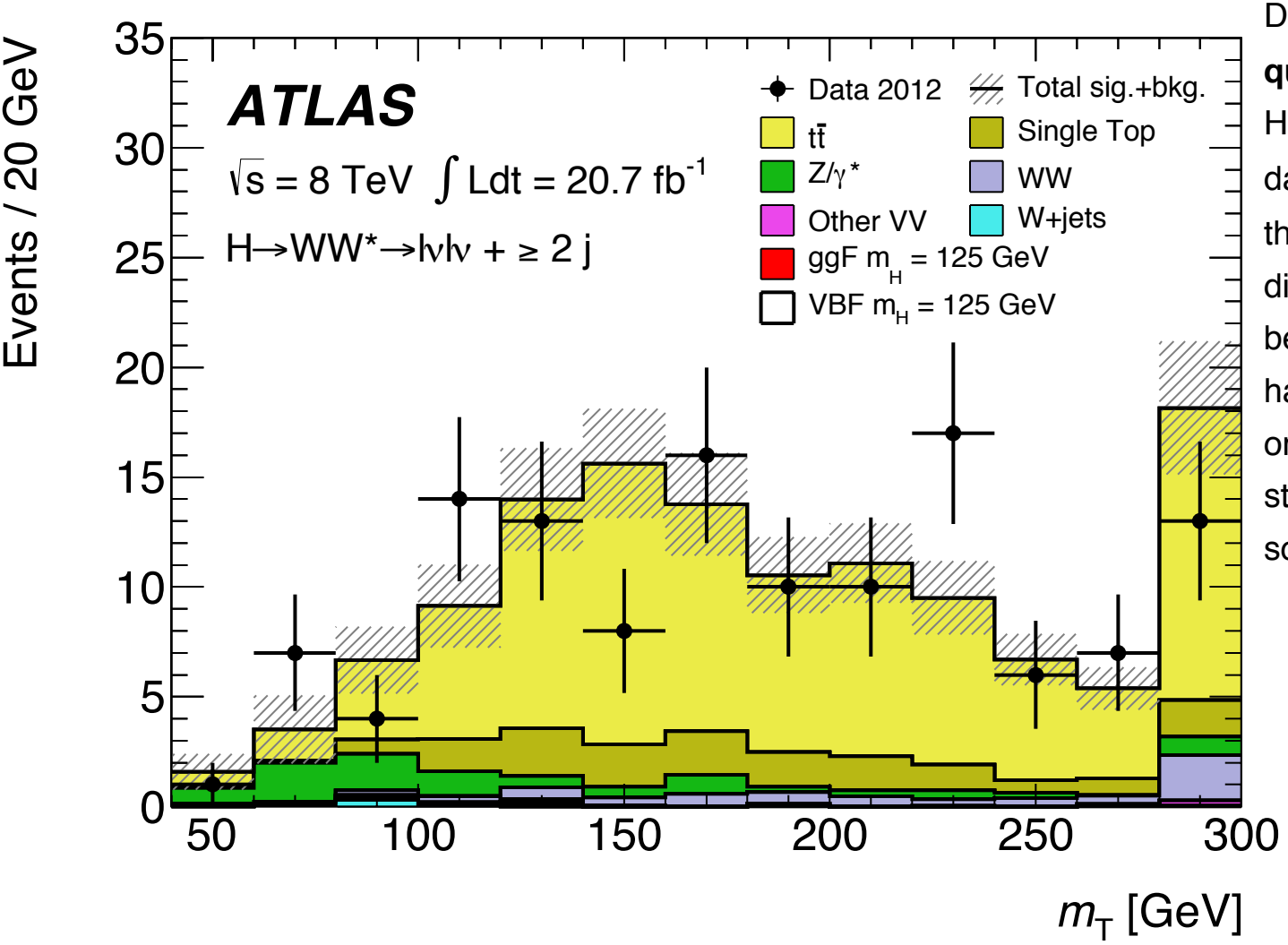

Caption

Distributions of **mT** in the **Njet ≥ 2 top-quark background control region** for the H→ WW∗→ lνlν analysis of the 8 TeV data. The MC expectation is normalised to the data. The right-most bin in the Njet ≥ 2 distribution contains events that would lie beyond the right edge of the figure. The hatched area represents the uncertainty on the signal and background yields from statistical, experimental, and theoretical sources.

Auxiliary Fig. 34a [2]

Hong

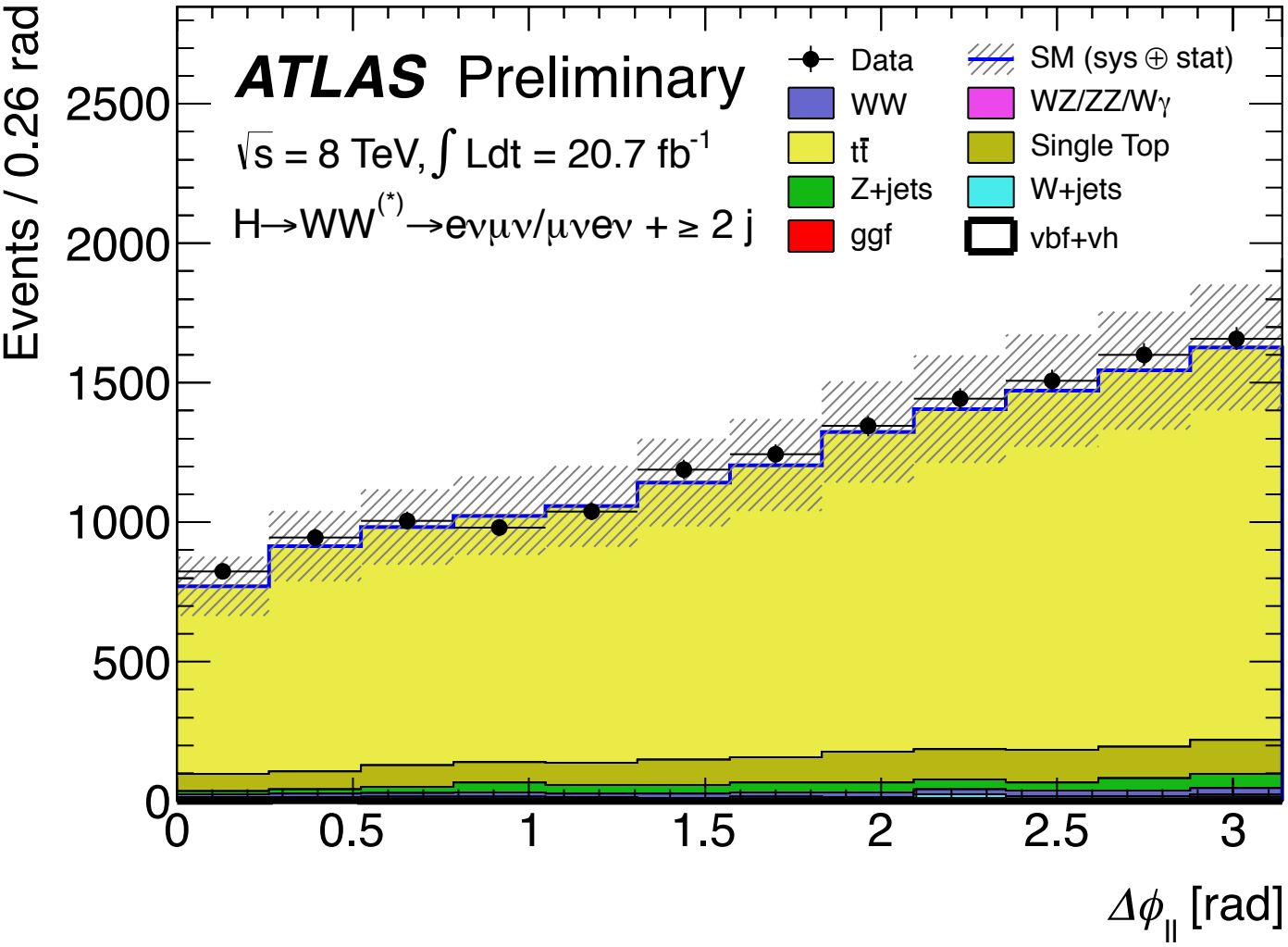

Caption

The **|ΔφlII** distribution **after the pTtot < 45 GeV cut in the top CR**, defined by the requirement of one and only one b tagged jet. pTtot is defined as the total transverse momentum of all leptons, jets and missing ET passing the selection. The shaded area represents the uncertainty on the signal and background yields from statistical, experimental, and theoretical sources.

Auxiliary Fig. 34b [2]

Hong

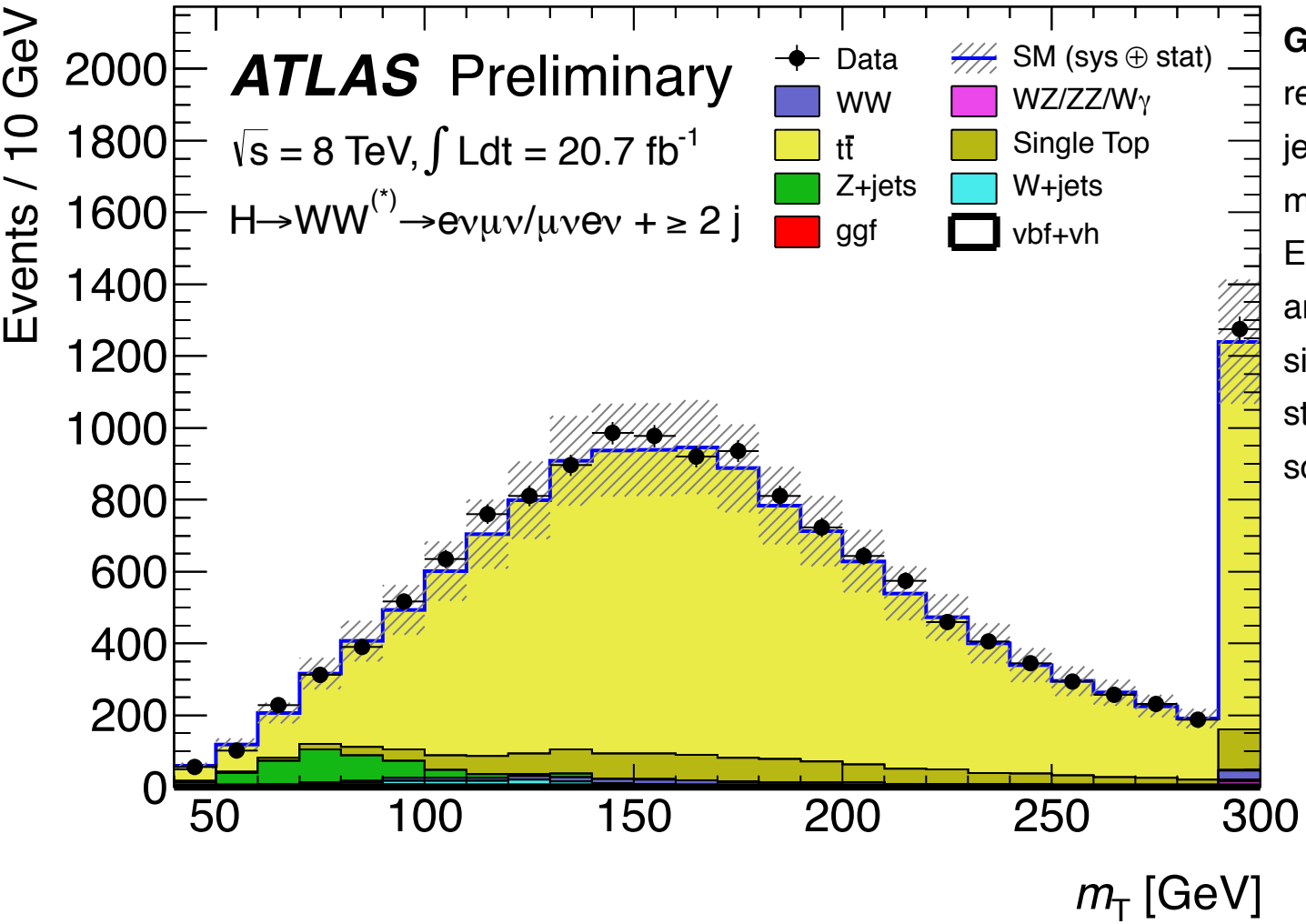

Caption

The **mT** distribution **after the pTtot < 45 GeV cut in the top CR**, defined by the requirement of one and only one b tagged jet. pTtot is defined as the total transverse momentum of all leptons, jets and missing ET passing the selection. The shaded area represents the uncertainty on the signal and background yields from statistical, experimental, and theoretical sources.

Auxiliary Fig. 34c [2]

Hong

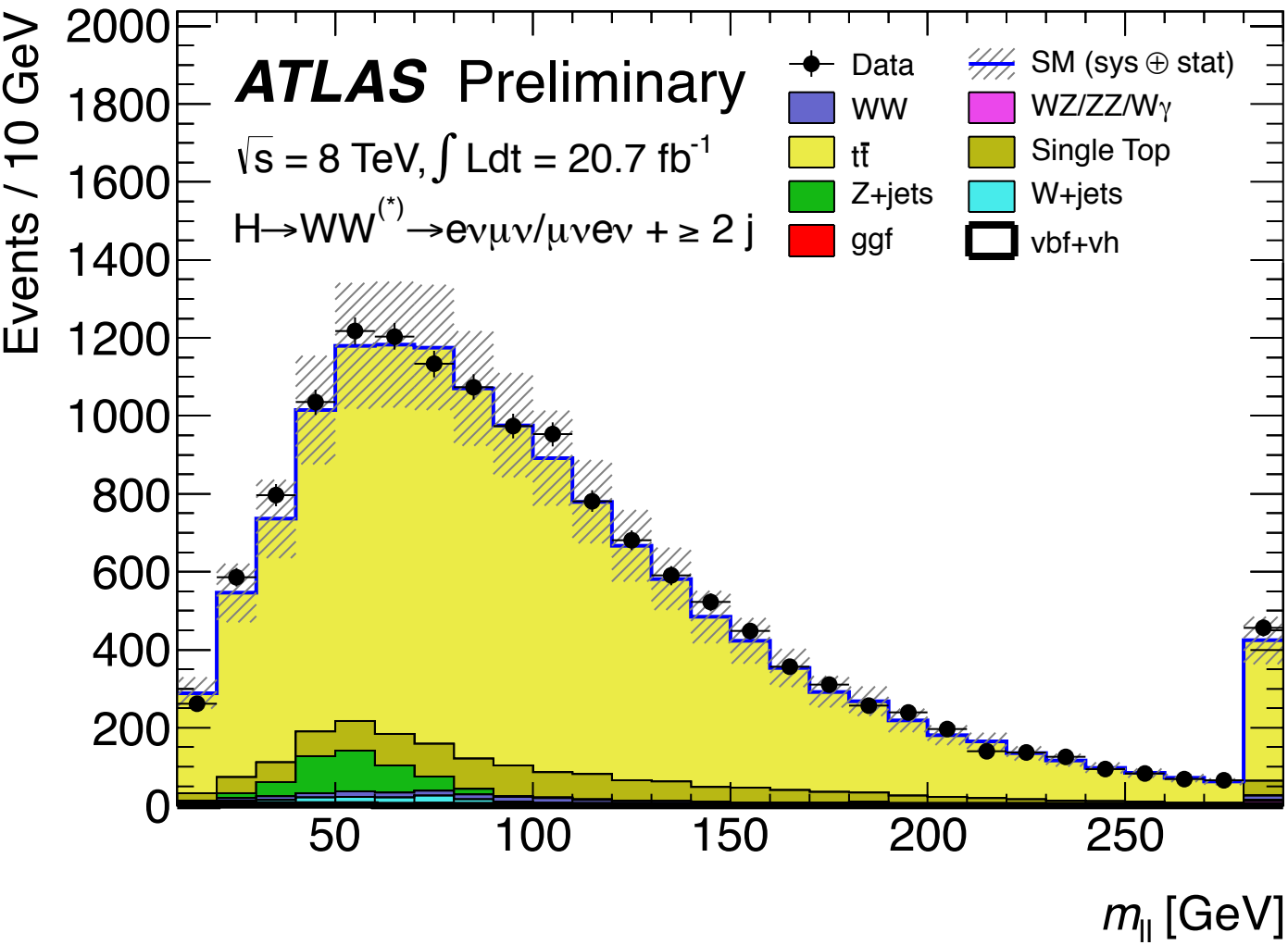

Caption

The **mll** distribution **after the pTtot < 45 GeV cut in the top CR**, defined by the requirement of one and only one b tagged jet. pTtot is defined as the total transverse momentum of all leptons, jets and missing ET passing the selection. The shaded area represents the uncertainty on the signal and background yields from statistical, experimental, and theoretical sources.

Auxiliary Fig. 31a [1]

Hong

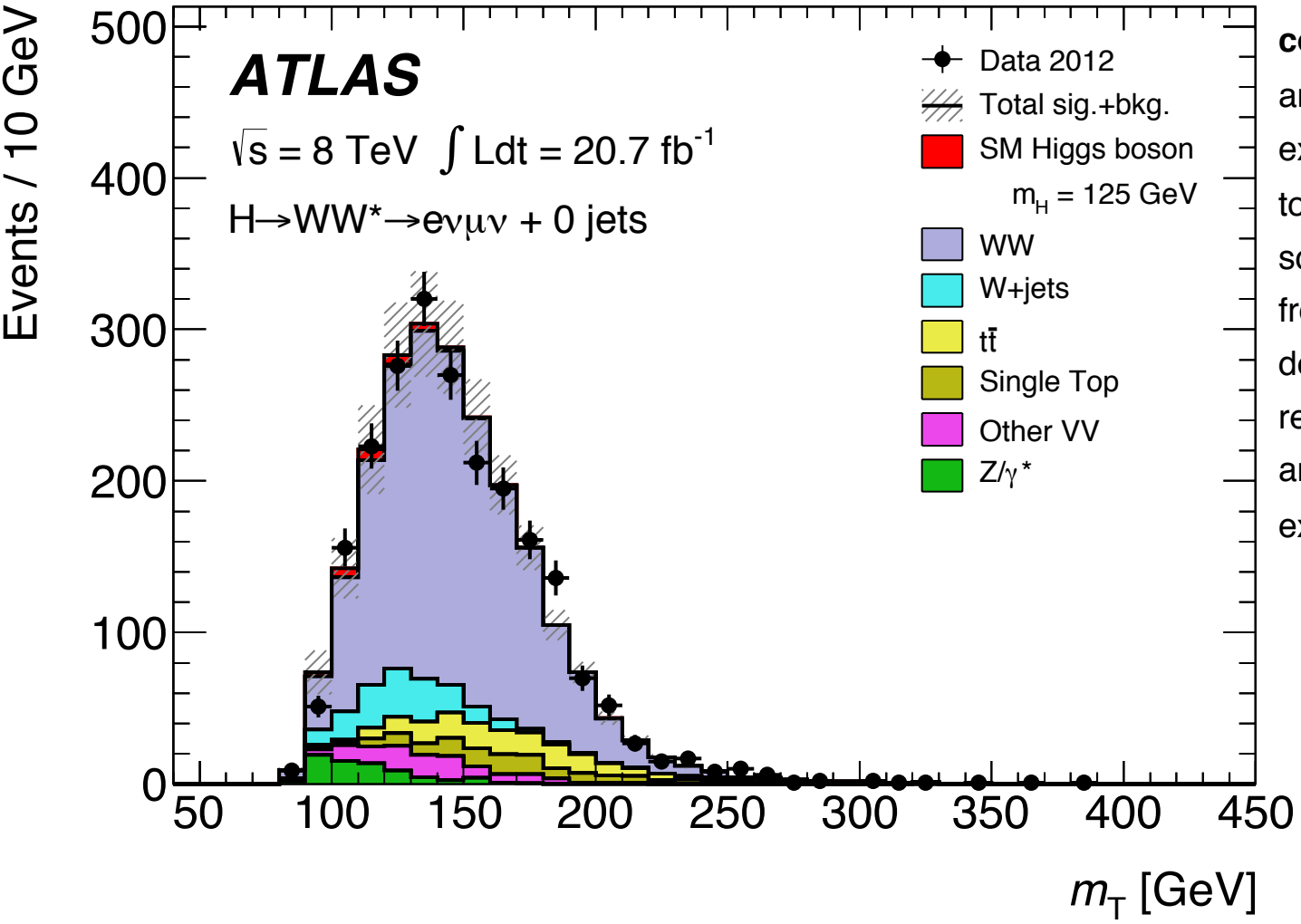

Caption

Distributions of **mT** in the **Njet = 0 WW control region** in the H→ WW∗→ lνlν analysis for the 8 TeV data. The MC expectation is normalised to the data. The top-quark and Z → ττ backgrounds are scaled using the normalisation derived from the corresponding control regions described in the text. The hatched area represents the uncertainty on the signal and background yields from statistical, experimental, and theoretical sources.

Auxiliary Fig. 31b [1]

Hong

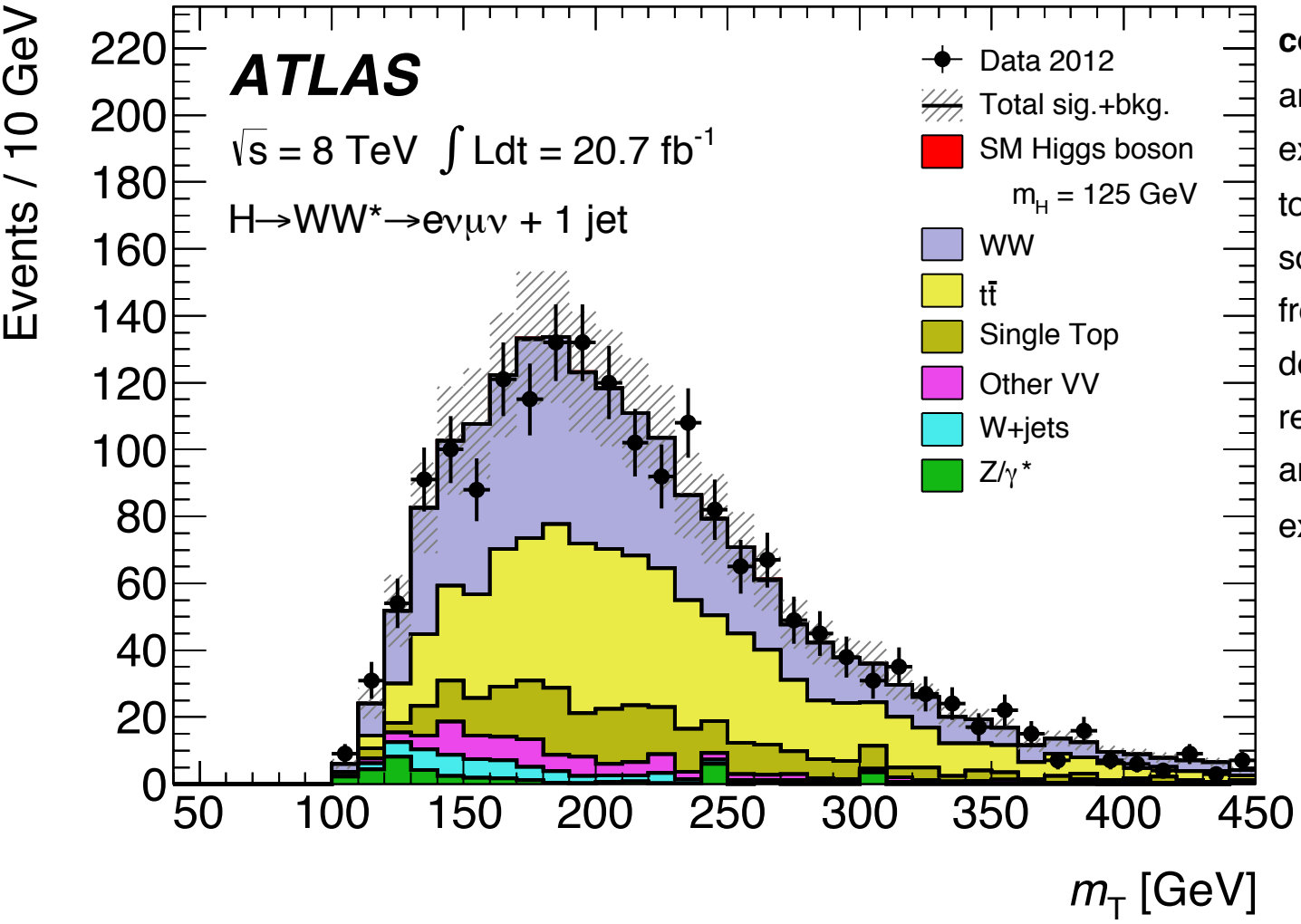

Caption

Distributions of **mT** in the **Njet = 1 WW control region** in the H→ WW∗→ lνlν analysis for the 8 TeV data. The MC expectation is normalised to the data. The top-quark and Z → ττ backgrounds are scaled using the normalisation derived from the corresponding control regions described in the text. The hatched area represents the uncertainty on the signal and background yields from statistical, experimental, and theoretical sources.

Auxiliary Fig. 32a [1]

Hong

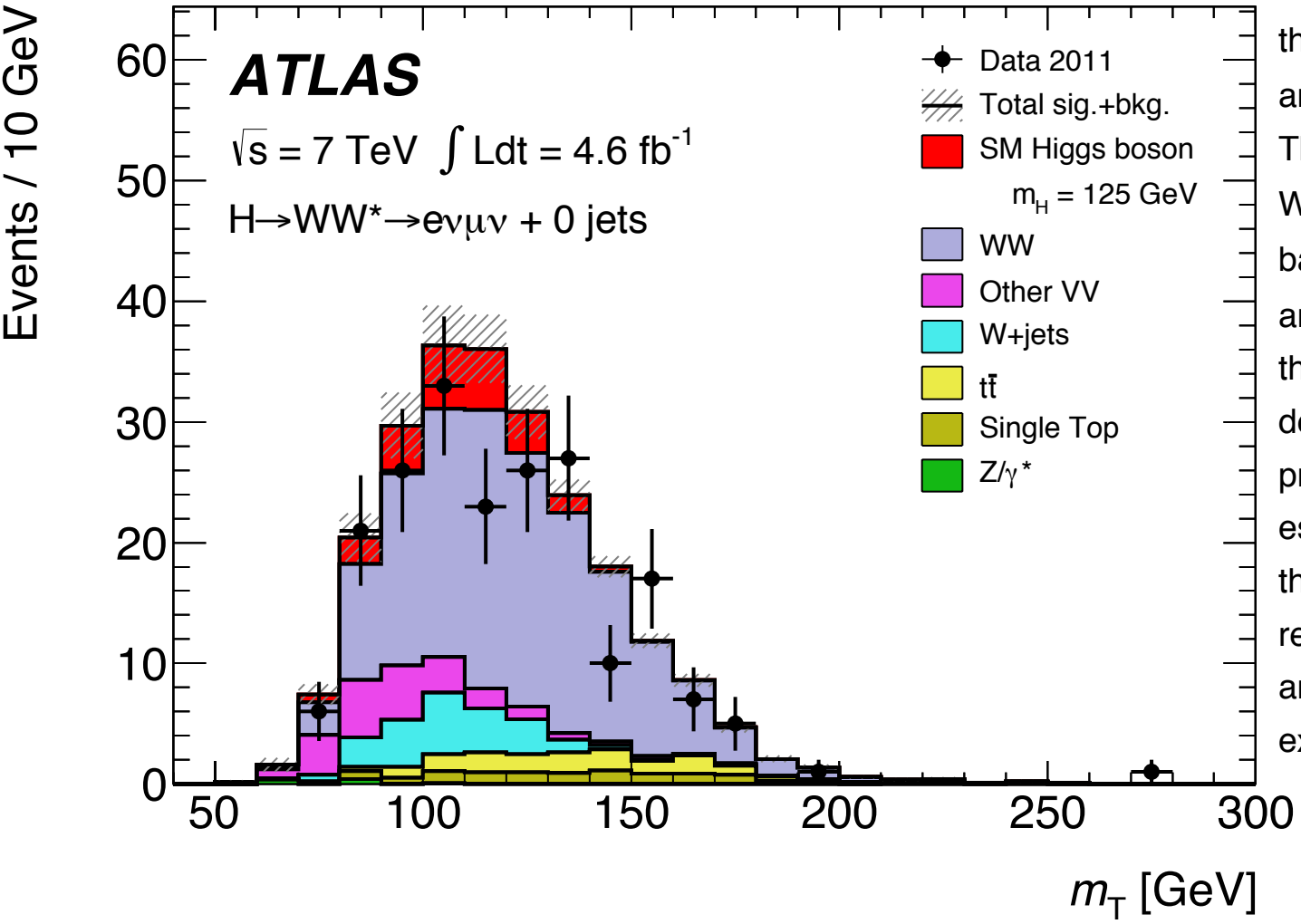

Caption

Distribution of transverse mass, **mT**, for the signal regions of the H→ WW∗→ lνlν analysis of the **7 TeV data with Njet = 0**. The plot is shown for the **eμ** channel. The WW, top-quark, and Z/γ∗ → ll backgrounds predicted by MC simulation are scaled using the normalisation from the corresponding control regions described in the text, and the W+jets prediction is from the data-driven estimate. The signal is stacked on top of the background. The hatched area represents the uncertainty on the signal and background yields from statistical, experimental, and theoretical sources.

Auxiliary Fig. 32b [1]

Hong

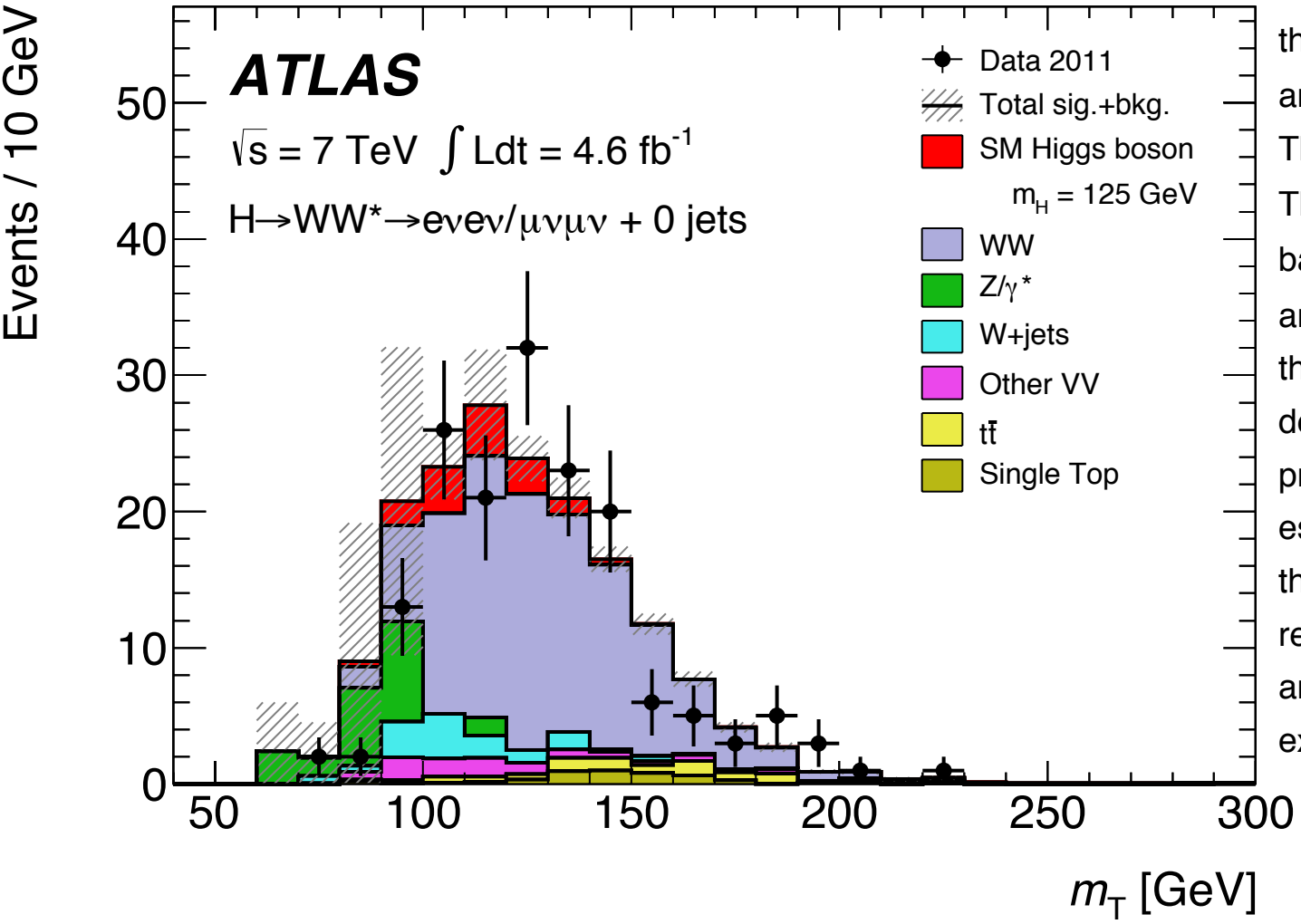

Caption

Distribution of transverse mass, **mT**, for the signal regions of the H→ WW∗→ lνlν analysis of the **7 TeV data with Njet = 0** . The plot is shown for the **ee/μμ** channel. The WW, top-quark, and Z/γ∗ → ll backgrounds predicted by MC simulation are scaled using the normalisation from the corresponding control regions described in the text, and the W+jets prediction is from the data-driven estimate. The signal is stacked on top of the background. The hatched area represents the uncertainty on the signal and background yields from statistical, experimental, and theoretical sources.

Auxiliary Fig. 32c [1]

Hong

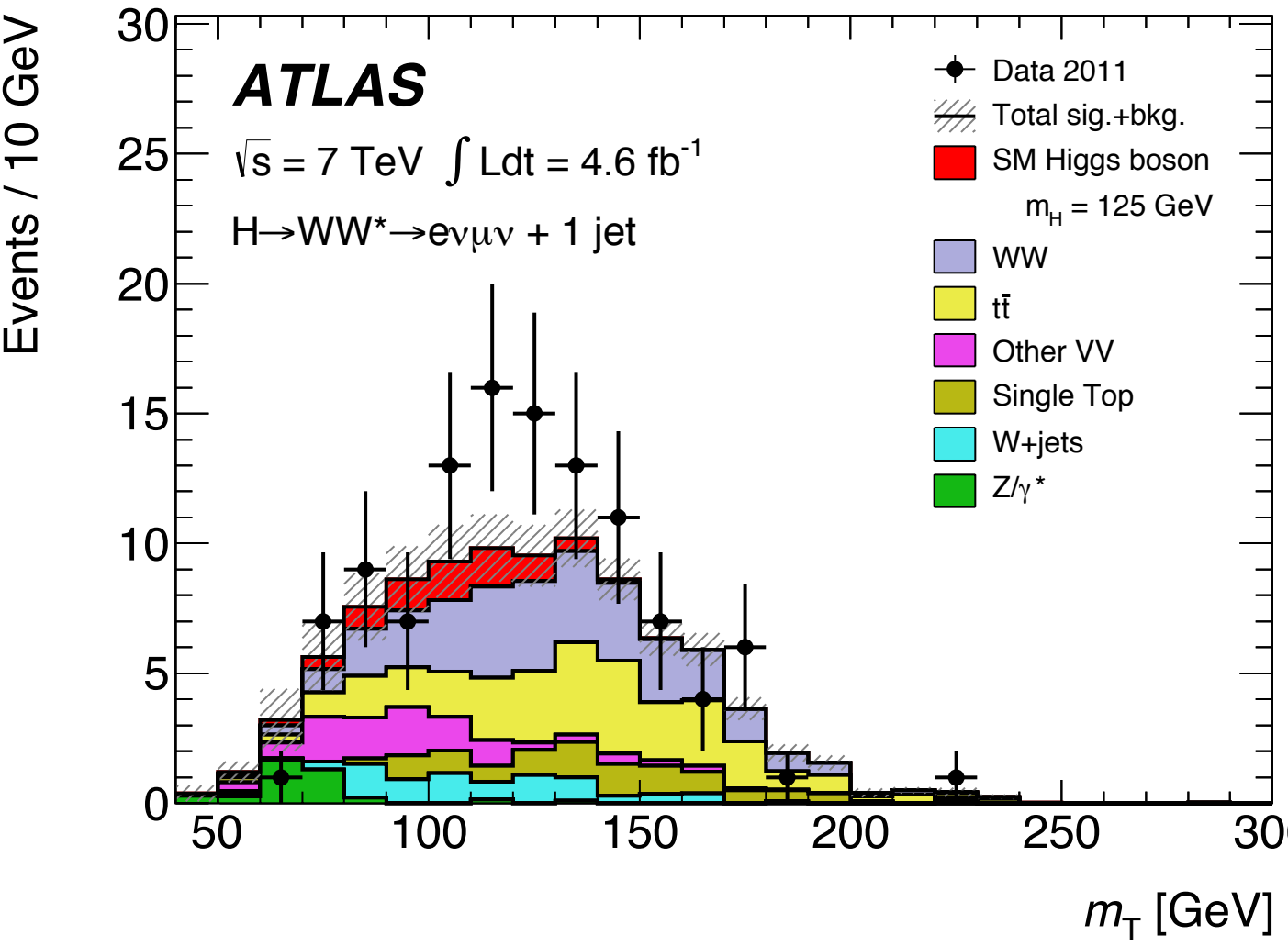

Caption

Distribution of transverse mass, mT, for the signal regions of the H→ WW∗→ lνlν analysis of the **7 TeV data with Njet = 1**. The plot is shown for the **eμ** channel. **Data with Njet ≥ 2 are included in the analysis but are not shown here due to the small number of events passing all selection.** The WW, top-quark, and Z/γ∗ → ll backgrounds predicted by MC simulation are scaled using the normalisation from the corresponding control regions described in the text, and the W+jets prediction is from the data-driven estimate. The signal is stacked on top of the background. The hatched area represents the uncertainty on the signal and background yields from statistical, experimental, and theoretical sources.

Auxiliary Fig. 32d [1]

Hong

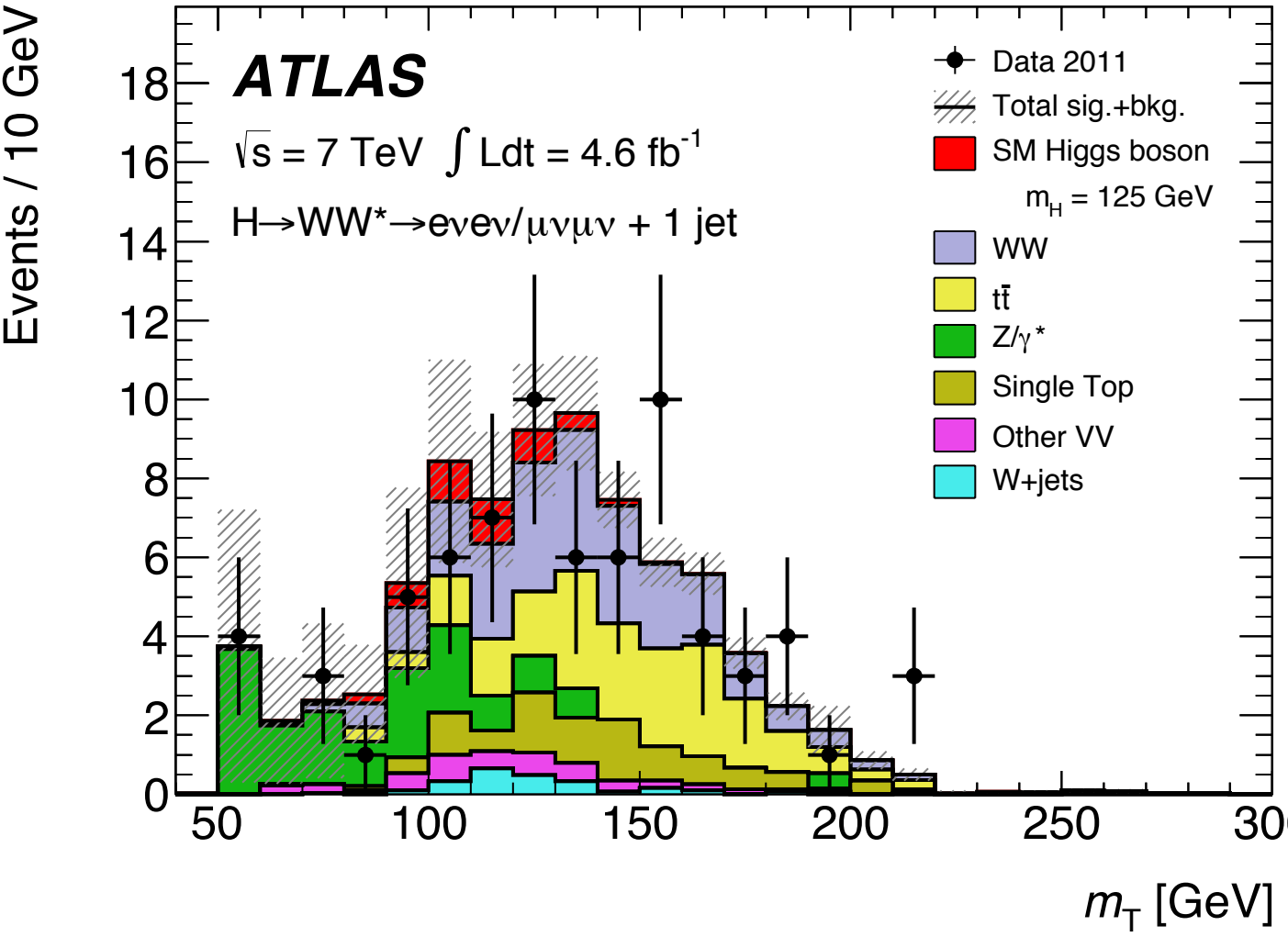

Caption

Distribution of transverse mass, **mT**, for the signal regions of the H→ WW∗→ lνlν analysis of the **7 TeV data with Njet = 1**. The plots are shown for the **ee/μμ** channels. **Data with Njet ≥ 2 are included in the analysis but are not shown here due to the small number of events passing all selection.** The WW, top-quark, and Z/γ∗ → ll backgrounds predicted by MC simulation are scaled using the normalisation from the corresponding control regions described in the text, and the W+jets prediction is from the data-driven estimate. The signal is stacked on top of the background. The hatched area represents the uncertainty on the signal and background yields from statistical, experimental, and theoretical sources.

Auxiliary Fig. 33 [1]

Hong

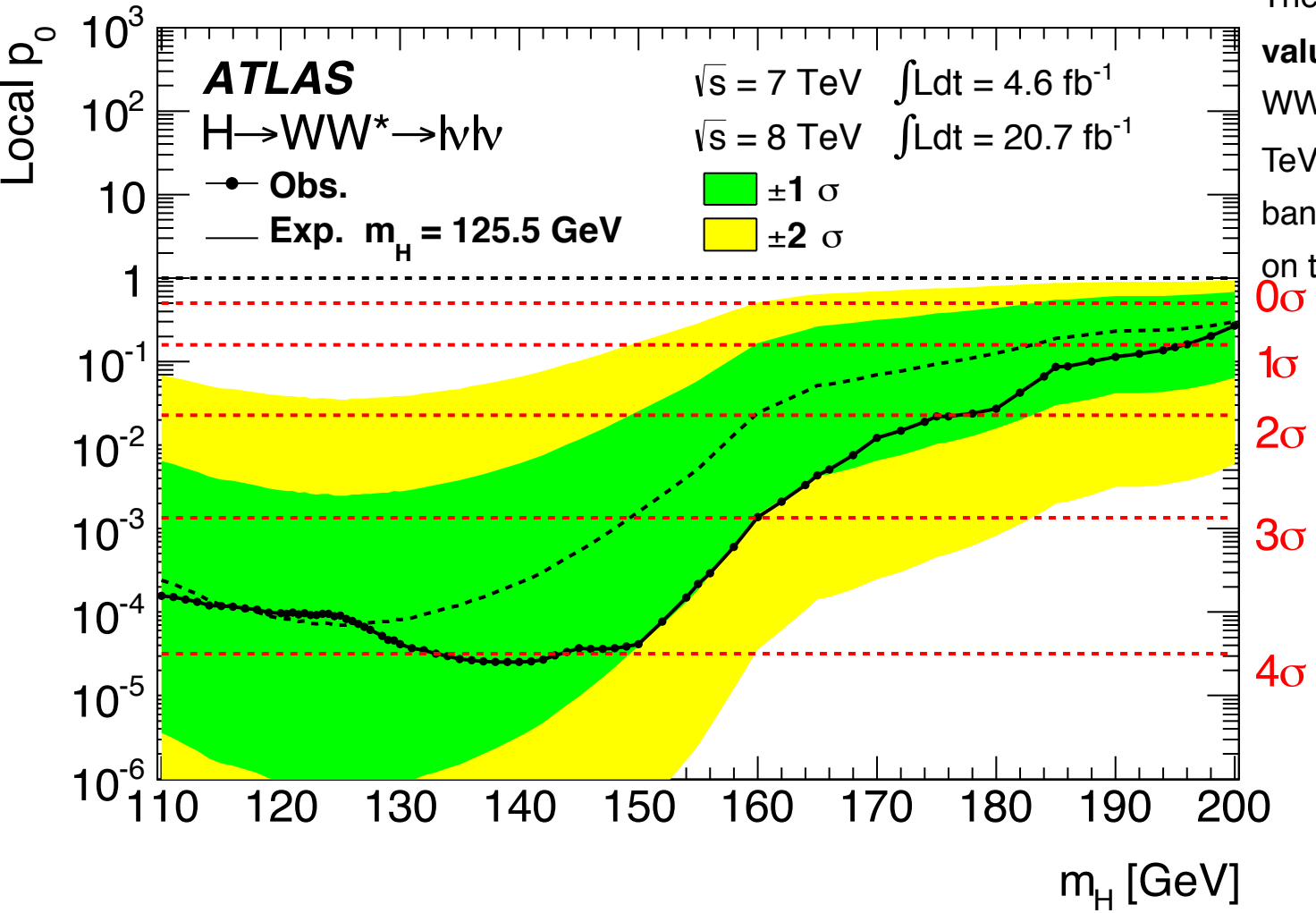

Caption

The expected and observed **local p0 values** as a function of mH for the H→ WW∗→ lνlν analysis of the combined 7 TeV and 8 TeV data. The green (yellow) band indicates the ±1σ (±2σ) uncertainty on the expected p0 curve.

Auxiliary Fig. 34 [1]

Hong

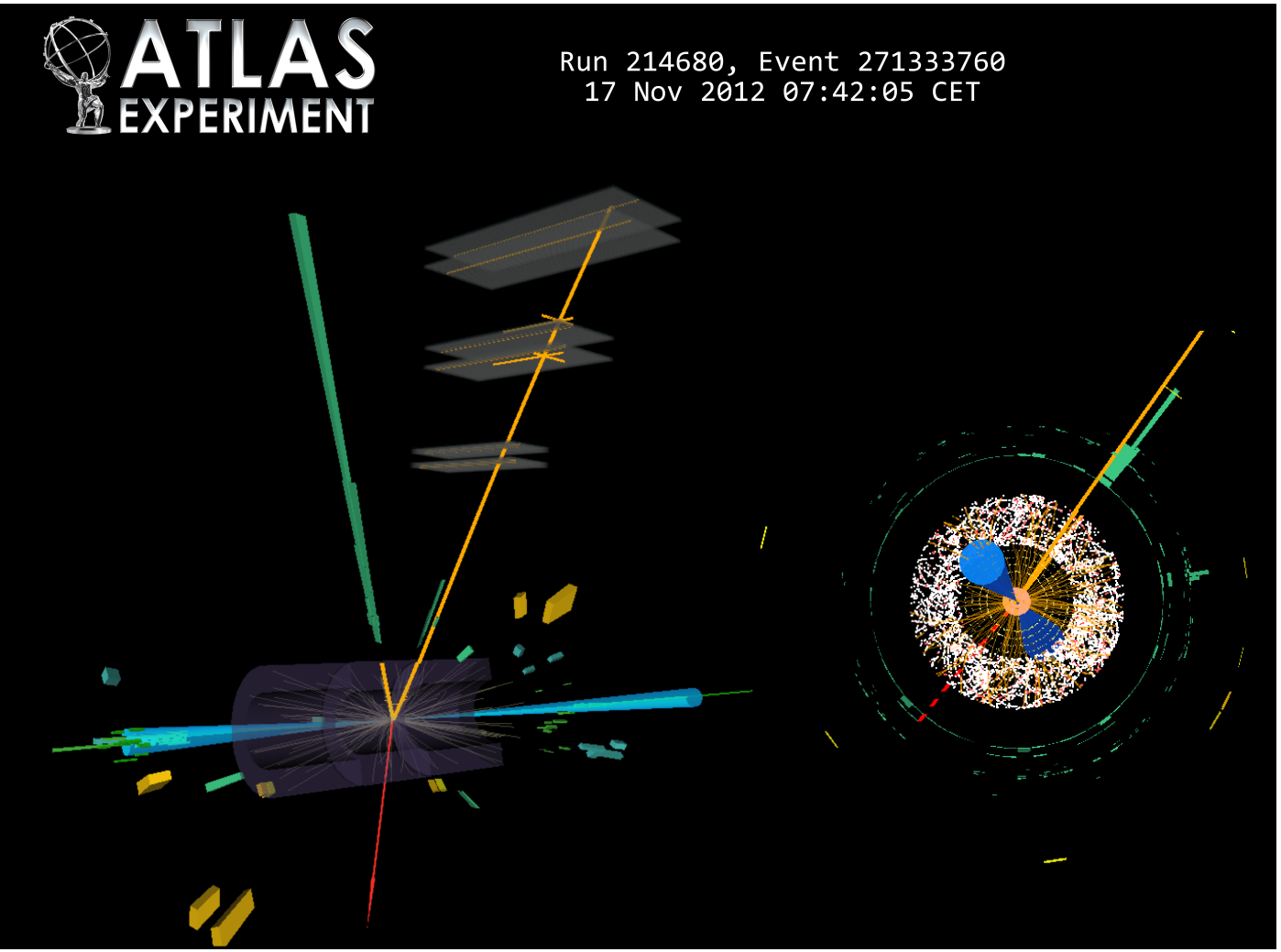

Caption

A **candidate event for H→WW*→evμv +2 jets produced via VBF**. The event variables are: mjj =1.5 TeV, lΔyjj l=6.6, mll =21 GeV, and mT = 95 GeV. For the figure on the left (starting from the top left going clockwise): the pT of the electron (thick green line) is 51 GeV, the pT of the muon (orange line) is 15 GeV, the pT of the jet (right cyan cone) is 68 GeV, the Emiss (thin dotted red line on the left) is 33 GeV, and the pT of the jet (left cyan cone) is 42 GeV. A view transverse to the beam direction is given on the right; here the Emiss is represented as a thick dotted line.

Auxiliary Fig. 32a [2]

Hong

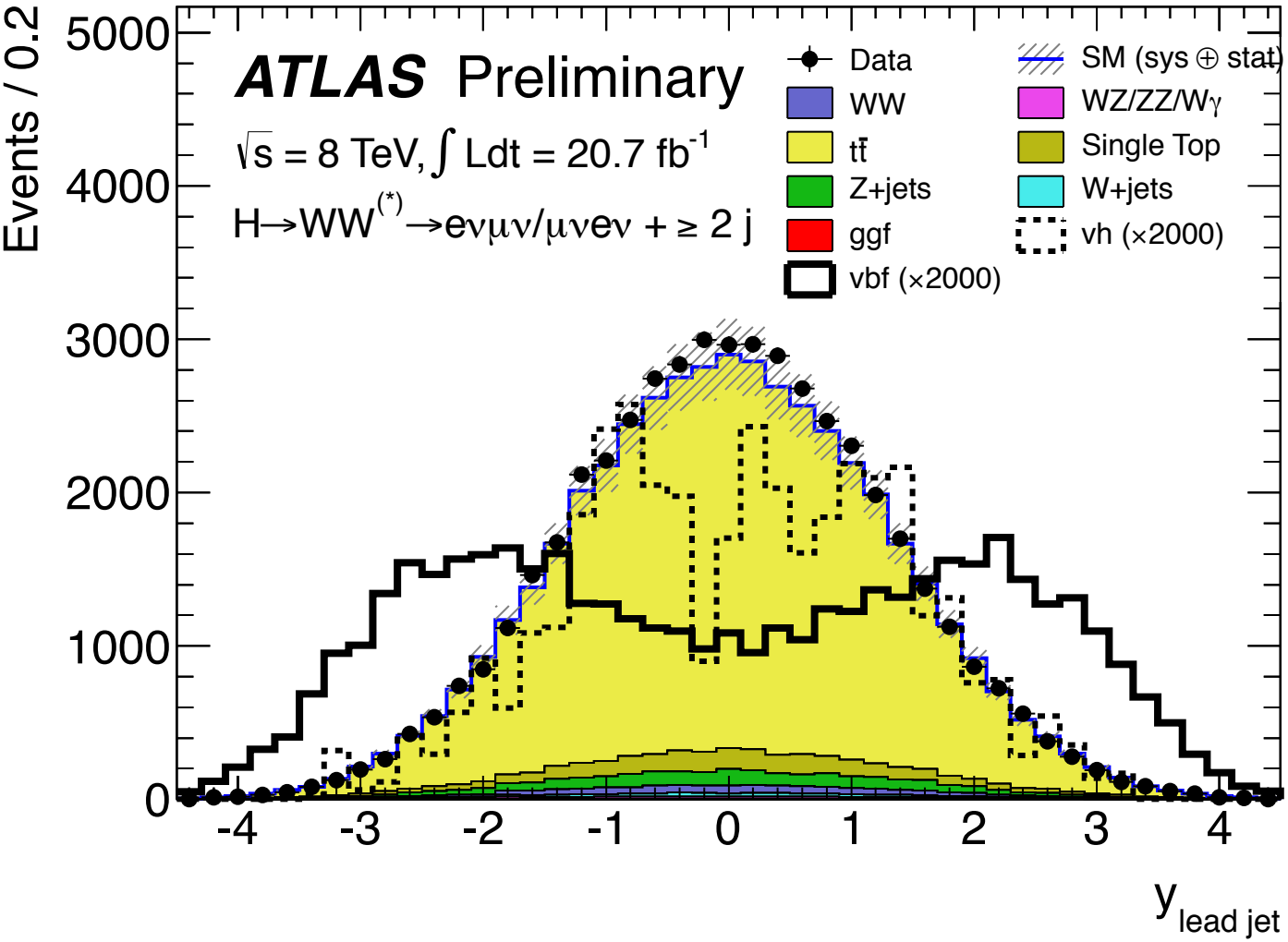

Caption

Rapidity distributions of the **leading jet**. The distribution is shown at the 2 jets requirement, the **signal is magnified by a factor 2000** to show the peculiar forward distribution of jets from the VBF process. The shaded area represents the uncertainty on the signal and background yields from statistical, experimental, and theoretical sources.

Auxiliary Fig. 32b [2]

Hong

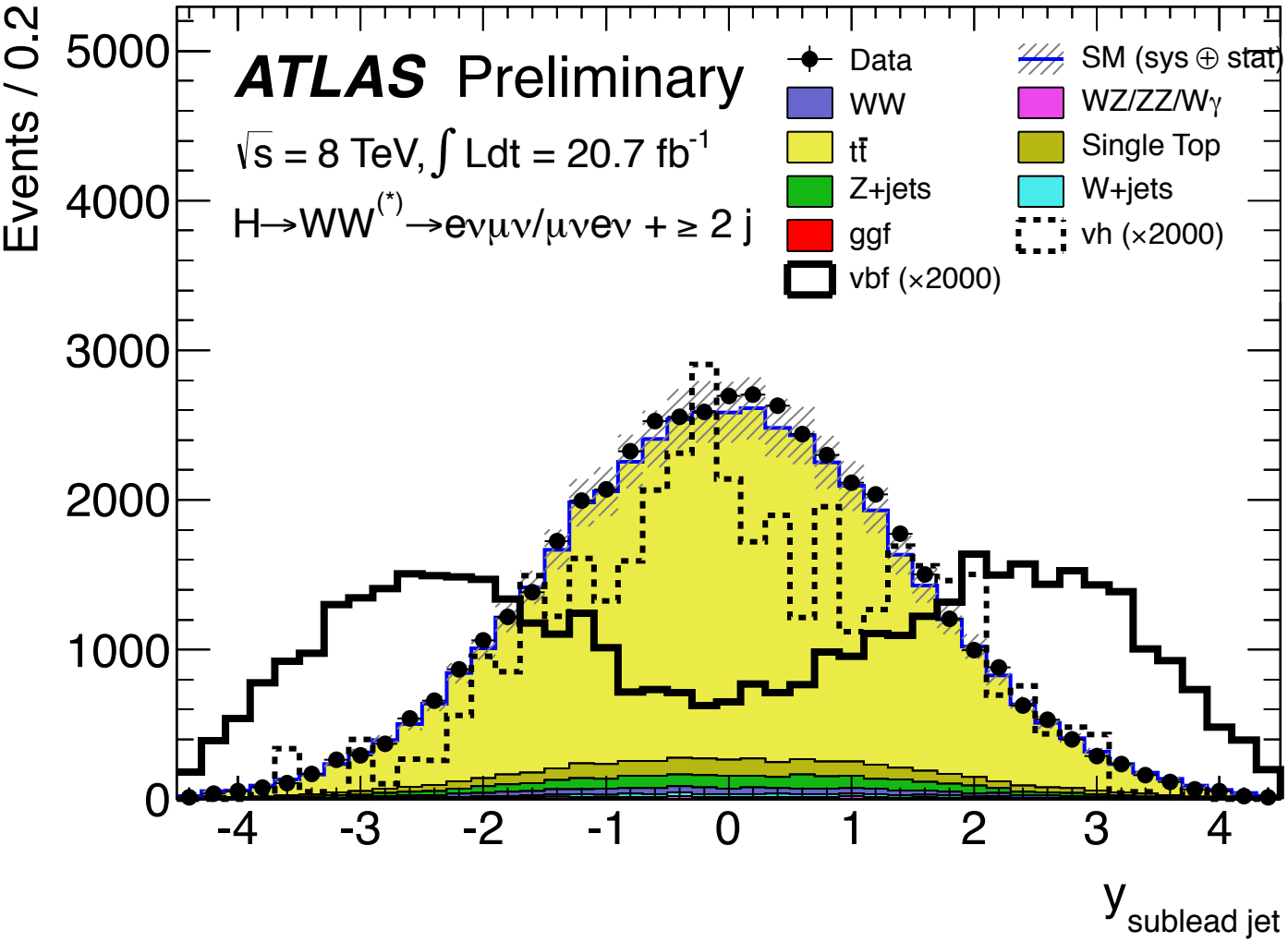

Caption

Rapidity distributions of the **subleading jet**. The distribution is shown at the 2 jets requirement, the **signal is magnified by a factor 2000** to show the peculiar forward distribution of jets from the VBF process. The shaded area represents the uncertainty on the signal and background yields from statistical, experimental, and theoretical sources.

Auxiliary Fig. 35a [1]

Hong

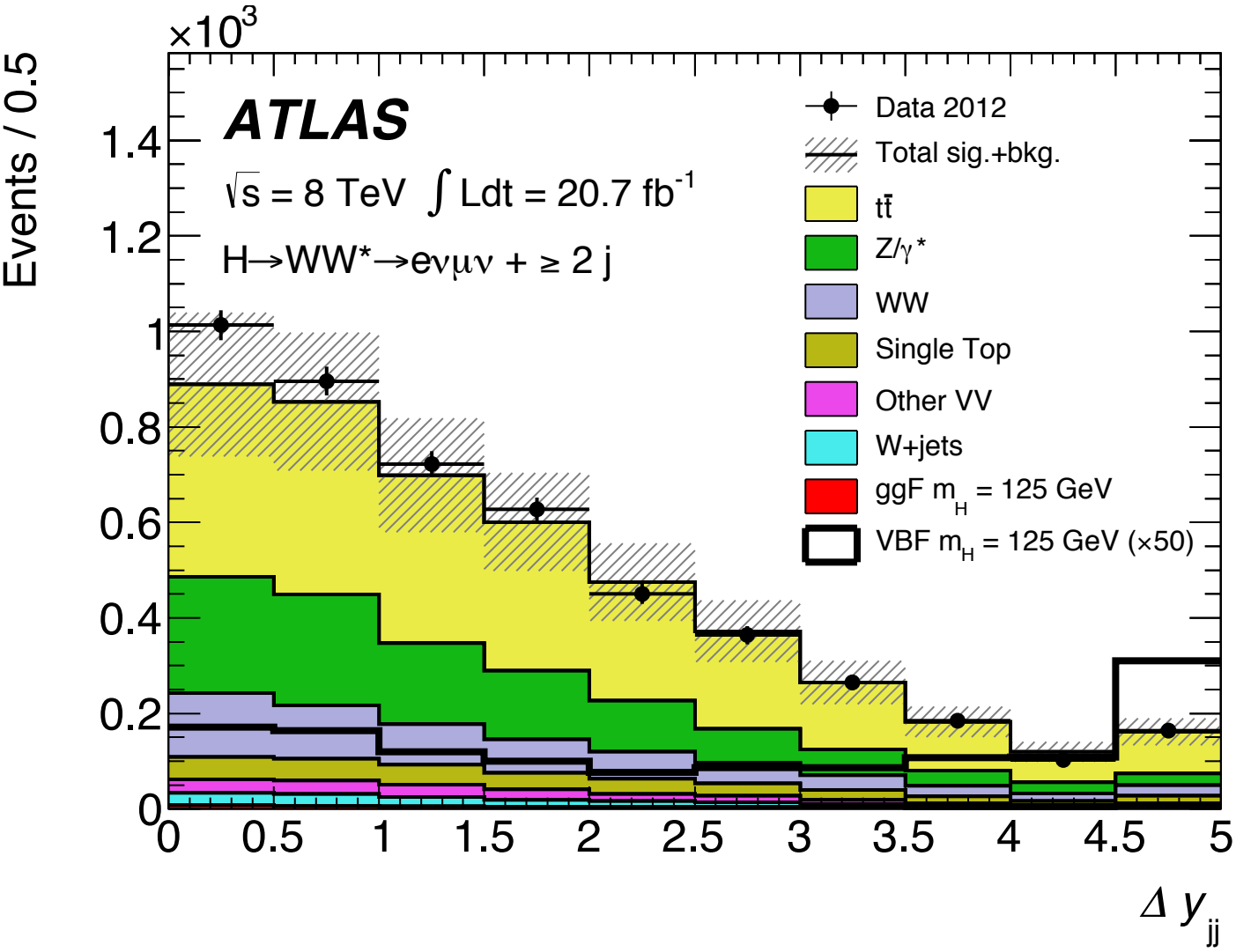

Caption

The **|Δyjj|** distribution for the H→WW*→lνlν analysis for **eμ** with **Njet ≥2**, **after the b-jet veto and |ptot|<45 GeV requirements**. The top-quark background is normalised using the corresponding control region, and Z+jets is normalised to the data-driven estimate. The expected **VBF signal magnified by a factor of 50** is also shown. The hatched area represents the uncertainty on the signal and background yields from statistical, experimental, and theoretical sources.

Auxiliary Fig. 35b [1]

Hong

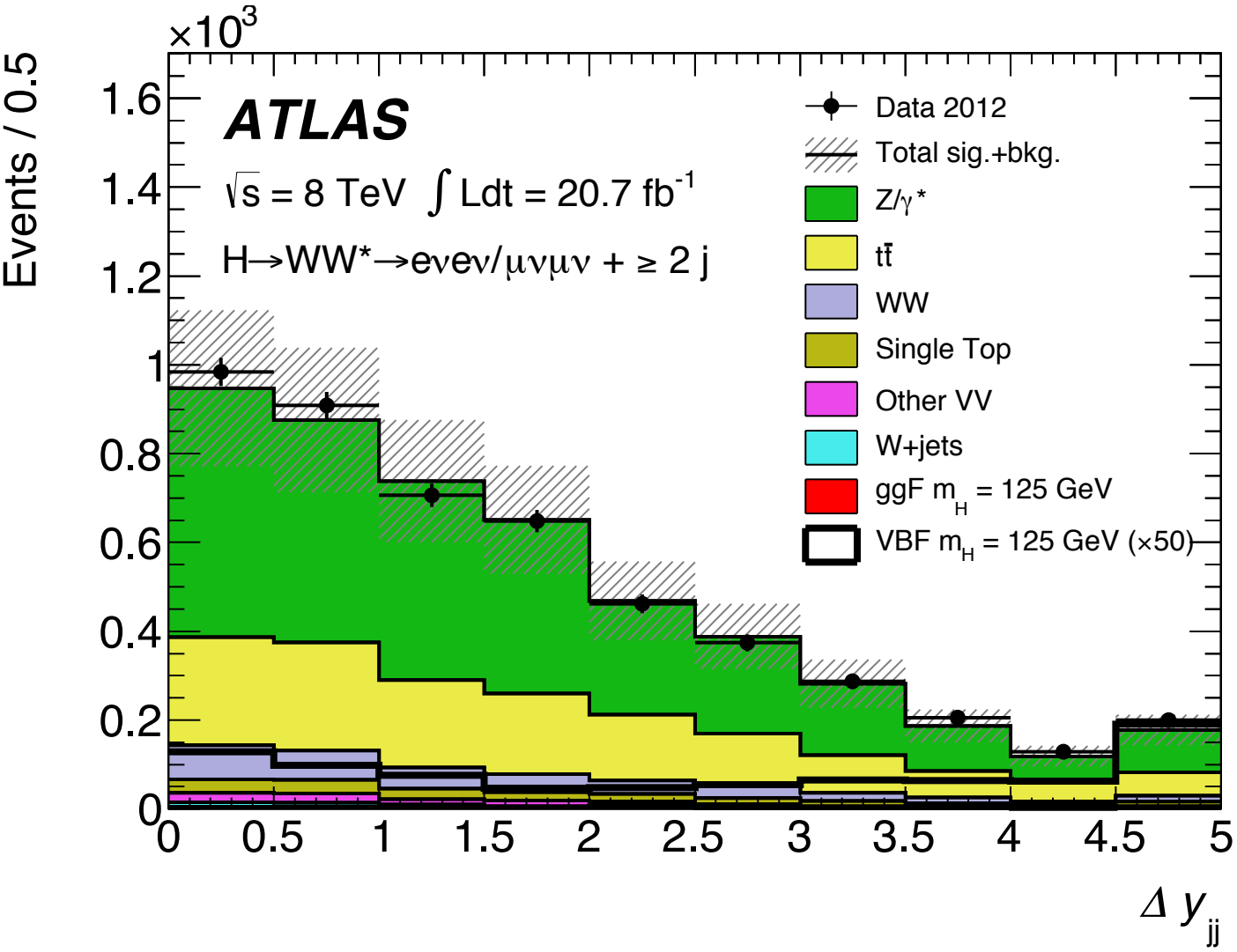

Caption

The **|Δyjj|** distribution for the H→WW*→lνlν analysis for **ee/μμ** with **Njet ≥2**, **after the b-jet veto and |ptot| <45 GeV requirements**. The top-quark background is normalised using the corresponding control region, and Z+jets is normalised to the data-driven estimate. The expected **VBF signal magnified by a factor of 50** is also shown. The hatched area represents the uncertainty on the signal and background yields from statistical, experimental, and theoretical sources.

Auxiliary Fig. 35c [1]

Hong

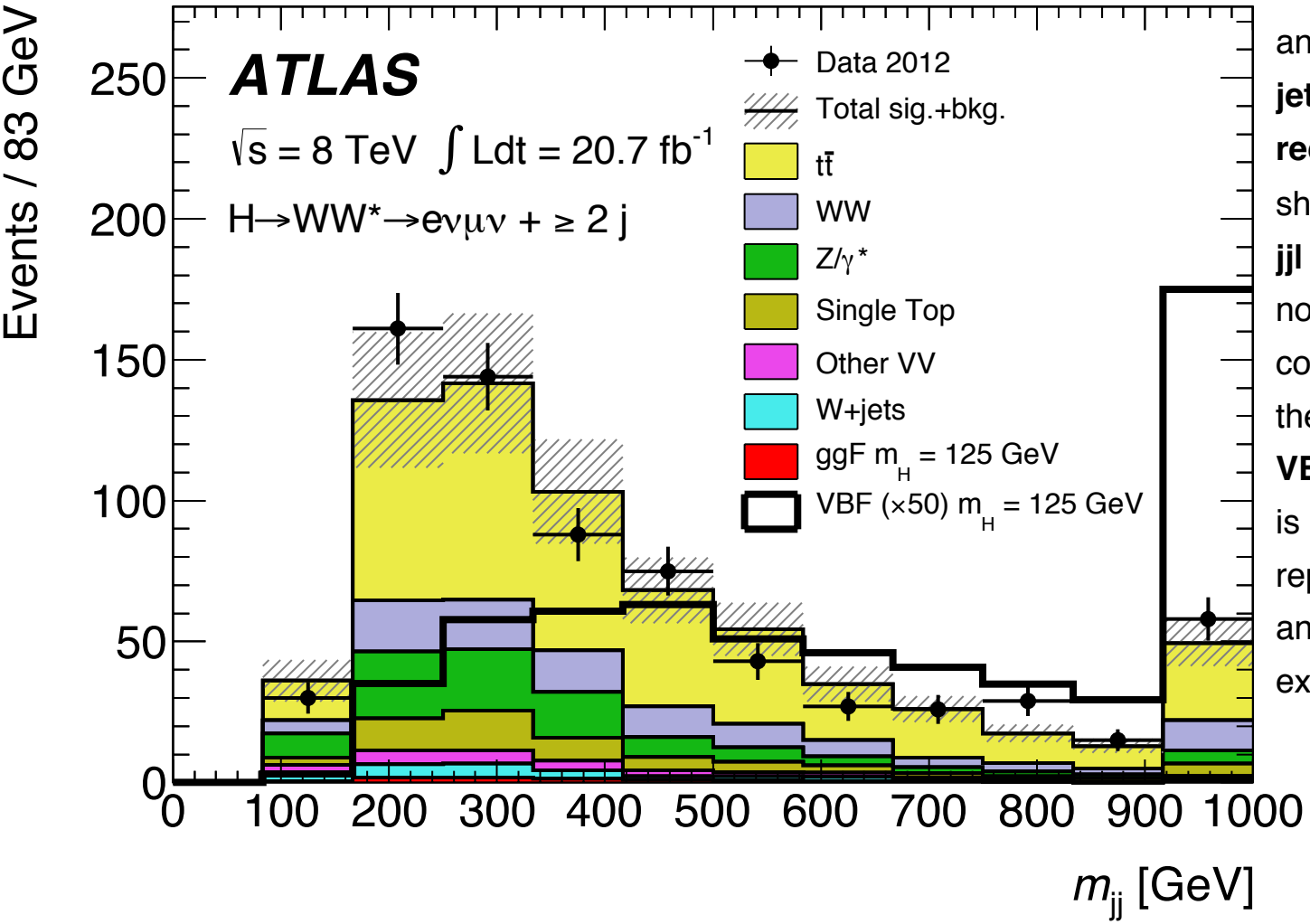

Caption

The **mjj** distribution for the H→WW*→lνlν analysis for **eμ** with **Njet ≥2**, **after the b-jet veto and |ptot|<45 GeV requirements**. The mjj distribution is shown **after the additional selection |Δy jj| > 2.8**. The top-quark background is normalised using the corresponding control region, and Z+jets is normalised to the data-driven estimate. The expected **VBF signal magnified by a factor of 50** is also shown. The hatched area represents the uncertainty on the signal and background yields from statistical, experimental, and theoretical sources.

Auxiliary Fig. 35d [1]

Hong

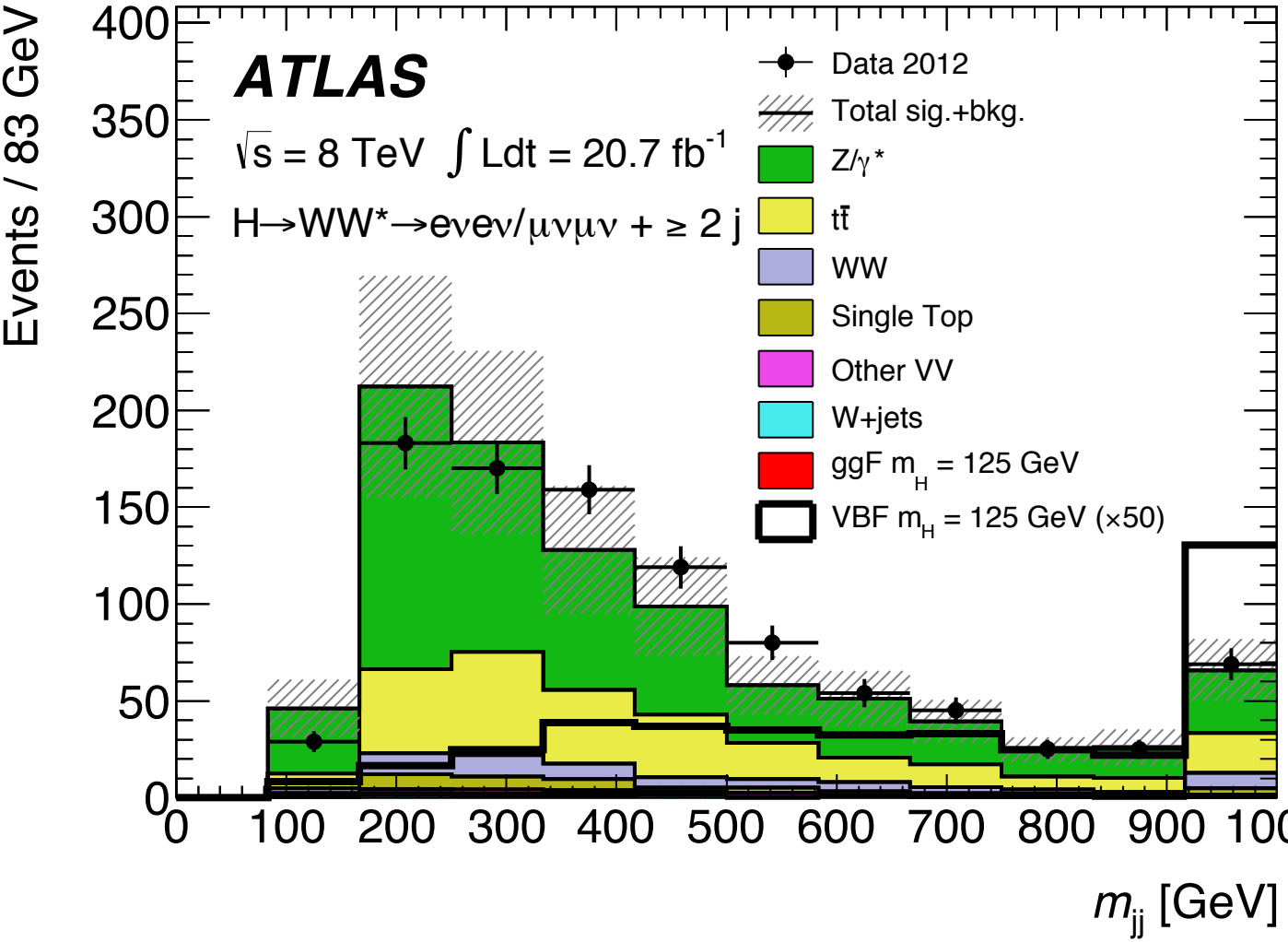

Caption

The **mjj** distributions for the H→WW*→lνlν analysis for **ee/μμ** with **Njet ≥2**, **after the b-jet veto and |ptotl <45 GeV requirements**. **The mjj distribution is shown after the additional selection | Δy jj | > 2.8.** The top-quark background is normalised using the corresponding control region, and Z +jets is normalised to the data-driven estimate. **The expected VBF signal magnified by a factor of 50 is also shown.** The hatched area represents the uncertainty on the signal and background yields from statistical, experimental, and theoretical sources.

Auxiliary Fig. 36a [1]

Hong

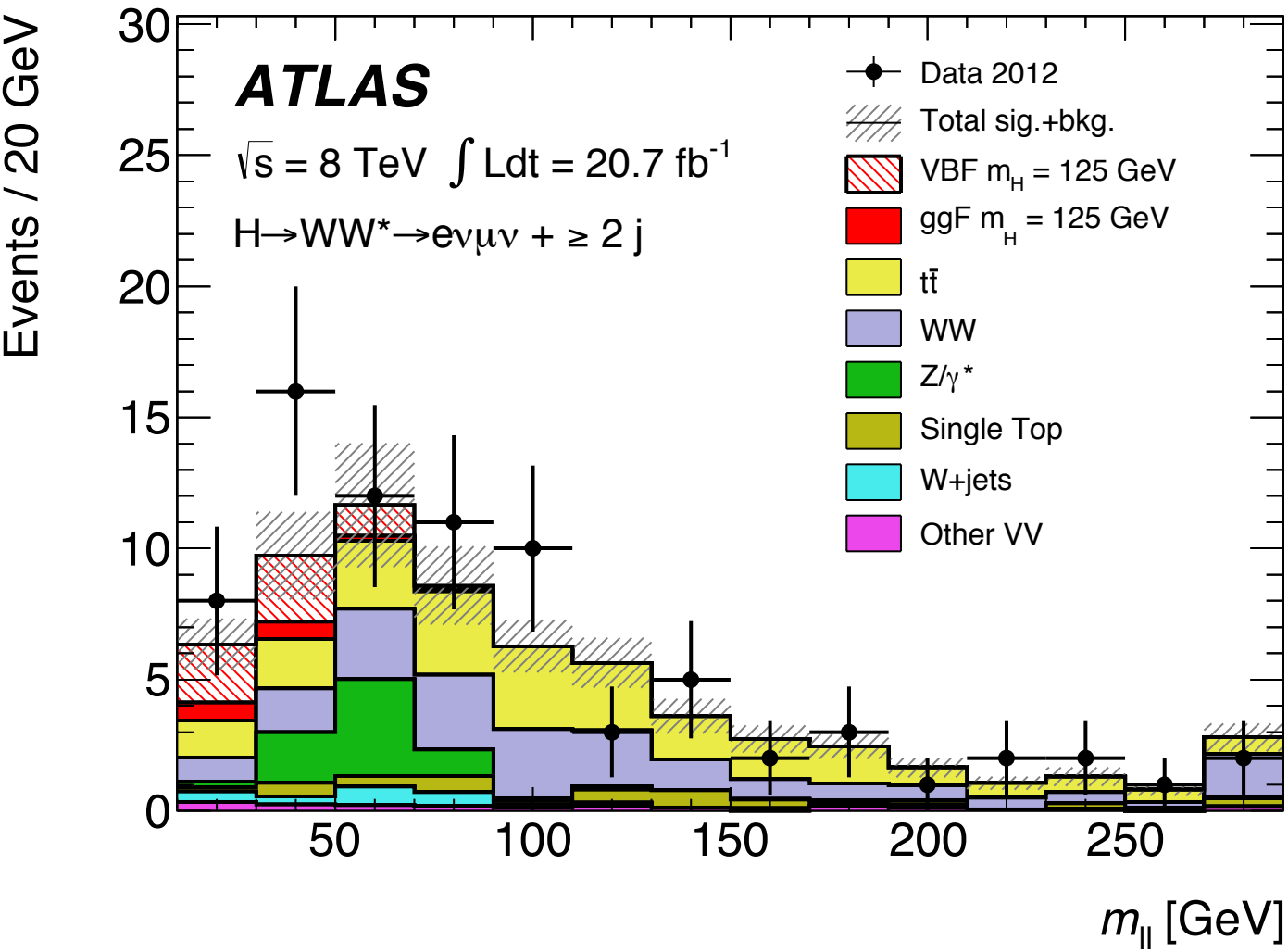

Caption

The **mll** distributions for the H→ WW∗→ lνlν analysis for **eμ** with **Njet ≥ 2**, **after the outside lepton veto requirement, which accepts only events with both leptons between the two tagging jets**. The top-quark background is normalised using the corresponding control region, and Z+jets is normalised to the data-driven estimate. The hatched area represents the uncertainty on the signal and background yields from statistical, experimental, and theoretical sources.

Auxiliary Fig. 36b [1]

Hong

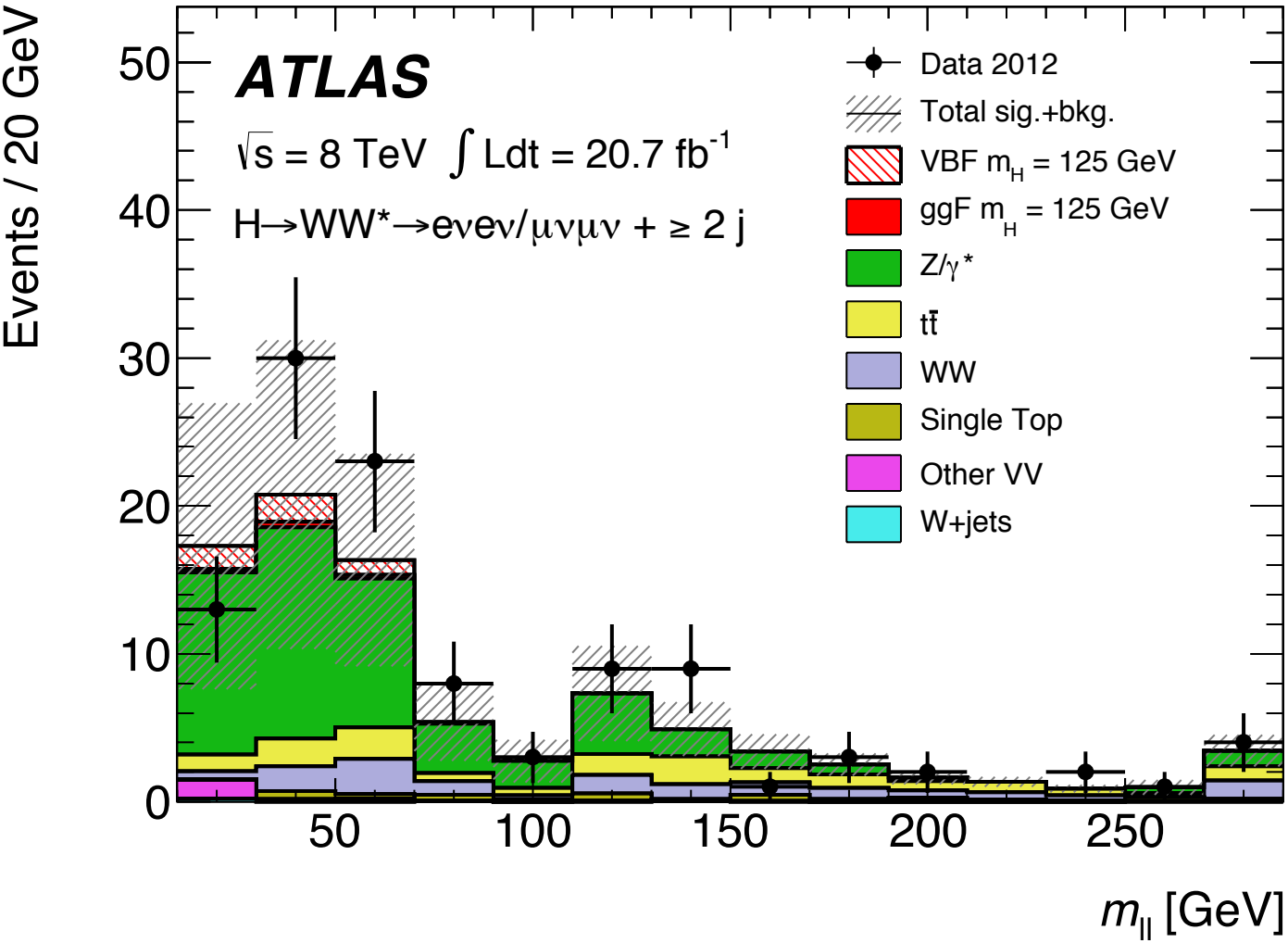

Caption

The **mll** distributions for the H→ WW∗→ lνlν analysis for **ee/μμ** with **Njet ≥ 2, after the outside lepton veto requirement, which accepts only events with both leptons between the two tagging jets**. The top-quark background is normalised using the corresponding control region, and Z+jets is normalised to the data-driven estimate. The hatched area represents the uncertainty on the signal and background yields from statistical, experimental, and theoretical sources.

Auxiliary Fig. 36c [1]

Hong

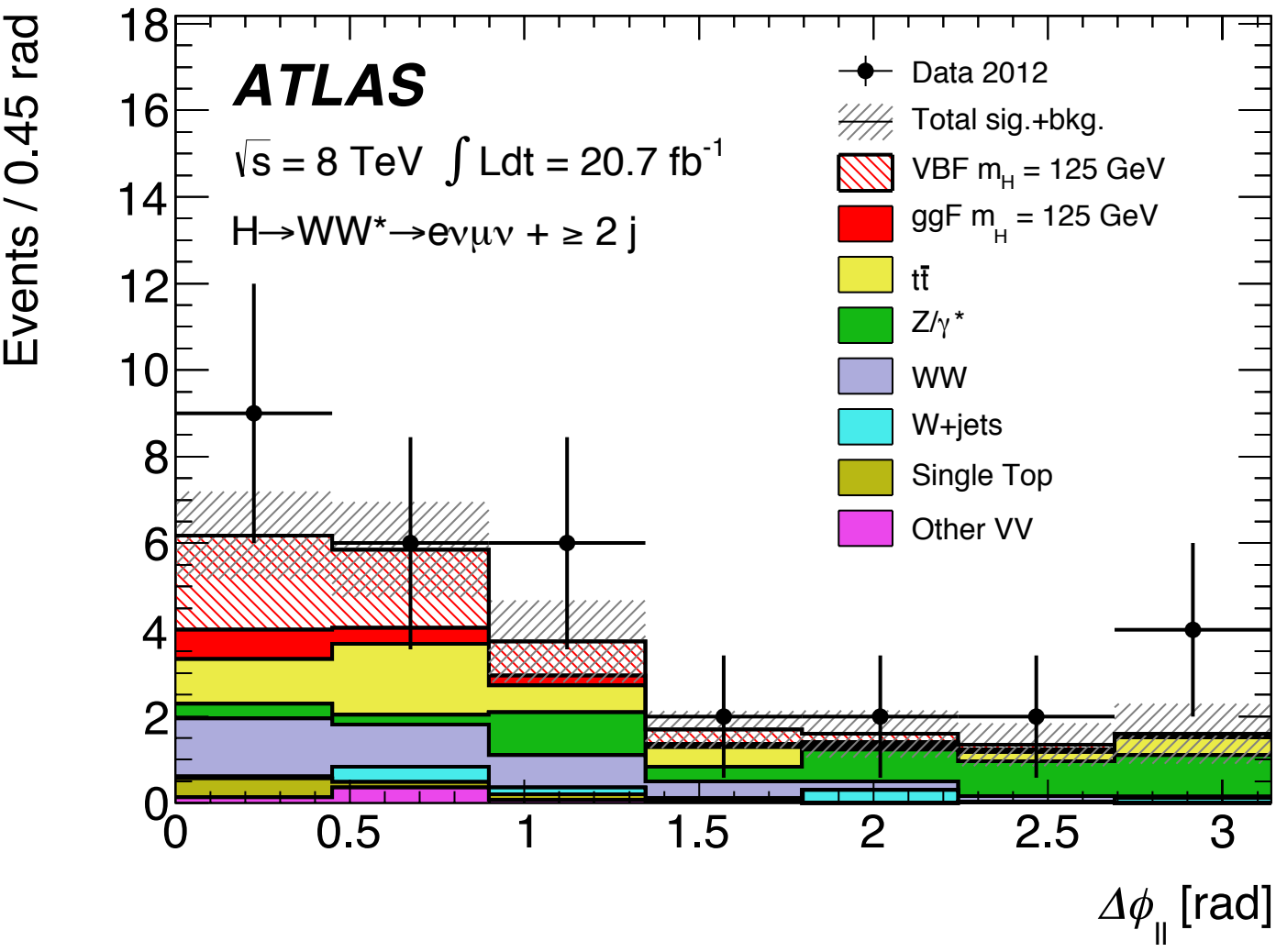

Caption

The **ΔφII** distributions for the H→ WW∗→ lνlν analysis for **eμ** with **Njet ≥ 2, after the outside lepton veto requirement, which accepts only events with both leptons between the two tagging jets**. **For the ΔφII distribution, the mII < 60 GeV selection is also made.** The top-quark background is normalised using the corresponding control region, and Z+jets is normalised to the data-driven estimate. The hatched area represents the uncertainty on the signal and background yields from statistical, experimental, and theoretical sources.

Auxiliary Fig. 36d [1]

Hong

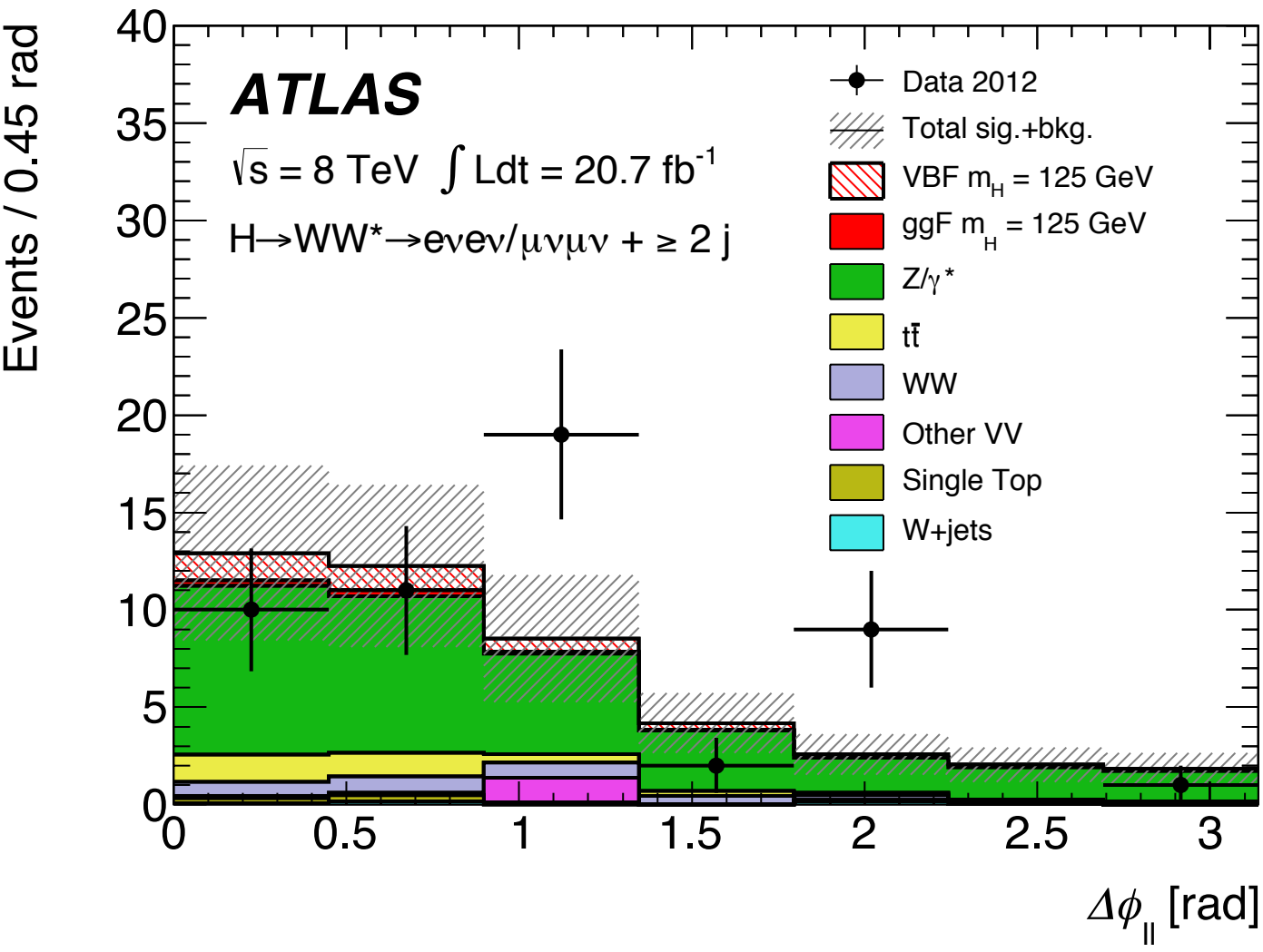

Caption

The **ΔφII** distributions for the H→ WW∗→ lνlν analysis for **ee/μμ** with **Njet ≥ 2, after the outside lepton veto requirement, which accepts only events with both leptons between the two tagging jets**. **For the ΔφII distribution, the mII < 60 GeV selection is also made.** The top-quark background is normalised using the corresponding control region, and Z+jets is normalised to the data-driven estimate. The hatched area represents the uncertainty on the signal and background yields from statistical, experimental, and theoretical sources.

Auxiliary Fig. 37 [1]

Hong

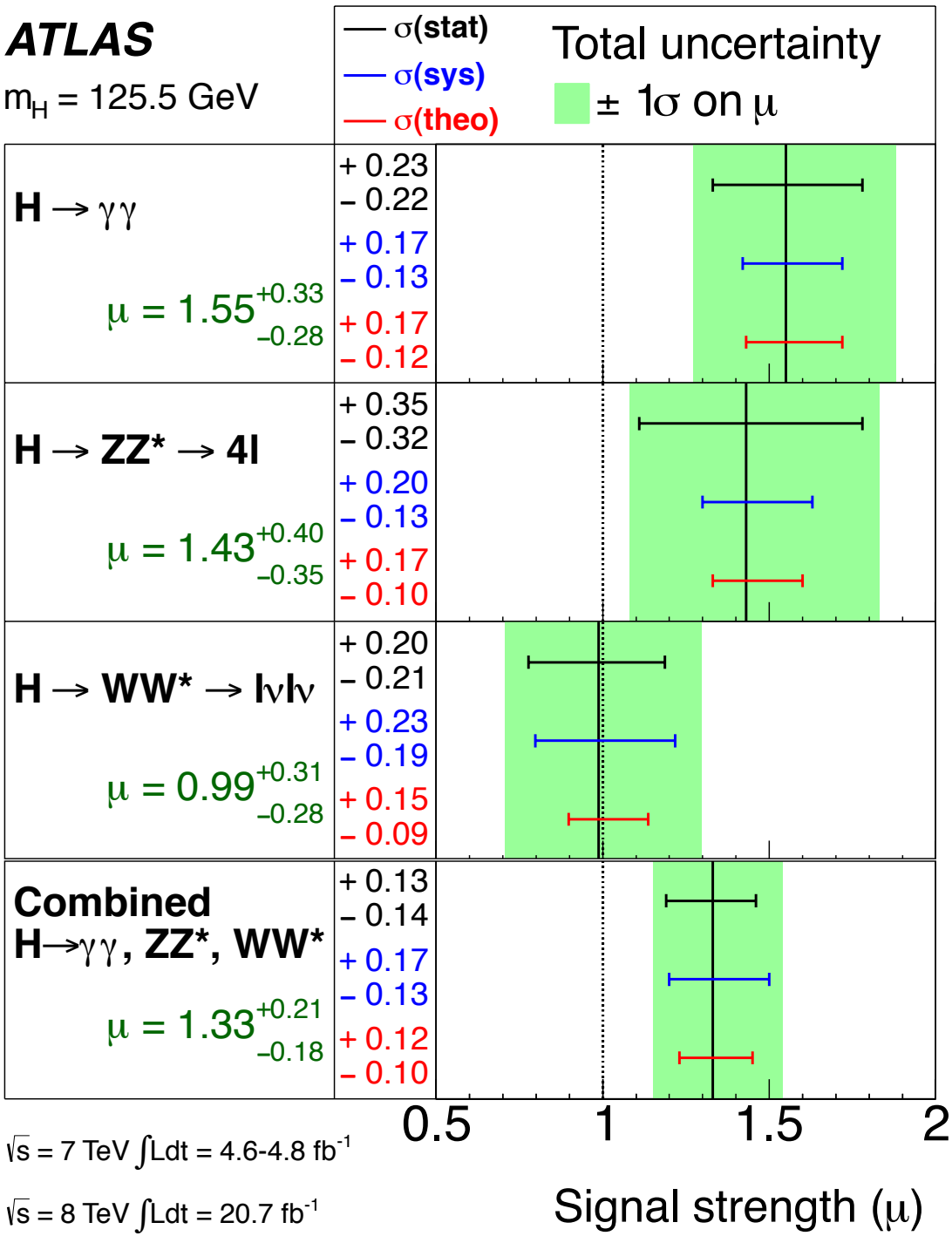

Caption

The **measured production strengths** for a Higgs boson of mass mH =125.5 GeV, normalised to the SM expectations, for diboson final states and their combination. The best-fit values are shown by the solid vertical lines. The total ±1σ uncertainty is indicated by the shaded band, with the individual contributions from the statistical uncertainty (top), the total (experimental and theoretical) stematic un- certainty (middle), and the theory uncertainty (bottom) on the signal cross section (from QCD scale, PDF, and branching ratios) shown as superimposed error bars.

Auxiliary Fig. 41a [1]

Hong

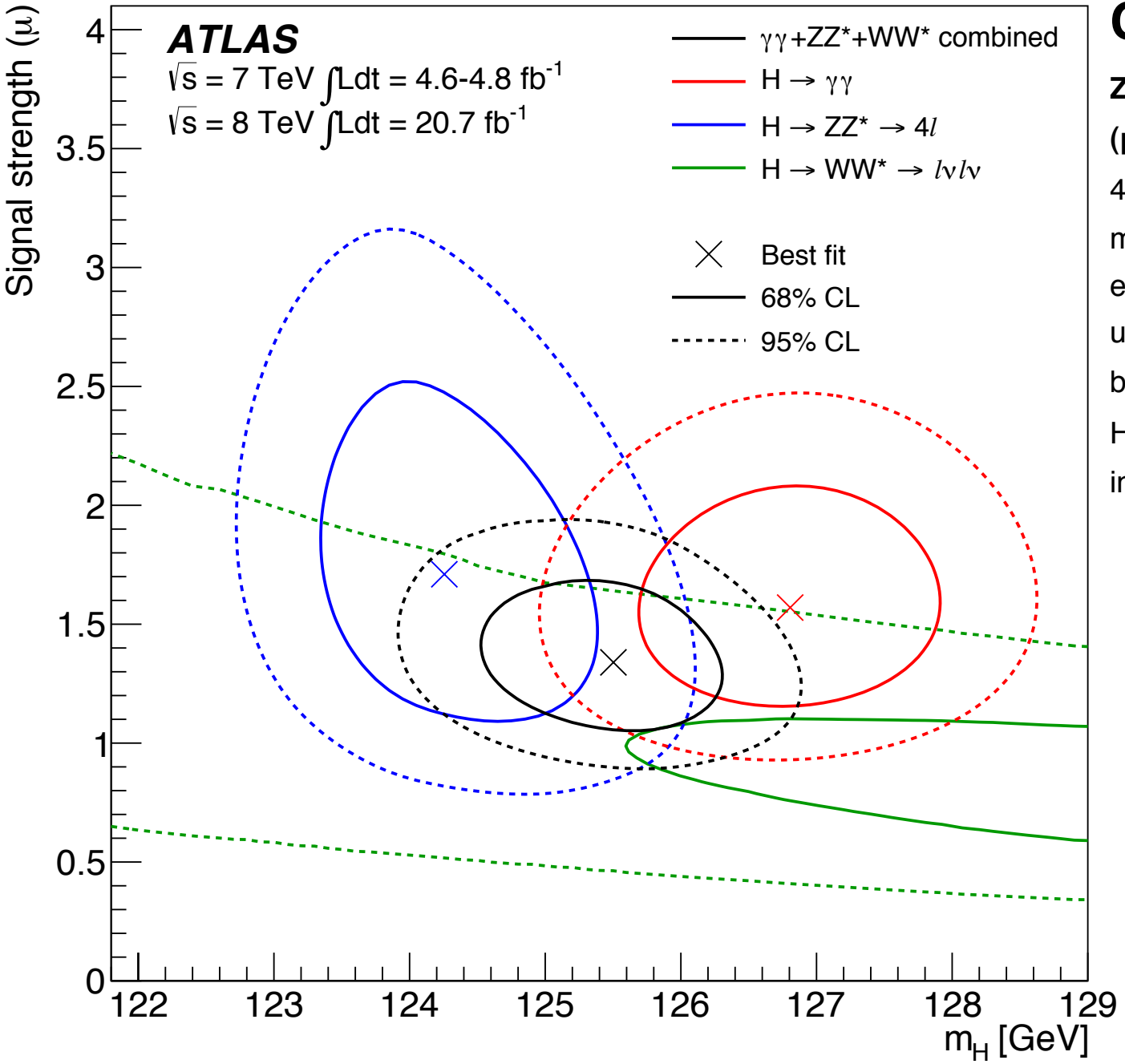

Caption

Zoomed-in likelihood contours in the (μ, mH) plane for the H → γγ, H→ ZZ∗→ 4l and H→ WW∗→ lνlν channels. The markers indicate the best-fit estimates in each case. Mass scale systematic uncertainties are treated as uncorrelated between the H → γγ, H→ ZZ∗→ 4l and H→ WW∗→ lνlν channels for the individual contours.

Auxiliary Fig. 41b [1]

Hong

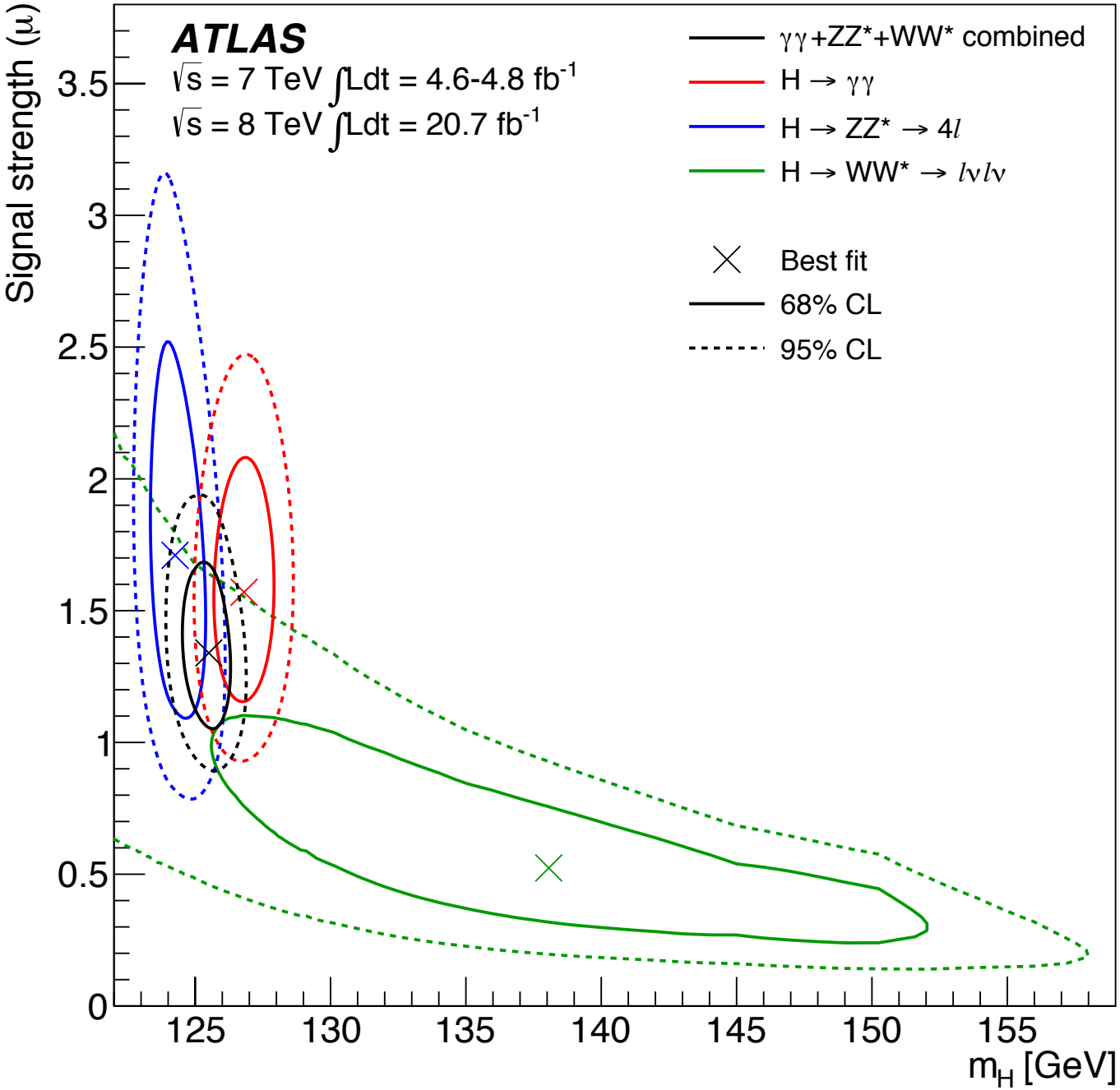

Caption

Zoomed-out likelihood contours in the (μ, mH) plane for the H → γγ, H→ ZZ∗→ 4l and H→ WW∗→ lνlν channels. The markers indicate the best-fit estimates in each case. Mass scale systematic uncertainties are treated as uncorrelated between the H → γγ, H→ ZZ∗→ 4l and H→ WW∗→ lνlν channels for the individual contours.

Auxiliary Fig. 42 [1]

Hong

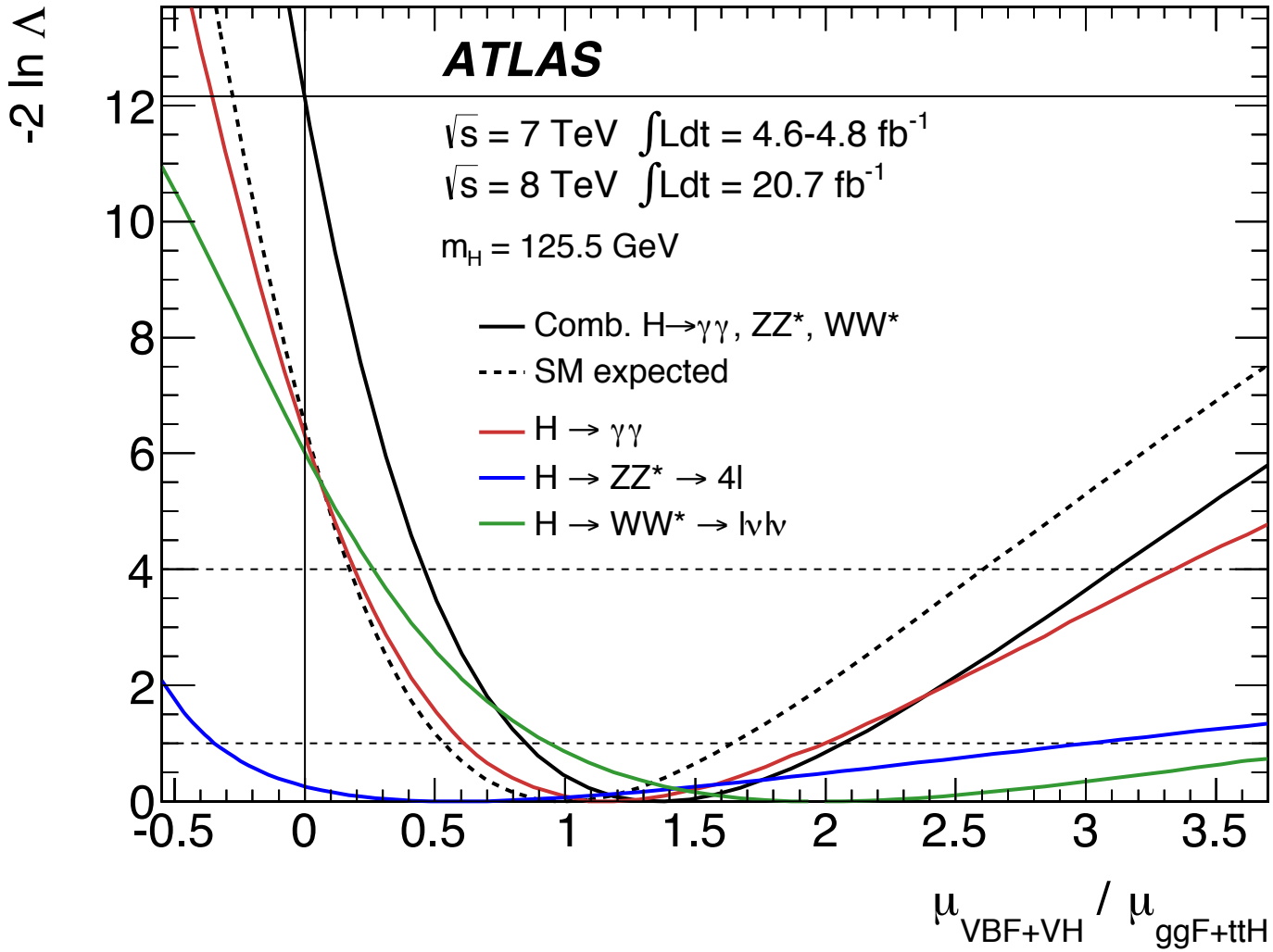

Caption

Likelihood curves for the ratio μVBF +VH/μggF+ttH for the H → γγ, H→ZZ*→4l and H→WW*→lνlν channels and their combination for a Higgs boson mass mH =125.5 GeV.The branching ratios (including possible non-SM contributions) cancel in the ratio μVBF +VH/μggF+ttH, hence the measurements from the four channels can be combined. The branching ratio dependence is contained in the signal strength factors μggF+ttH · BXX/BXX (with XX=γγ, ZZ and SM WW), which are profiled independently for the three final states. The dashed curve shows the SM expectation for the combination. The horizontal dashed lines indicate the 68% and 95% confidence levels.

Auxiliary Fig. 16a [2]

Hong

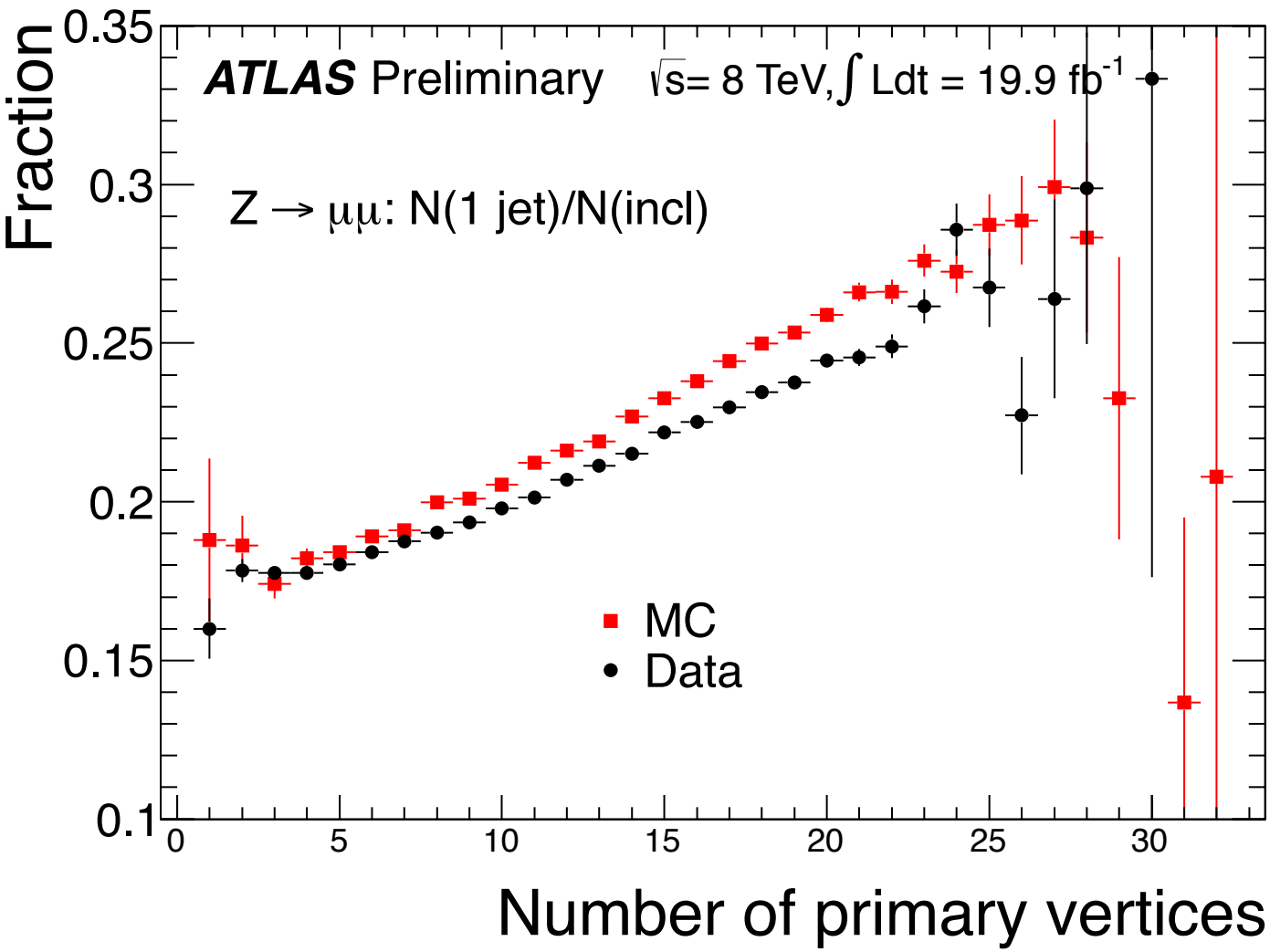

Caption

The **ratio of Z→μμ + 1-jet events to all Z→μμ candidates as a function of the number of reconstructed primary vertices** in the event with **no JVF requirement**. Uncertainties are statistical.

Auxiliary Fig. 16b [2]

Hong

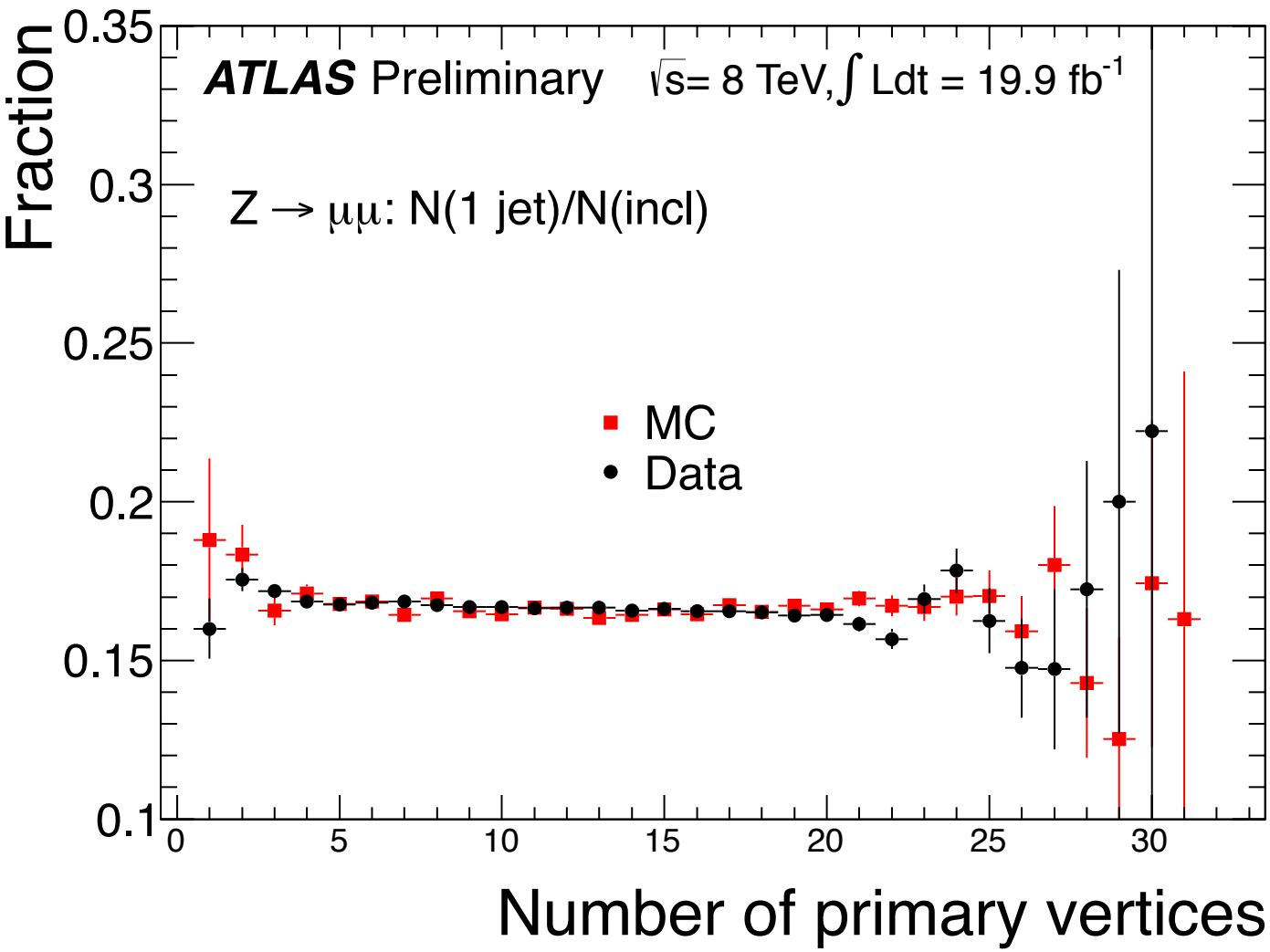

Caption

The **ratio of Z→μμ + 1-jet events to all Z→μμ candidates as a function of the number of reconstructed primary vertices** in the event with the | JVF | > 0.5 requirement. Uncertainties are statistical.

That’s all!